

Familial Alzheimer's disease mutations in presenilins disrupt endoplasmic reticulum calcium leak

APPROVED BY SUPERVISORY COMMITTEE

Ilya Bezprovanny, PhD

Matthew Goldberg, PhD

Lisa Monteggia, PhD

Gang Yu, PhD

Acknowledgements

“The ultimate measure of a man is not where he stands in times of comfort and convenience but where he stands in times of challenges and controversy” MLK. My journey in graduate school was a long roller coaster ride, it was rigged with many ups and downs; however, the overall experience was one of great enlightenment. This voyage would have not be possible without the guidance of one of the world’s greatest scientific minds, Dr. Ilya Bezprovanny. I learned how to maintain a mature composure in stressful situations, how to be productive in a cutting edge laboratory and how to think as an independent scientist. To learn these traits and be able to overcome my challenges would have not been possible without the support of Dr. Ilya Bezprovanny, a prodigy of science. Thankful words cannot explain the gratitude I have for the training, advice, patience and Dr. Bezprovanny’s endless emphasis on the importance of doing great science. It was an honor to have worked for him and I will forever cherish “my scientific age of reasoning” in his laboratory. Special thanks to my thesis committee Drs Matthew Goldberg, Lisa Monteggia and Gang Yu; without their guidance I would have not have smooth patches in my graduate school life. My sincere gratitude to the DBS training grant from the University of Texas Southwestern Medical school and the NIH Predoctoral Fellowship for Minority students (F31-AG0316920).

I would also like to thank Dr. Lee Monroe for giving me “my make a wish” so that I could have obtained an undergraduate education from a HBCU. In addition, I would like to thank Dr. George Ordway for giving me the opportunity to get my feet in the door of Basic Science and Dr. Dwight German for giving me the chance to work in the

laboratory in the infancy of my scientific journey. Without their initial efforts and mentorship I would have never had the chance to develop an interest in neurodegeneration.

I would like to extend my sincere gratitude to all my laboratory members both past and present for their expertise and knowledge over the years - Huiping Tu, Tieshan Tang, Youngie Ma, Tianhua Lei, Hua Zhang, Xi Chen, Jun Wu, Jing Liu, Xuesong Chen, Emin Ozkan, Huarui Liu, Yu Fu, Xinmei, Hewen Ma, Xiangmei Kong, Suyu Sun, Volodymyr Rybalchenko, Hongyu Wang, Yuemei Li, Yali Zhao, Qin Li, Janet Young and Leah Benson. Without their input; whether scientific or administrative, my thesis project would have not been this fruitful because they provided a nurturing environment for science. Special thanks to our collaborator Bart de Strooper, Alexandria Tolia and Sam Gandy, they provided us with cell lines, DNA constructs and scientific advice that were crucial in developing our calcium leak model for Alzheimer's disease.

Finally, I would like to thank my family for putting up with me over the years. Special thanks to my mother, Arlene Hall-Bryan. She mothered and fathered me through the passage of time; without her love and sacrifice I would have not made it thus far. I dedicate this to you mom.

Familial Alzheimer's disease mutations in presenilins disrupt endoplasmic
reticulum calcium leak

By

Omar Lloyd Nelson

DISSERTATION

Presented to the faculty of the Graduate School of Biomedical Sciences

The University of Texas Southwestern Medical Center at Dallas

In Partial Fulfillment of the Requirements

For the Degree of

DOCTOR OF PHILOSOPHY

The University of Texas Southwestern Medical Center at Dallas

Dallas, Texas

April 2009

Copyright

By

Omar Lloyd Nelson, 2009

All rights reserved

Introductory Abstract

Familial Alzheimer's disease mutations in presenilins disrupt endoplasmic
reticulum calcium leak

Omar Lloyd Nelson

The University of Texas Southwestern Medical Center at Dallas, 2009

Supervising Professor: Ilya Bezprozvanny, PhD

Alzheimer disease (AD) is the most common form of progressive dementia in adults over the age of 65 years. AD is a fatal brain disease and it currently affects about 27 million people worldwide. It is speculated that the number of people affected by AD will quadruple by 2050. The presence of amyloid beta plaque serves a pathological hallmark for AD, since it was first described by Alois Alzheimer's in 1906. The major risk factors for developing AD are age, mutations in presenilins (PS1 and PS2), mutations in the amyloid precursor protein (APP), cardiovascular diseases, open heart surgery, diabetes, brain injury/head trauma, Apolipoprotein E-e4 (APOE-e4) and the (P86L) mutation in the CALHM1(Calcium homeostasis modulator 1) gene. Multiple missense mutations have been reported in presenilin-1 (PS1), presenilin-2 (PS2) and the amyloid precursor proteins (APP), which are linked to familial AD (FAD). Presenilins are known

to function as the catalytic subunit of the γ -secretase complex and FAD mutations in presenilins affect APP processing, leading to the accumulation of A β 42 peptide and amyloid plaque formation in AD brains. In addition to abnormal APP processing, several FAD mutations in presenilins have been linked to abnormal calcium (Ca^{2+}) signaling. Our laboratory recently discovered that presenilin holoproteins function as endoplasmic reticulum (ER) Ca^{2+} leak channels and that FAD mutations in presenilins affected this function. Our findings potentially provided an explanation for Ca^{2+} signaling abnormalities resulting from FAD mutations in presenilins. The goal of my thesis project is to establish a connection between presenilins FAD mutations and ER Ca^{2+} signaling. For these studies we utilized the lipid bilayer reconstitution technique and Ca^{2+} imaging experiments. In order to establish such a connection I examined the effects of FAD PS1 mutation, FAD PS2 mutation, FAD APP mutation, a mutation in tau and sporadic AD cases on ER Ca^{2+} leak. In addition, I will map the conductance pore of PS1 using cysteine substitution in transmembrane 6, 7 and 9. These data will help to evaluate the “ Ca^{2+} hypothesis of AD” and will contribute to selecting optimal strategies for treatment of AD.

Publications

Prior Publications:

Xi Chen, Tie-shan Tang, Huiping Tu, **Omar Nelson**, Mark Pook, Robert Hammer, Nobuyuki Nukina, Ilya Bezprozvanny. Deranged Calcium Signaling and Neurodegeneration in Spinocerebellar Ataxia 3. 2009, **J. Neuroscience** 28:12713-12724

Nelson O, Tu H, Lei T, Bentahir M, De Strooper B and Bezprozvanny I Familial Alzheimer disease–linked mutations specifically disrupt Ca^{2+} leak function of presenilin 1 **J. Clin. Invest.** 2007 May; 117 (5): 1230-9

Tu H.P., **Nelson O**, Bezprozvanny A, Wang Z, Lee S-F, Hao Y-H, Serneels L, De Strooper B, Yu G, and Bezprozvanny I (2006). Presenilins form ER calcium leak channels, a function disrupted by familial Alzheimer's disease-linked mutations. **Cell**, v 126, pp 981-993.

German DC, **Nelson O**, Liang F, Liang CL, Games D. The PDAPP mouse model of Alzheimer's disease: locus coeruleus neuronal shrinkage. **J Comp Neurol.** 2005 Nov 28; 492 (4): 469-76.

Liang CL, **Nelson O**, Yazdani U, Pasbakhsh P, German DC. Inverse relationship between the contents of neuromelanin pigment and the vesicular monoamine transporter-2: human midbrain dopamine neurons. **J Comp Neurol.** 2004 May 17; 473(1): 97-106.

Publications in preparation:

Liu J, Tang TS, Tu H, **Nelson O**, Herndon E, Huynh DP, Stefan-M.

Pulst SM, Bezprozvanny I. Deranged calcium signaling and neurodegeneration in spinocerebellar ataxia type 2. **J. Neuroscience** 2009(under revision)

Nelson O, Liu H and Bezprozvanny I. Calcium signaling defects in Familial Alzheimer's disease patients. Relevance for Alzheimer's disease. (awaiting submission to Neurobio of Dis.)

Nelson O, Tolia A, Horr  K, De Strooper B and Bezprozvanny I. Role of Presenilin 1 transmembrane domain 6, 7 and 9 on Endoplasmic Reticulum Calcium leak. (awaiting submission to J. Bio. Chem.)

LIST OF FIGURES

FIGURE 1 - FAD -LINKED MUTATIONS IN PRESENILIN.....	5
FIGURE 2 – HUMAN A β STAIN.....	6
FIGURE 3 – AMYLOID CASCADE HYPOTHESIS OF AD.....	5
FIGURE 4 – CALCIUM HYPOTHESIS OF AD.....	7
FIGURE 5 – PRESENILINS AS A CHANNEL AND A γ -SECRETASE.....	9
FIGURE 6 – RECOMBINANT PRESENILIN FORM CALCIUM CHANNELS IN PLANAR LIPID BILAYERS.....	31
FIGURE 7 – RESCUE OF CALCIUM SIGNALING DEFECTS IN DKO MEFS WITH PS1-FAD MUTANTS.....	32
FIGURE 8 – SUMMARY OF PS1-FAD RESCUE EXPERIMENTS.....	33
FIGURE 9 - CALCIUM SIGNALS IN STABLE DKO RESCUE LINES.....	34
FIGURE 10 – RESCUE OF CALCIUM SIGNALING DEFECTS IN DKO MEFS WITH PS1-FTD MUTANTS.....	35
FIGURE 11 – SUMMARY OF PS1-FTD RESCUE EXPERIMENTS.....	36
FIGURE 12 – CALCIUM SIGNALS IN HUMAN PRIMARY FIBROBLASTS FROM THE FAD PATIENT.....	37
TABLE 1.....	38
FIGURE 13 – MOLECULAR MODEL OF PRESENILINS.....	56
FIGURE 14 – CALCIUM SIGNALS IN LYMPHOBLAST FROM THE FAD PATIENT.....	57
FIGURE 15 – CALCIUM SIGNALS IN HUMAN LYMPHOBLAST FROM FAD PATIENTS.....	58

FIGURE 16 – SUMMARY OF PS1-FAD RESCUE EXPERIMENTS.....	59
FIGURE 17 – SUMMARY OF CWP PS1-ASSOCIATED RESCUE EXPERIMENTS.....	60
FIGURE 18 – EFFECT OF UNCLEAVABLE PS1-M292D AND γ -SECRETASE MUTANT ON ER CALCIUM LEAK.....	61
FIGURE 19 – CALCIUM SIGNALS IN PS1 TARGETING CONTSTRUCT (dTAG).....	62
FIGURE 20 - MOLECULAR MODEL OF PRESENILINS.....	63
FIGURE 21 – CYS-LESS mPS1 AND CYSTEINE MUTANTS.....	77
FIGURE 22 – CYS-LESS mPS1 RESCUES ER CALCIUM LEAK PATHWAY IN STABLY TRANSFECTED DKO CELLS.....	78
FIGURE 23 – SUMMARY OF TM6, 7 AND 9 IO RELEASEABLE CALCIUM ER POOL.....	79
FIGURE 24 – MPS1- Δ LOOP DOES NOT ER CALCIUM LEAK PATHWAY IN STABLY TRANSFECTED DKO CELLS.....	80
TABLE 2.....	81
FIGURE 25- HELICAL REPRESENTATION OF TM 6, 7 AND 9.....	82
FIGURE 26- THE MODEL OF CALCIUM DYSREGULATION IN AD.....	89
FIGURE 27- CHEMIICAL REACTION OF CYSTEINE SIDE-CHAIN MODIFICATION WITH MTS REAGENT.....	94
FIGURE 28-SUBSTITUTED-CYSTEINE-ACCESSIBILTY METHOD (SCAM).....	95
FIGURE 29- PScDKO MICE IO RELEASABLE CALCIUM POOL.....	96

LIST OF ABBREVIATIONS

A β - amyloid beta

AD - Alzheimer's disease

APP - amyloid precursor protein

APOE - apolipoprotein E

BK- bradykinin

BLM - planar lipid bilayer

Ca²⁺ - calcium

CWP - cotton wool plaque

ER - endoplasmic reticulum

FAD - Familial Alzheimer's disease

FTD - frontotemporal dementia

IO- ionomycin

NFT - neurofibrillary tangle

MEF- mouse embryonic fibroblast

PS1 - presenilin 1

PS2 - presenilin 2

TM - transmembrane

SP - spastic paraparesis

TABLE OF CONTENTS

ACKNOWLEDGEMENTS.....	ii
INTRODUCTORY ABSTRACT.....	vi
PUBLICATIONS.....	viii
LIST OF FIGURES.....	x
LIST OF ABBREVIATIONS.....	xii

CHAPTER ONE

GENERAL INTRODUCTION.....	2
RESEARCH DESIGN AND METHODS.....	9

CHAPTER TWO

ENDOPLASMIC RETICULUM CALCIUM LEAK FUNCTION OF PRESENILIN 1 DISRUPTED BY MUTATATIONS LINKED TO FAMILIAL ALZHEIMER'S DISEASE BUT NOT BY MUTATIONS ASSOCIATED WITH FRONTOTEMPORAL DEMENTIA.....	15
ABSTRACT.....	16
INTRODUCTION.....	17
RESULTS.....	18
DISCUSSION.....	27
FIGURES.....	31

CHAPTER THREE

CALCIUM SIGNALING DEFECTS IN FAMILIAL ALZHEIMER'S DISEASE PATIENT: RELEVANCE FO ALZHEIMER'S DISEASE.....	40
ABSTRACT.....	41
INTRODUCTION.....	42
RESULTS.....	43
DISCUSSION.....	52
FIGURES.....	56

CHAPTER FOUR

THE ROLE OF PRESENILIN 1 TRANSMEMBRANE DOMAIN 6, 7 AND 9 ON ENDOPLASMIC RETICULUM CALCIUM LEAK.....	64
ABSTRACT.....	65
INTRODUCTION.....	66
RESULTS.....	69
DISCUSSION.....	73
FIGURES.....	77

CHAPTER FIVE

CONCLUSIONS AND FUTURE EXPERIMENTS.....	83
CONCLUSIONS.....	84
FUTURE EXPERIMENTS.....	90
BIBLIOGRAPHY.....	97

CHAPTER ONE

General Introduction, Research Design and Methods

General Introduction

Alzheimer disease (AD, OMIM entry 104300) is the most common form of progressive dementia in the elderly. It is a neurodegenerative disorder that is characterized by the neuropathological findings of intracellular neurofibrillary tangles (NFT) and extracellular amyloid plaques that accumulate in vulnerable brain regions (hippocampus and cortex) that are mainly involved in cognitive function (memory, attention, language and problem solving). The major risk factors for developing AD are age, mutations in presenilins (PS1 and PS2), mutations in the Amyloid precursor protein (APP), cardiovascular diseases, open-heart surgery, diabetes, brain injury/head trauma, Apolipoprotein E-e4 (APOE-e4) and a rare polymorphism in the CALHM1 (Calcium homeostasis modulator 1) gene. Approximately 25-40% of the AD patients reported have genetic factors that are involved in the disease pathology. The ϵ 4 allele of the apolipoprotein E gene (APOE) that is located on 19q13.2 chromosomal region was identified as a major risk factor contributing to the pathogenesis of AD in about 20% of the cases (Corder, Saunders et al. 1993; Saunders, Strittmatter et al. 1993). The involvement of other AD risk genes is currently under investigation. In approximately 1-2% of the early onset (< 65 years old) cases; AD segregates as an autosomal dominant trait in families (familial AD, FAD). Molecular genetics studies uncovered three genes that are linked to FAD – the A β amyloid precursor protein gene (APP) located in 21q21 region (Levy, Carman et al. 1990; Goate, Chartier-Harlin et al. 1991), the presenilin-1 gene (PSEN1) located in 14q24.3 region and presenilin-2 gene (PSEN2) located in 1q31-q42 region (Levy-Lahad, Wasco et al. 1995; Rogaeve, Sherrington et al. 1995; Sherrington, Rogaeve et al. 1995). Together, mutations in these 3 genes are responsible for the majority of all known FAD cases. Currently there is 24 FAD-linked mutations have been identified in

APP gene, 156 FAD-linked mutations have been identified in PSEN1 and 10 FAD-linked mutations have been identified in PSEN2 (<http://www.molgen.ua.ac.be/ADMutations/>). The presence of senile plaques with a dense core that is mainly composed of the Amyloid β peptide ($A\beta$) (Fig 2B) that surrounds degenerating neurons, which accumulates hyperphosphorylated tau, serves as a key pathological hallmark for Alzheimer's disease. Dense core senile plaques appear in most cases of AD with mutations in PS1; however, there are certain PS1 mutations that are associated with a variant plaque, known as cotton wool plaques (CWP)(Fig 2A), which consist of large round $A\beta$ deposits primarily positive for $A\beta$ 42(Steiner, Revesz et al. 2001) usually devoid of a compact amyloid core and lacking neuritic pathology (Crook, Verkkoniemi et al. 1998). Three missense mutations in PS1 is suggested to be linked to frontal temporal dementia (FTD) (Hutton 2004), a disease which is characterized by the shrinkage of the frontal and temporal lobes of the brain. Because of the similarity in the pathological and clinical manifestations of sporadic and familial AD, it is generally assumed that studies of FAD will provide a clue to the understanding of AD pathogenesis, better treatments for AD or eventually a cure.

My thesis mainly focuses on the studying of FAD-causing mutations in PS1 because of material availability and more animal models with mutations in PS1. Mammalian PS1 and PS2 are synthesized as 50 kDa polypeptides and localized to the endoplasmic reticulum (ER) membrane (Yu, Chen et al. 1998; Annaert, Levesque et al. 1999). According to the latest biochemical data, presenilins span the membrane 9 times with the amino-terminus in the cytosol and carboxy-terminus in the ER lumen (Laudon, Hansson et al. 2005; Oh and Turner 2005; Spasic, Tolia et al. 2006)(Fig 1). Previously, an 8 transmembrane (TM) domain model was widely used (Tandon and Fraser 2002).

Most FAD-linked missense mutations in PS1 are located within transmembrane domains (Fig 1). Both PS1 and PS2 holoproteins undergo endoproteolysis in the cytosolic loop between TM domains 6 and 7 (Fig 1), resulting in the generation of a 35 kD amino-terminal fragment (PS-NTF) and a 18-20 kD carboxy-terminal fragment (PS-CTF) which remain associated with each other (Thinakaran, Borchelt et al. 1996; De Strooper, Beullens et al. 1997; Yu, Chen et al. 1998). Endoproteolytic cleavage of presenilins occurs only after it has been incorporated into a ~440 kDa complex which also contains nicastrin, aph-1 and pen-2 subunits (Fig 5) (Edbauer, Winkler et al. 2003; Kimberly, LaVoie et al. 2003; Takasugi, Tomita et al. 2003; Lazarov, Fraering et al. 2006). The assembly of presenilins with nicastrin, aph-1 and pen-2 is coordinated with exit from the ER and translocation into the Golgi apparatus (LaVoie, Fraering et al. 2003; Takasugi, Tomita et al. 2003; Spasic, Tolia et al. 2006). Following assembly, the “mature” complex of PS-NTF: PS-CTF, nicastrin, aph-1 and pen-2 travel towards the cell surface and get incorporated into the plasma membrane (Fig 5).

Our laboratory recently discovered that not only could PSs function as the catalytic subunit of γ -secretase complex; they also function as a Ca^{2+} leak channel before incorporation in the γ -secretase complex (Fig 5). In addition, we discovered that many FAD PSs mutations affected its ability to function as a Ca^{2+} leak channel.

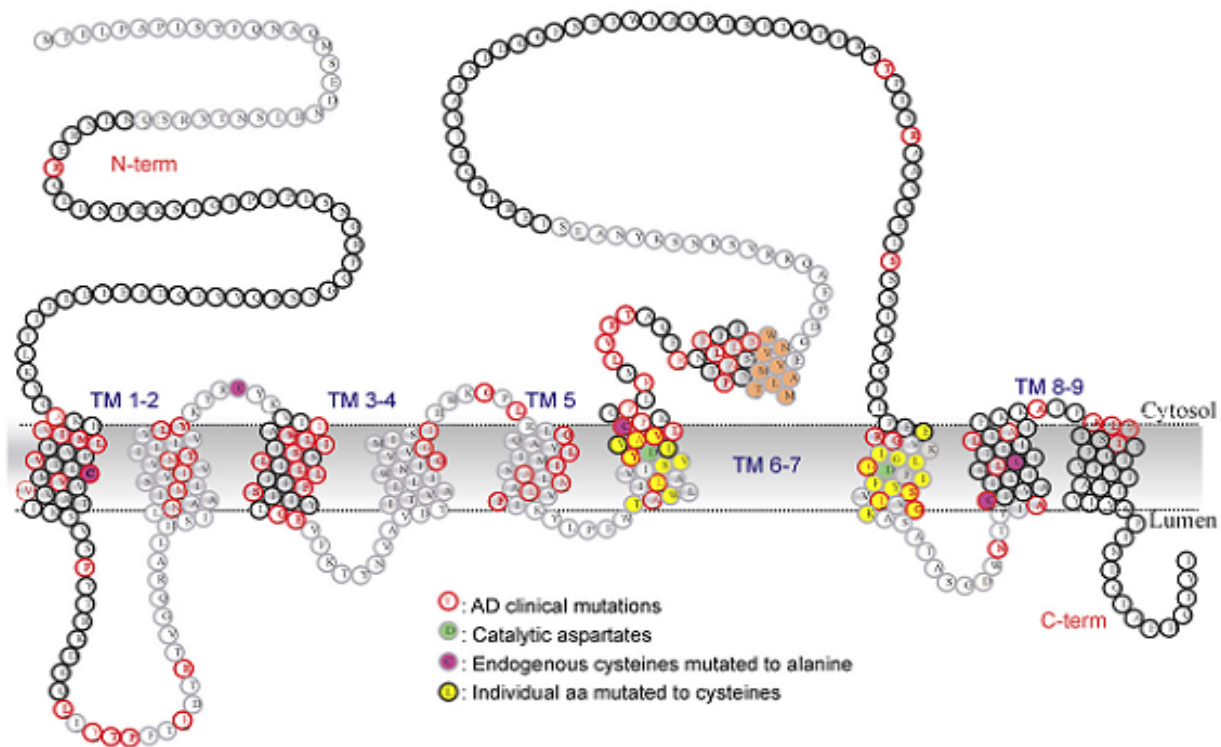


Fig 1. FAD-linked mutations in PS1. From (Tolia et al., 2008)

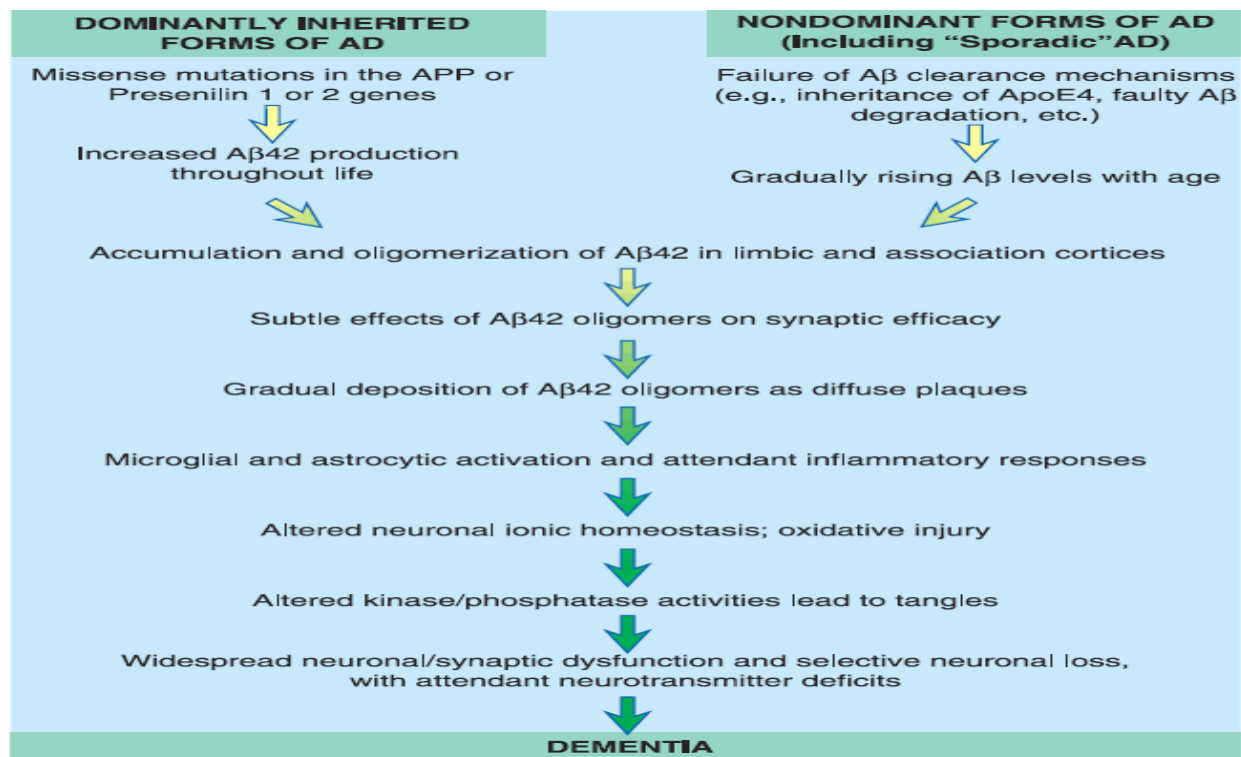
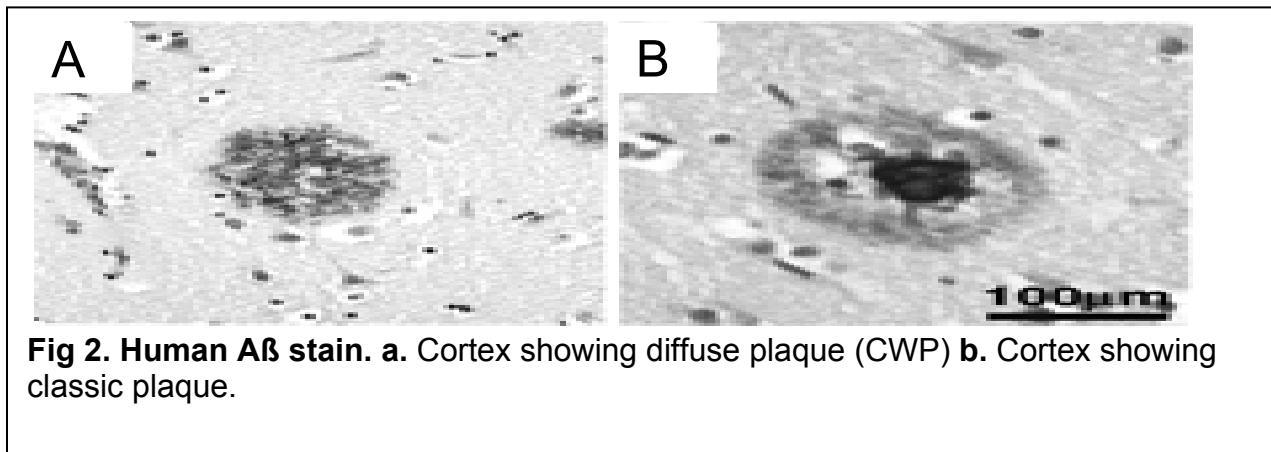


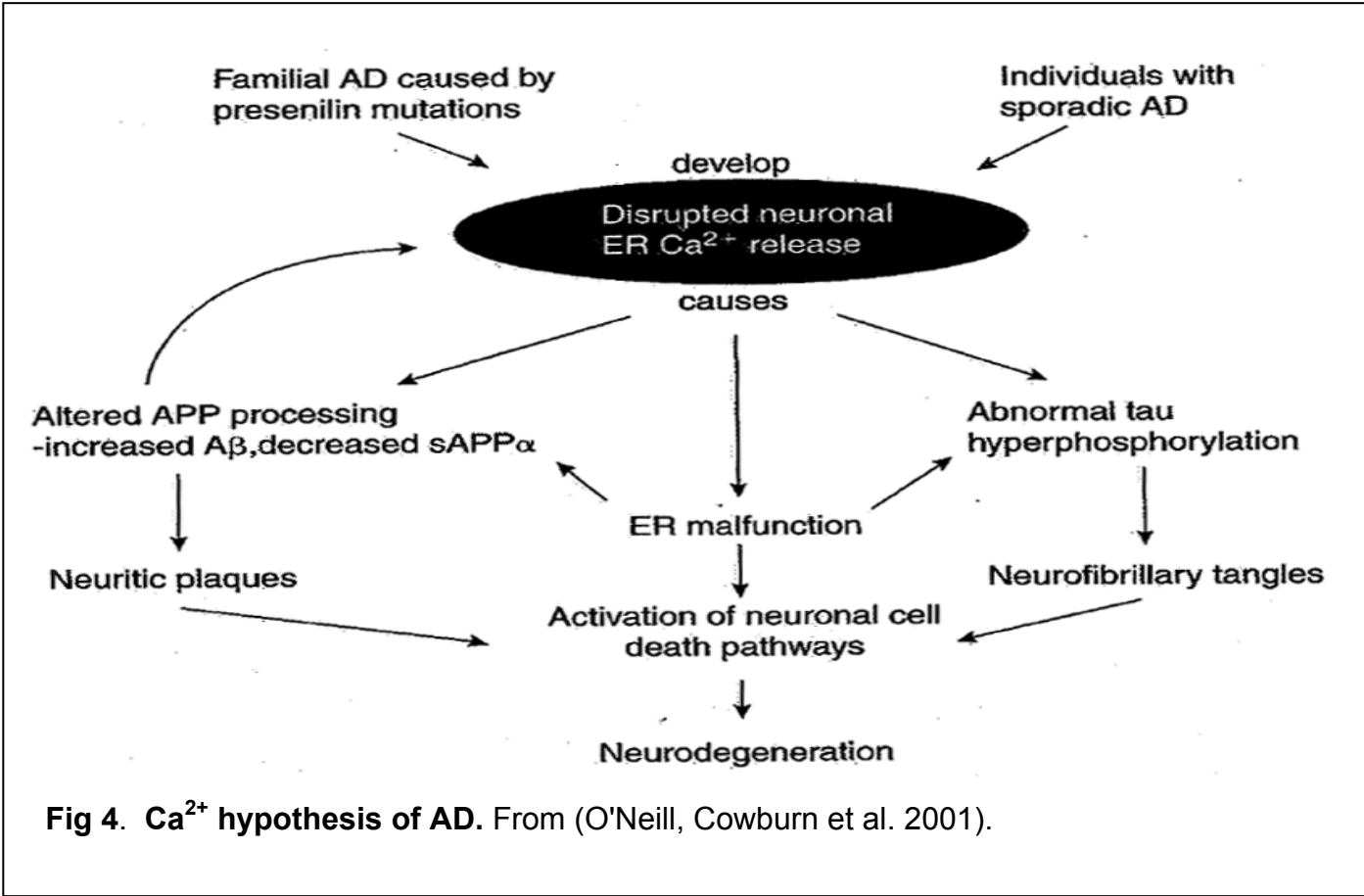
Fig 3. Amyloid cascade hypothesis of AD. From (Selkoe 2002)



Presenilins as components of γ -secretase complex. Amyloid cascade hypothesis of AD

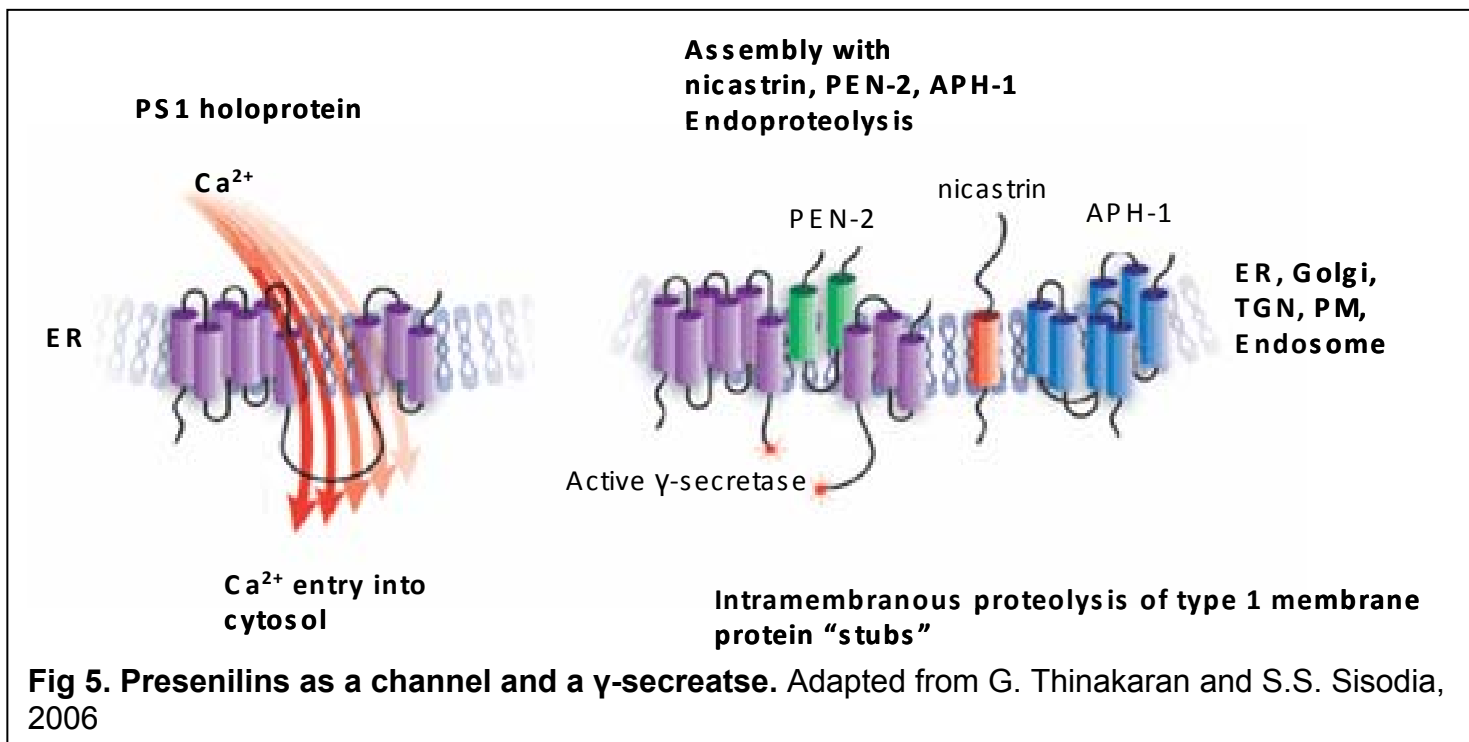
The “mature” complex of presenilins, nicastrin, aph-1 and pen-2 subunits functions as a γ -secretase involved in the processing (transmembrane cleavage) of Notch, amyloid precursor protein (APP), N- and E-cadherins and several additional type 1 transmembrane proteins (Edbauer, Winkler et al. 2003; Kimberly, LaVoie et al. 2003; Takasugi, Tomita et al. 2003). Genetic and biochemical evidence suggest that presenilins act as the catalytic subunits of γ -secretase (De Strooper, Saftig et al. 1998; De Strooper, Annaert et al. 1999; Struhl and Greenwald 1999; Wolfe, Xia et al. 1999). The key aspartates in TM6 and TM7 of presenilins (D257 and D385 in PS1) form the catalytic site of γ -secretase (Fig 1). The amyloid β -peptide (A β) released following γ -secretase cleavage of APP is a principal component of senile plaques that accumulate in the brains of AD patients (Glennner and Wong 1984; Masters, Simms et al. 1985). A combination of biochemical and genetic evidence provide strong support to the “amyloid cascade hypothesis” of AD (Hardy and Selkoe 2002; Selkoe 2002; Tanzi and Bertram

2005). According to this hypothesis missense FAD mutations in APP or presenilins result in increased amyloidogenic A β 42 peptide (or an increase in the A β 42:A β 40 ratio) production due to dysregulated APP cleavage by γ -secretase (Fig 3). Similar accumulation of A β 42 also occurs in “sporadic” AD cases for reasons, which remain poorly understood (Fig 3). Increased A β 42 levels lead to the formation of A β 42 aggregates and toxic oligomers, which induce local activation of microglia and eventually lead to loss of synapses and neurodegeneration in AD brains (Fig 3). The “amyloid cascade hypothesis” of AD is the main driving force behind most current efforts on developing AD therapeutics (Hardy and Selkoe 2002; Selkoe 2002; Tanzi and Bertram 2005).



Presenilins and Ca²⁺ signaling. Ca²⁺ hypothesis of AD

A number of studies point to dysfunctional ER Ca²⁺ signaling in AD brains. It has been reported that the number of inositol 1,4,5-trisphosphate receptors (InsP₃R), ER Ca²⁺ release channels, is significantly reduced in the cortex and hippocampus of AD brains (Young, Kish et al. 1988; Garlind, Cowburn et al. 1995; Kurumatani, Fastbom et al. 1998). Similar reduction was reported for ryanodine receptor (RyanR), another ER Ca²⁺ release channel (Kelliher, Fastbom et al. 1999). The reduction in InsP₃R and RyanR levels was observed early in AD pathology, suggesting that dysregulation of ER Ca²⁺ signaling is one of the early events occurring in AD brains. Further connection between Ca²⁺ signaling and AD emerged from analysis of Ca²⁺ signaling in cells expressing FAD mutations of presenilins. Ca²⁺ signaling defects were observed in studies with fibroblasts from presenilin FAD patients (Ito, Oka et al. 1994), in presenilins FAD cellular and animal models (Mattson, LaFerla et al. 2000; LaFerla 2002; Smith, Green et al. 2005) and in cells from PS1 and PS2 knockout mice (Yoo, Cheng et al. 2000; Herms, Schneider et al. 2003; Ris, Dewachter et al. 2003; Takeda, Asahi et al. 2005). These results provided experimental support to the “Ca²⁺ hypothesis of AD”, which states that disturbed Ca²⁺ dyshomeostasis contributes to neurodegeneration in AD (Fig 4) (Khachaturian 1989; Mattson, LaFerla et al. 2000; O'Neill, Cowburn et al. 2001; LaFerla 2002; Smith, Green et al. 2005). Our laboratory recently discovered that in addition to acting as a γ -secretase, presenilins also function as passive ER Ca²⁺ leak channels (Fig 5) (Tu, Nelson et al. 2006). Our results provided a mechanistic explanation to Ca²⁺ signaling defects observed in presenilins FAD mutant cells and further supported the “Ca²⁺ hypothesis of AD” (Fig 4).



Research design and Methods

Expression constructs and recombinant baculoviruses

The wild type PS1 expression construct and generation of PS1 baculovirus has been previously described (Tu, Nelson et al. 2006). The PS1-G384A and PS1-A246E constructs were kindly provided by Dr Christine Van Broeckhoven (Cruts, Backhovens et al. 1995) and the PS1-L166P construct was kindly provided by Dr Christian Haass (Haass 1997). PS1- Δ E8 was obtained from Sam Gandy and cloned into pcDNA3. The A79V, L85P, L113P, M139V, G183V, G217D, V261F, P264L, E273A, E280G, P284H, T291P, Rins352, G384A, N405S, C410Y, L420R, A426P, A431E and P436Q mutations in wild type PS1 sequence were generated by the Quick-change site-directed mutagenesis kit (Stratagene) and verified by sequencing. The PS1-FAD constructs were cloned into pFastBac1 baculovirus vector (Invitrogen) and recombinant PS1-FAD baculoviruses were generated using Bac-to-Bac system (Invitrogen) as previously described for wild type PS1 (Tu, Nelson et al. 2006). The high titer baculoviral stocks

were obtained by amplification of generated viruses in Sf9 cells. For expression in DKO cells all the FAD and FTD constructs were cloned into pcDNA3 mammalian expression vector (Invitrogen). In transient transfection “rescue” experiments DKO cells were transfected using Lipofectamine (Invitrogen) by pEGFP-C3 plasmid (Clontech) or by a 1:3 mixture of pEGFP-C3 and PS-expression plasmids (in pcDNA3). The Ca²⁺ imaging experiments were performed and analyzed as described below 48h after transfection. The transfected cells were identified by GFP imaging using GFP filter cube (Chroma) prior to Fura-2 Ca²⁺ imaging as previously described (Tu, Nelson et al. 2006).

BLM reconstitution experiments

Wild type and mutant presenilins were expressed in Sf9 cells as previously described (Tu, Nelson et al. 2006). The ER microsomes were isolated from Sf9 cell homogenates by differential centrifugation as previously described (Tu, Miyakawa et al. 2002) and stored at –80°C. The expression of presenilin in Sf9 cells was confirmed by Western blotting of isolated microsomal preparations with monoclonal anti-PS1 antibodies (MAB5232, Chemicon). The samples used for Western blotting were maintained at 37°C prior to loading on the gel. The isolated ER microsomes were fused with planar lipid bilayers (BLM) and recordings of presenilin-supported currents were performed and analyzed as previously described (Tu, Nelson et al. 2006). In these experiments the *trans* (intraluminal) side of the BLM contained 50 mM Ba²⁺/HEPES (pH 7.35) and the *cis* (cytosolic) side contained 100 mM Tris/HEPES (pH 7.35). The *cis* chamber was held at virtual ground and the *trans* chamber was voltage clamped (OC-725 bilayer clamp, Warner Instruments) to 0 mV, +10 mV and –10 mV as indicated. The current across the BLM was amplified (OC-725C), filtered at 5 kHz, digitized (Digidata 1200, Axon

Instruments), and stored on a computer hard drive and recordable optical discs. For presentation the current traces were digitally filtered at 200 Hz (pClamp 6.0, Axon Instruments). For off-line computer analysis, the stationary noise analysis method was used as previously described (Tu, Nelson et al. 2006). Using WinEDR V2.4.3 software (Dempster 2001), the currents were filtered at 100 Hz and the mean current (I) and the current variance (δ^2) were determined for the currents measured before addition of ER microsomes (I_{BLM} and δ_{BLM}^2) and after fusion of ER microsomes (I_{PS} and δ_{PS}^2) in the same experiment. The unitary size of PS-mediated currents (i_{PS}) was then estimated for each experiment from the “noise analysis equation”: $i_{\text{PS}} = (\delta_{\text{PS}}^2 - \delta_{\text{BLM}}^2) / (I_{\text{PS}} - I_{\text{BLM}})$ as previously described (Tu, Nelson et al. 2006).

Ca²⁺ imaging experiments

The PS-DKO MEF cells and the hPS1, L166P, A246E, G384A stable rescue lines were previously described (Herreman, Serneels et al. 2000; Bentahir, Nyabi et al. 2006). Human primary fibroblasts from PS1-A246E a 56 year old FAD symptomatic patient (AG06840) and the hF control primary fibroblasts from a 62 year old unaffected spouse (AG08701) were obtained from the Coriell Cell Repositories. Ca²⁺ imaging experiments with all MEFs and hF cells were performed as previously described (Tu, Nelson et al. 2006). Briefly, the cells were cultured on poly-D-lysine (Sigma) coated 12 mm round glass coverslips and loaded with 5 μM Fura-2-AM (Molecular Probes) in HCSS buffer (120 mM NaCl, 5.4 mM KCl, 0.8 mM MgCl₂, 2 mM CaCl₂, 15 mM glucose, and 20 mM HEPES, pH 7.3) for 45 minutes at 37°C. For Ca²⁺ imaging experiments the coverslips were mounted onto a recording/perfusion chamber (RC-26G, Warner Instrument) positioned on a movable stage of an Olympus IX-70 inverted microscope and washed

with HCSS-Ca²⁺ deficient buffer (buffered with EGTA to 50 nM Ca²⁺). In Ca²⁺ imaging experiments the cells were intermittently excited by 340 nm and 380 nm UV light (DeltaRam illuminator, PTI) using a Fura-2 dichromic filter cube (Chroma Technologies) and 60× UV-grade oil-immersed objective (Olympus). The emitted light was collected by an IC-300 camera (PTI), and the images were digitized by the ImageMaster Pro software (PTI). Baseline (6 min) measurements were obtained prior to bath application of drugs. The drugs – 300 nM bradykinin (BK) and 5 μM ionomycin (IO) (both from Sigma) were dissolved in HCSS-Ca²⁺ deficient buffer prior to application to the cells. Images at 340 nm and 380 nm excitation wavelengths were captured every 2 s and shown as 340/380 image ratios at time points as indicated. Background fluorescence was determined according to manufacturer's (PTI) recommendations and subtracted. The absolute values of free cytosolic Ca²⁺ concentrations [Ca²⁺] in these experiments were determined from the equation (Grynkiewicz, Poenie et al. 1985).

$$[\text{Ca}^{2+}] = K_d \frac{[R - R_{\min}]}{[R_{\max} - R]} \frac{s_{f,380}}{s_{b,380}}$$

where $K_d = 140$ nM is the affinity of Fura-2 for Ca²⁺, R is the experimentally determined 340/380 ratio, R_{\max} is the 340/380 ratio for Fura-2 saturated with Ca²⁺ (determined by application of 20 mM Ca²⁺ and 10 μM ionomycin at the end of the experiment), R_{\min} is the 340/380 ratio for Ca²⁺-free Fura-2 (determined by addition of 10 mM EGTA following R_{\max} determination), and $s_{f,380}/s_{b,380}$ is the ratio of fluorescence intensity of Ca²⁺-free and Ca²⁺-bound form of Fura-2 at 380 nm ($s_{f,380}/s_{b,380} = 2$ in our experiments).

ER Ca²⁺ measurements

The ER Ca²⁺ levels in MEF cells were measured using Mag-Fura-2 (Hofer 1999) as previously described (Tu, Nelson et al. 2006) using the PTI Ca²⁺ imaging setup described above. Briefly, the cells were first loaded with 2 μM Mag-Fura-2-AM (Molecular Probes) in HCSS buffer for 30 min at 37°C and permeabilized by application of 10 μM digitonin in the intracellular buffer (125 mM KCl, 25 mM NaCl, 10 mM HEPES, 0.1 mM MgCl₂, pH 7.3) containing 170 nM free Ca²⁺ (clamped by 5 mM EGTA) and 3 mM ATP. Mag-Fura-2 signals were collected as 340/380 ratios for the duration of the experiment, then the ER membrane was permeabilized with 5 μM ionomycin and the cells were washed by ATP-free and Ca²⁺-free calibration buffer (125 mM KCl, 25 mM NaCl, 10 mM HEPES, pH 7.3) containing 0.8 mM EGTA. The Mag-Fura-2 signals were calibrated in the presence 10 μM ionomycin by using a series of calibration buffers with free Ca²⁺ clamped to defined concentrations by 1 mM nitrilotriacetic acid (NTA) as previously described (Tu, Nelson et al. 2006). Based on these calibration results, the 340/380 Mag-Fura-2 ratios were converted to [Ca²⁺]_{ER} concentrations by using an empirical formula:

$$[\text{Ca}^{2+}]_{\text{ER}} = 141 (R - 0.49) / (1.42 - R)$$

where [Ca²⁺]_{ER} is intraluminal ER Ca²⁺ concentration in μM and R is the 340/380 ratio reported by Mag-Fura-2 in our experiments.

Ca²⁺ imaging experiments in Lymphoblast

The lymphoblasts cell lines shown as Family number and genotype [(62390:WT, 62384:PS1-M139V, 62787:PS1-M146L, 62533:PS1-K239E, 62752:PS1-V261F, 62746:PS1-P264L, 62166:PS1-R269G, 62546:PS1-C410Y, 62493:PS1-A426P, 62652:PS1-

A431E, 62751: PS1- Δ E9, 62410: PS2-N141I, 62450: tau-R406W, 62728: APP-V717L, 62073: old sporadic AD (OAD), 62459: young sporadic AD (YAD1) and 62755: young sporadic AD (YAD2)] were obtained from the National Cell Repository for Alzheimer's disease (NCRAD). Standard lymphoblast culture procedures were used. Lymphoblasts were maintained in RPMI 1640 medium (Sigma Chemical Co.) supplemented with 10% fetal bovine serum (FBS) (Gemini), 100 μ g/ml streptomycin and 100 U/ml penicillin (Sigma Chemical Co.) at 37 °C in an atmosphere of 5% CO₂ /95% air. For Ca²⁺ imaging experiments the cells were loaded with fura-2/AM (Molecular Probes)(3 μ M) in HCSS buffer (120 mM NaCl, 5.4 mM KCl, 0.8 mM MgCl₂, 2 mM CaCl₂, 15 mM glucose, and 20 mM HEPES, pH 7.3) for 45 min at 37°C. The cells were then washed with HCSS buffer by centrifugation and resuspended in HCSS-Ca²⁺ deficient buffer (buffered with EGTA to 170 nM Ca²⁺) for ionomycin experiments. Once the cells were resuspended, they were challenged with 5 μ M ionomycin to evaluate ER Ca²⁺ contents, the increase in 340/380 ratio was used to detect the increase in cytosolic calcium levels. The Ca²⁺ measurements were performed with 1.8 ml of cell suspension (1 \times 10⁶ cells) in a 2ml quartz cuvette using the Felix system (PTI). At the end of each experiment, the 340/380 Fura-2 ratios were calibrated by consecutive additions of 10 μ M ionomycin, 2 mM CaCl₂ and 20 mM EDTA. The 340/380 Fura-2 ratios were converted to free Ca²⁺ concentration in the cuvette by using the equation from (Grynkiewicz, Poenie et al. 1985).

CHAPTER TWO

Endoplasmic reticulum calcium leak function of presenilin 1 disrupted by mutations linked to familial Alzheimer's disease but not by mutations associated with frontotemporal dementia

Abstract

Mutations in presenilin 1 (PS1) and presenilin 2 (PS2) are responsible for approximately 40% of all early onset familial Alzheimer's disease (FAD) cases in which a genetic cause has been identified. In addition, a number of mutations in PS1 have been associated with the occurrence of frontal temporal dementia (FTD) although a formal proof of their causal involvement has not been provided. Presenilins are highly conserved transmembrane proteins that support cleavage of the amyloid precursor protein by γ -secretase. Recently, we discovered that presenilins also function as passive endoplasmic reticulum calcium (Ca^{2+}) leak channels (Tu et al., 2006. Cell, v 126: pp 981-993). We further found that PS1-M146V, PS1- Δ E9 and PS2-N141I FAD mutations in presenilins affected their ER Ca^{2+} leak function (Tu et al., 2006. Cell, v 126: pp 981-993). Here we used planar lipid bilayer reconstitution assays and Ca^{2+} imaging experiments with PS-null mouse embryonic fibroblasts (MEF) to analyze ER Ca^{2+} leak function of six additional PS1 FAD mutants and three known PS1 mutations suggested to be linked to FTD. We demonstrate that L166P, A246E, E273A, G384A and P436Q FAD mutations in PS1 abolished ER Ca^{2+} leak function of PS1. In contrast, ER Ca^{2+} leak function of PS1 appeared unaffected by A79V FAD mutation in our experiments. Similar to FAD A79V, neither of the FTD-associated mutations in PS1 (L113P, G183V and Rins352) affected ER Ca^{2+} leak function in our experiments. We validated our findings using Ca^{2+} imaging experiments with primary fibroblasts obtained from PS1-A246E FAD human patients. Our results indicate that many FAD mutations in presenilins are "loss of function" mutations for ER Ca^{2+} leak activity. In contrast, none of the FTD-associated mutations affected ER Ca^{2+} leak function of PS1, indicating that the

observed effects are disease-specific. Our observations are consistent with the potential role of disturbed Ca^{2+} homeostasis in AD pathogenesis.

Introduction

Alzheimer's disease (AD) is the most common form of age-related dementia in human beings over the age of 65 years. AD affects about 2% of the population in industrialized countries. The understanding of the molecular processes that leads to the pathogenesis of AD is immensely important to combat this neurological disease. Most cases of AD are idiopathic and characterized by late onset (>60 years of age). A small fraction of AD cases (familial AD, FAD) are characterized by an earlier onset and genetic inheritance. Mutations in presenilin-1 (PS1) and presenilin-2 (PS2) account for about 40% of all known FAD cases (Tandon and Fraser 2002). Three missense mutations in PS1 suggested to be linked to frontal temporal dementia (FTD) (Hutton 2004), a disease that is characterized by the shrinkage of the frontal and temporal lobes of the brain. In addition to changes in APP processing, many FAD mutations in presenilins result in deranged calcium (Ca^{2+}) signaling (reviewed in (Smith, Green et al. 2005)). Although a connection between FAD mutations in presenilins and abnormal Ca^{2+} signaling has been known for over a decade (Ito, Oka et al. 1994), the mechanistic explanation to these findings has been controversial (Smith, Green et al. 2005). Recently, we discovered that presenilins function as passive endoplasmic reticulum Ca^{2+} leak channels (Tu, Nelson et al. 2006). We further found that PS1-M146V, PS1- Δ E9 and PS2-N141I FAD mutations in presenilins affected their ER Ca^{2+} leak function (Tu, Nelson et al. 2006). Here we used planar lipid bilayer reconstitution assays and Ca^{2+} imaging experiments with PS-null mouse embryonic fibroblasts (MEF) to analyze

ER Ca²⁺ leak function of six additional PS1 FAD mutants. Our results indicate that many FAD mutations in PS1 disrupt ER Ca²⁺ leak function. These observations provide further support for the contribution of disturbed Ca²⁺ homeostasis to AD pathogenesis (Khachaturian 1989; Mattson, LaFerla et al. 2000; LaFerla 2002; Smith, Green et al. 2005). We further discovered that none of the three suggested FTD-associated PS1 mutations affected ER Ca²⁺ leak function of PS1. These results indicate that effects of FAD mutations on ER Ca²⁺ leak function of presenilins are disease-specific.

Results

Calcium channel function of PS1 FAD mutants in planar lipid bilayers

The predicted structure of presenilins includes nine transmembrane domains (Laudon, Hansson et al. 2005; Spasic, Tolia et al. 2006) (Fig 6A), which is consistent with potential ion channel or transporter function. In the previous study we discovered that presenilin holoproteins function as passive endoplasmic reticulum Ca²⁺ leak channels (Tu, Nelson et al. 2006). We further discovered that PS1-M146V, PS1-ΔE9 and PS2-N141I FAD mutations (Fig 6A) affected their ER Ca²⁺ leak function, whereas PS1-D257A γ -secretase catalytic mutation was without effect (Tu, Nelson et al. 2006). Here we set out to test ER Ca²⁺ leak function of six additional PS1 FAD mutants - A79V, L166P, A246E, E273A, G384A, and P436Q (Fig 6A). Baculoviruses encoding these 6 selected FAD PS1 mutants were generated and recombinant wild type PS1 and PS1 FAD mutants were expressed in Sf9 cells. Western blotting analysis confirmed that wild type PS1 and all six FAD PS1 mutants expressed at similar levels in baculovirus-infected Sf9 cells (Fig 6B). To study ion channel function of recombinant PS1 and the PS1 FAD mutants, we performed planar lipid bilayer (BLM) reconstitution experiments with ER microsomes from baculovirus-infected Sf9 cells. These experiments were

performed as described in our previous study of the ion channel function of PS1 (Tu, Nelson et al. 2006). Ba^{2+} ions (50 mM on *trans* side) were used in these experiments as a current carrier. We did not detect ion currents across the BLM prior to fusion of ER microsomes (Fig 6C, first column) or following fusion of microsomes from non-infected Sf9 cells (Fig 6C, second column). In contrast, when microsomes from PS1-infected Sf9 cells were fused to the BLM, Ba^{2+} currents were observed in our experiments (Fig 6C, third column), consistent with our previous findings (Tu, Nelson et al. 2006). Previous report indicated that the function of ER Ca^{2+} leak pathway maybe modulated by millimolar levels of cytosolic ATP levels (Hofer, Curci et al. 1996). We evaluated effects of ATP on PS1-mediated current activity in bilayers, but did not observe significant effects (data not shown). By using noise analysis, we estimated that the unitary current size of PS1-supported channel was equal to 0.046 ± 0.004 pA ($n = 3$) in the absence of ATP and 0.041 ± 0.005 pA ($n = 3$) in the presence of 5 mM ATP on the cytosolic (*cis*) side of the bilayer. In further bilayer experiments we determined that the PS1-A79V mutants supported Ba^{2+} currents across the BLM similar to the wild type PS1 (Fig 6C, forth column), but the other five mutants tested in our experiments were not active in the BLM (Fig 6C, columns 5 – 9). By applying previously described “noise analysis” algorithm (Tu, Nelson et al. 2006) we estimated that at 0 mV transmembrane potential the unitary Ba^{2+} current size was equal to 0.04 ± 0.01 pA ($n = 5$) for PS1-supported currents and 0.035 ± 0.003 pA ($n = 4$) for currents supported by PS1-A79V mutant (Table 1). Noise analysis further confirmed the absence of detectable ion channel activity in experiments with L166P, A246E, E273A, G384A and P436Q FAD mutants of PS1 (Table 1).

Rescue of Ca²⁺ signaling defects in PS DKO mouse embryonic fibroblasts with FAD PS1 mutations

In the previous study (Tu, Nelson et al. 2006) we describe Ca²⁺ signaling defects in PS1/2 double knockout (DKO) mouse embryonic fibroblasts (MEF) (Herreman, Serneels et al. 2000). Specifically, we found that the amplitude of bradykinin (BK)-induced Ca²⁺ release (mediated by inositol 1,4,5-trisphosphate ER Ca²⁺ channels) is twice higher in DKO MEFs than in wild type (WT) MEFs (Tu, Nelson et al. 2006). We further found that application of the Ca²⁺ ionophore ionomycin resulted in more massive and longer lasting Ca²⁺ signals in DKO cells than in MEF cells (Tu, Nelson et al. 2006), and that intraluminal ER Ca²⁺ levels were significantly elevated in DKO cells when compared to WT cells (Tu, Nelson et al. 2006). As described in the previous study, all of these observations could be explained by defective ER Ca²⁺ leak pathway in DKO cells (Tu, Nelson et al. 2006). To evaluate ER Ca²⁺ leak function of wild type PS1 and selected PS1 FAD mutants we performed a series of “rescue” experiments. In these experiments, DKO fibroblasts were transfected by EGFP plasmid alone (EGFP control) or EGFP plasmid together with the presenilin expression constructs and analyzed by Fura-2 Ca²⁺ imaging 48 hours after transfection. The transfected cells in these experiments were identified by GFP fluorescence (Fig 7, first column).

The resting Ca²⁺ levels in transfected DKO cells were estimated from Fura-2 340/380 ratio measurements. We found that the average basal Ca²⁺ level in DKO cells transfected with EGFP plasmid was equal to 186 ± 32 nM (n = 33) (Fig 8A). The average basal Ca²⁺ levels in DKO cells co-transfected with EGFP and L166P, A246E, E273A, G384A, P436Q mutant PS1 expression plasmids were not significantly different

from DKO cells transfected with EGFP plasmid alone (Fig 8A). In contrast, the mean basal Ca^{2+} level in DKO cells transfected with (EGFP + PS1) plasmid combination was equal to 263 ± 47 nM ($n = 21$), significantly higher ($p < 0.05$) than in DKO cells transfected with EGFP alone (Fig 8A). The mean basal Ca^{2+} level in DKO cells co-transfected with EGFP and A79V PS1 mutant plasmid was equal to 257 ± 34 nM ($n = 40$), also significantly higher ($p < 0.05$) than in DKO cells transfected with EGFP alone. To explain these results we reasoned that expression of wild type PS1 and PS1-A79V mutant plasmids, but not the other five FAD PS1 mutants tested in our study increases passive Ca^{2+} leak from the ER and elevates basal cytosolic Ca^{2+} levels in transfected DKO cells.

When transfected DKO cells were challenged with 300 nM BK, large transient Ca^{2+} signals were observed in EGFP, (EGFP + L166P), (EGFP + A246E), (EGFP + E273A), (EGFP + G384A) and (EGFP + P436Q)-transfected cells (Fig 7, rows 1, 4-8). In contrast, significantly smaller Ca^{2+} signals were induced by BK in DKO cells transfected with (EGFP + PS1) and (EGFP + A79V) combinations (Fig 7, rows 2 and 3). On average, the difference between peak and basal Ca^{2+} levels ($\Delta[\text{Ca}^{2+}]$) in BK-stimulated cells was equal to 732 ± 103 nM ($n = 33$) for EGFP-transfected cells, 271 ± 53 nM ($n = 21$) for (EGFP + PS1)-transfected cells, and 253 ± 39 nM ($n = 40$) for (EGFP + A79V)-transfected cells (Fig 8A, Table 1). The peak responses in DKO cells transfected with other FAD mutants were not significantly different from the peak Ca^{2+} responses in cell transfected with EGFP plasmid alone (Fig 8A, Table 1). Thus, transfection of DKO cells with wild type PS1 and A79V expression constructs reduced the amplitude of BK-induced Ca^{2+} responses to levels observed in experiments with WT MEFs (Fig 8A, Table 1), whereas expression of L166P, A246E, E273A, G384A and P436Q FAD

mutants had no significant effect on the amplitude of BK-induced responses (Fig 8A, Table 1).

In the next series of experiments, we evaluated the size of the ionomycin-sensitive Ca^{2+} pool in PS1- transfected DKO cells. Ionomycin is an ionophore that induces formation of Ca^{2+} -permeable pores in cellular membranes, leading to complete emptying of ER Ca^{2+} stores independently from the InsP_3R activation. In agreement with the previous findings (Tu, Nelson et al. 2006), we found that the addition of 5 μM ionomycin (IO) induced large and long-lasting elevation of cytosolic Ca^{2+} levels in EGFP-transfected DKO cells, but smaller in amplitude and shorter in duration Ca^{2+} elevation in (EGFP + PS1)-transfected cells (data not shown). To estimate the size of IO-sensitive Ca^{2+} pool, we calculated the area under the IO-induced Ca^{2+} signals. On average, the area under the IO-induced Ca^{2+} curve was equal to $52 \pm 11 \mu\text{M}\cdot\text{sec}$ ($n = 19$) for EGFP-transfected DKO cells, $33 \pm 9 \mu\text{M}\cdot\text{sec}$ ($n = 21$) for (EGFP + PS1)-transfected DKO cells, and $31 \pm 14 \mu\text{M}\cdot\text{sec}$ ($n = 18$) for (EGFP + A79V)-transfected DKO cells (Fig 8B, Table 1). Transfection with other FAD mutants had no significant effect on the size of IO-sensitive Ca^{2+} pool (Fig 8B, Table 1). To determine the effect of PS1 constructs expression on ER Ca^{2+} levels, we directly measured Ca^{2+} concentration in the ER ($[\text{Ca}^{2+}]_{\text{ER}}$) of transfected DKO MEFs with low-affinity Ca^{2+} imaging dye Mag-Fura-2 (Hofer 1999). Consistent with the previous findings (Tu, Nelson et al. 2006) we found that $[\text{Ca}^{2+}]_{\text{ER}}$ levels were equal to $183 \pm 42 \mu\text{M}$ ($n = 18$) in EGFP-transfected DKO cells, $108 \pm 21 \mu\text{M}$ ($n = 17$) in (EGFP + PS1)-transfected DKO cells, and $114 \pm 28 \mu\text{M}$ ($n = 23$) in (EGFP + A79V)-transfected DKO cells (Fig 8C, Table 1). The $[\text{Ca}^{2+}]_{\text{ER}}$ levels in DKO cells transfected with other FAD mutants were not significantly different from the $[\text{Ca}^{2+}]_{\text{ER}}$ levels in DKO cells transfected with EGFP plasmid alone (Fig 8C, Table 1). From these

results we concluded that expression of wild type PS1 and A79V PS1 FAD mutant, but not L166P, A246E, E273A, G384A and P436Q FAD mutants, restores the size of IO-sensitive Ca^{2+} pool and the $[\text{Ca}^{2+}]_{\text{ER}}$ levels in DKO cells to the levels observed in wild type MEF cells (Fig 8C, Table1).

To rule out potential artifacts resulting from transient overexpression of PS1 constructs in DKO cells, we performed a series of Ca^{2+} imaging experiments with DKO MEFs stably transfected with wild type PS1 (hPS1 line), and L166P, A246E, and G384A FAD rescue constructs. The expression of PS1 rescue constructs in these stable lines was confirmed by Western blotting (Fig 9A). In Ca^{2+} imaging experiments with these cells we found that the addition of ionomycin induced large Ca^{2+} responses in DKO, L166P, A246E, and G384A cell lines and much smaller Ca^{2+} responses in wild type MEF and hPS1 rescue cell lines (Fig 9B). By calculating an area under IO-induced Ca^{2+} curve, we determined that the content of IO-sensitive Ca^{2+} stores was significantly lower in wild type and HPS1 rescue cells than in DKO, L166P, A246E, and G384A rescue cells (Fig 9C, Table 1). In agreement with ionomycin results, direct measurements of $[\text{Ca}^{2+}]_{\text{ER}}$ levels with Mag-Fura-2 yielded $183 \pm 42 \mu\text{M}$ ($n = 32$) in DKO cells, $97 \pm 19 \mu\text{M}$ ($n = 27$) in wild type MEFs, $93 \pm 15 \mu\text{M}$ ($n = 31$) in HPS1 cells, $178 \pm 19 \mu\text{M}$ ($n = 43$) in L166P cells, $191 \pm 23 \mu\text{M}$ ($n = 29$) in A246E cells and $186 \pm 31 \mu\text{M}$ ($n = 37$) in G384A cells (Fig 9D, Table 1). Thus, similar to transient transfection experiments (Fig 8), we found that the stable expression of wild type PS1 but not L166P, A246E, and G384A FAD mutants in DKO cells restored IO-sensitive Ca^{2+} pool content and $[\text{Ca}^{2+}]_{\text{ER}}$ concentration to wild type MEF levels (Figs 9C, 9D, Table 1).

Rescue of Ca²⁺ signaling defects in PS DKO mouse embryonic fibroblasts with FTD PS1 mutations

Human genetic studies identified three missense mutations in PS1 sequence (L113P, G183V, and Rins352) which are associated with frontotemporal dementia (FTD) (Raux, Gantier et al. 2000; Rogaeva, Fafel et al. 2001; Amtul, Lewis et al. 2002; Tang-Wai, Lewis et al. 2002; Dermaut, Kumar-Singh et al. 2004) (reviewed in (Hutton 2004)) (Fig 6A). Do these potential FTD-associated mutations in PS1 affect ER Ca²⁺ leak function? To answer this question we performed a series of “rescue” experiments by transiently transfecting DKO cells with PS1-FTD expression plasmids (L113P, G183V, and Rins352) together with EGFP plasmid. In parallel control experiments DKO cells were transfected with EGFP plasmid alone and with EGFP plasmid together with wild type PS1 expression plasmid. The transfected cells were identified by GFP fluorescence (Fig 10, first column) and Ca²⁺ imaging experiments with transfected cells were performed using Fura-2 fluorescent dye as described above. When Fura-2 images (Fig 10, columns 2-5) were analyzed, we determined that the resting basal Ca²⁺ levels in DKO cells transfected with EGFP plasmid alone was on average 179 ± 27 nM (n=26), while the basal Ca²⁺ levels in EGFP + PS1, EGFP + PS1-L113P, EGFP + PS1-G183V and EGFP + PS1-Rins352 were 246 ± 38 nM (n=31), 259 ± 56 nM (n=27), 253 ± 34 nM (n=39) and 234 ± 29 nM (n=34), respectively (Fig 11A). The resting basal Ca²⁺ level was significantly ($p < 0.05$) higher in PS1 and PS1-FTD transfected DKO cells when compared to DKO cells transfected with EGFP alone (Fig 11A).

When transfected DKO cells were challenged with 300 nM BK, large transient Ca²⁺ signals were observed in EGFP transfected cells (Fig 10, row 1). In contrast,

significantly smaller Ca^{2+} signals were induced by BK in DKO cells transfected with EGFP + PS1, EGFP + PS1-L113P, EGFP + PS1-G183V and EGFP + PS1-Rins352 combinations (Fig 10, rows 2-5). On average, the difference between peak and basal Ca^{2+} levels ($\Delta[\text{Ca}^{2+}]$) in BK-stimulated DKO cells was equal 689 ± 99 nM (n=26) for EGFP-transfected cells, 261 ± 45 nM (n=31) for (EGFP +PS1)-transfected cells, 288 ± 61 nM (n=27) for (EGFP + L113P)-transfected cells, 237 ± 51 nM (n=39) for (EGFP + G183V)-transfected cells and 247 ± 37 nM (n=34) for (EGFP + Rins352)-transfected cells (Fig 11A). The amplitude of BK-induced Ca^{2+} transients was significantly ($p < 0.05$) lower in PS1 and PS1-FTD transfected DKO cells when compared to DKO cells transfected with EGFP alone (Fig 11A).

Consistent with BK experiments, we found that the application of 5 μM ionomycin (IO) induced large and long-lasting elevation of cytosolic Ca^{2+} levels in EGFP-transfected DKO cells, but smaller in amplitude and shorter in duration Ca^{2+} increase DKO cells transfected with wild type PS1 or PS1-FTD mutants (data not shown). By integrating an area under IO-induced Ca^{2+} transients, we found that the average content of IO-sensitive Ca^{2+} stores was equal to 55 ± 14 $\mu\text{M}\cdot\text{sec}$ (n = 27) for EGFP-transfected DKO cells, 22 ± 7 $\mu\text{M}\cdot\text{sec}$ (n = 21) for DKO cells transfected with (EGFP + PS1), 25 ± 11 $\mu\text{M}\cdot\text{sec}$ (n =39) for DKO cells transfected with (EGFP + L113P), 31 ± 13 $\mu\text{M}\cdot\text{sec}$ (n =31) for DKO cells transfected with (EGFP + G183V) and 28 ± 11 $\mu\text{M}\cdot\text{sec}$ (n =26) for DKO cells transfected with (EGFP + Rins352) (Fig 11B). The content of the IO-sensitive Ca^{2+} stores was significantly ($p < 0.05$) smaller in PS1 and PS1-FTD transfected DKO cells when compared to the DKO cells transfected with EGFP alone (Fig 11B).

Ca²⁺ signaling defects in human FAD primary fibroblasts

To establish the relevance of our results for human FAD, we obtained a sample of primary human fibroblasts derived from a 56 year old symptomatic patient with A246E mutation in PS1 (AG06840). The human fibroblasts (hF) from a non-affected 62 year old spouse (which does not harbor any known FAD mutations) were also obtained to facilitate the control experiments (AG08701). The hF and A246E primary fibroblasts were used in Fura-2 Ca²⁺ imaging experiments by following the same procedures as described above for MEF cells. In these experiments we determined that the mean basal Ca²⁺ level was equal to 217 ± 37 nM ($n = 43$) in control hF cells. In A246E fibroblasts the mean basal Ca²⁺ level was equal to 173 ± 26 nM ($n = 54$), significantly lower ($p < 0.05$) than in control hF cells. We further discovered that the application of 300 nM BK induced larger Ca²⁺ responses in A246E fibroblasts than in control hF cells (Figs 12A and 12B). On average, the amplitude of BK-induced Ca²⁺ responses was equal to 318 ± 71 μ M ($n = 43$) in hF cells and 629 ± 114 μ M ($n = 54$) in A246E cells (Fig 12C, Table 1). The enhanced amplitude of BK-induced Ca²⁺ responses in hF-A246E fibroblasts was in agreement with the earlier observations made with human fibroblasts harboring the same mutation (Ito, Oka et al. 1994; Etcheberrigaray, Hirashima et al. 1998). Similar to experiments with BK, application of 5 μ M ionomycin (IO) induced larger Ca²⁺ transients in A246E cells than in control hF cells in our experiments (Fig 12D). As described above for MEF cells, we calculated the area under IO-induced Ca²⁺ curve to quantify the content of IO-sensitive Ca²⁺ stores in these cells. We found that the average content of IO-sensitive Ca²⁺ stores was equal to 19 ± 7 μ M.sec ($n = 56$) for hF cells and 37 ± 12 μ M.sec ($n = 63$) for A246E cells (Fig 12E, Table 1). Direct measurements of $[Ca^{2+}]_{ER}$ with Mag-Fura-2 yielded 84 ± 19 μ M Ca²⁺ ($n = 34$) in hF and

169 ± 27 μM Ca²⁺ (n = 41) in hF-A246E (Figs 12F, 12G, Table 1). From these experiments, we concluded that the intracellular Ca²⁺ stores are overfilled in primary fibroblasts from A246E patient when compared to hF fibroblasts from non-affected family member. The Ca²⁺ signaling defects observed in hF-A246E primary fibroblasts in our experiments were consistent with the previous studies of Ca²⁺ signaling in FAD fibroblasts (Ito, Oka et al. 1994; Etcheberrigaray, Hirashima et al. 1998) (but also see (Zatti 2006)).

Discussion

Mutations in presenilin-1 (PS1) and presenilin-2 (PS2) account for majority of all known FAD cases (Tandon and Fraser 2002). Many FAD mutations in presenilins result in deranged calcium (Ca²⁺) signaling, but the mechanistic explanation to these finding has been controversial (reviewed in (Smith, Green et al. 2005)). Our recent discovery that presenilins function as ER Ca²⁺ leak channels (Tu, Nelson et al. 2006) provided a direct link between presenilins and Ca²⁺ signaling. The results in the present report and in the previous study (Tu, Nelson et al. 2006) indicate that most FAD mutations in presenilins have dramatic effect on their ability to function as ER Ca²⁺ leak channels. In our combined experiments we tested 8 FAD mutations in PS1 and 1 FAD mutation in PS2 (Table 1). From the 9 FAD mutations tested 7 mutations (M146V, L166P, A246E, E273A, G384A, P436Q mutations in PS1 and N141I/L mutation in PS2) abolished ER Ca²⁺ leak function of presenilins. This conclusion was based on the lack of channel activity in BLM experiments with the FAD mutants and by failure of these mutants to rescue Ca²⁺ signaling defects in PS DKO cells (Table 1). One FAD mutation (PS1-ΔE9) appear to be a “gain of function” mutation which enhanced Ca²⁺ channel activity of presenilins in BLM experiments (Tu, Nelson et al. 2006) (Table 1). Interestingly, ER

Ca²⁺ leak function was not affected by D257A mutation that abolishes γ -secretase function of PS1 (Tu, Nelson et al. 2006) (Table 1). As discussed in our previous publication (Tu, Nelson et al. 2006), “ER Ca²⁺ leak function” appear to be independent from their “ γ -secretase function”.

A single mutation from 9 FAD mutations tested (PS1-A79V) had no apparent effect on ER Ca²⁺ leak function in our experiments (Table 1). Interestingly, PS1-A79V mutation resulted in highly variable age of FAD onset and incomplete penetrance in one of the carrier families (Cruts, van Duijn et al. 1998). Typically FAD mutations have complete penetrance, and a few “incompletely penetrant” FAD-linked mutations such as PS1-E318G and PS1-T354I mutations appear to represent rare polymorphisms and are not pathogenic (Mattila, Forsell et al. 1998; Dermaut, Cruts et al. 1999; Goldman, Johnson et al. 2005; Lee, Medina et al. 2006). It remains to be determined if PS1-A79V mutation is pathogenic or if it is another example of a rare polymorphism. If it is pathogenic, our results suggest that abnormal Ca²⁺ signaling is not involved in the pathology resulting from this mutation. It is also possible that PS1-A79V mutation is a “partial loss of ER Ca²⁺ leak function” mutation, which cannot be detected in our bilayer and DKO “rescue” experiments geared at detecting “complete loss of ER Ca²⁺ leak function” phenotypes. The incomplete penetrance of PS1-A79V mutation discussed above may also be potentially consistent with a partial loss of function phenotype. More precise and sensitive experiments will be required to formally address this later possibility.

With exception of PS1-A79V and PS1- Δ E9, all other FAD-linked mutations tested in our experiments resulted in complete loss of ER Ca²⁺ leak function of presenilins (Table 1). These results are in sharp contrast to the results obtained with three known FTD-associated mutations in PS1, none of which appear to affect ER Ca²⁺ leak function of

PS1. Expression of FTD-linked L113P, G183V and Rins352 PS1 mutants rescued Ca^{2+} signals in DKO cells similar to expression of wild type PS1(Fig 10 and 11). These results suggest that either that these mutations are not pathogenic or that defects in ER Ca^{2+} leak pathway are not involved in FTD pathogenesis. In contrast to our findings, the Rins352 mutation in PS1 has been reported to be a loss of function mutation for the γ -secretase activity (Amtul, Lewis et al. 2002). However, recent study indicated that Rins352 mutation in PS1 is in fact not pathogenic and that FTD in the affected family results from mutation in the progranulin gene (Boeve, Baker et al. 2006). Further studies will be needed to determine the pathogenic status of L113P (Raux, Gantier et al. 2000) and G183V (Dermaut, Kumar-Singh et al. 2004) FTD-associated mutations in PS1. Additional investigation will also be required to analyze functional effects of two more recently described FTD-associated PS1 mutations L226F and L424H (Zekanowski, Golan et al. 2006).

Some of the FAD mutants analyzed in this and the previous study (PS1-M146V/L, PS2-N141I/L, PS1- Δ E9, PS1-A246Q/E) have been previously linked to abnormal Ca^{2+} signaling (Smith, Green et al. 2005). Our new results indicate that L166P, E273A, G384A, and P436Q FAD mutants in PS1 are also linked to abnormal Ca^{2+} signaling due to impaired ER Ca^{2+} leak function (Table 1). The impaired ER Ca^{2+} leak function of PS1 FAD mutants observed in this report and in our previous study (Tu, Nelson et al. 2006) is consistent with the increased InsP_3 -induced Ca^{2+} release in *Xenopus* oocytes expressing PS1-M146V and PS2-N141I FAD mutants (Leissring, Parker et al. 1999; Leissring, Paul et al. 1999; Leissring, LaFerla et al. 2001), in synaptosomes and cortical neurons from PS1-M146V mutant knock-in mouse (Begley, Duan et al. 1999; Stutzmann, Caccamo et al. 2004), in hippocampal neurons from PS2-N141I and PS1-

A246E transgenic mice (Schneider, Reverse et al. 2001) and in human fibroblasts from PS1-A246E patients (Etcheberrigaray, Hirashima et al. 1998). However, our results differ from the data obtained in studies of PS1-M146L, PS1-A246E and PS2-N141I FAD mutants recently reported by (Zatti 2006). In contrast to our findings, these authors found that expression of these FAD mutants causes either no effect or reduction of ER Ca^{2+} content and decreased InsP_3R -mediated Ca^{2+} release (Zatti 2006). The exact nature of this discrepancy is unclear at the moment and will require further investigation. The mutations analyzed in the present paper and in the previous study are spread across the sequence of presenilins and correspond to FAD cases with variable ages of onset (Table 1). From these results we could not detect any particular “hot spot” region or pattern that can be used to predict which mutations influence ER Ca^{2+} leak function of presenilins and which did not. With 156 FAD mutations identified in the sequence of PS1 and 10 FAD mutations in the sequence PS2 (Tandon and Fraser 2002; Larner and Doran 2006), future experimentation will be required to identify all FAD mutations in presenilins which affect their ER Ca^{2+} leak function. However, from the results obtained so far (Table 1) we can conclude that many FAD point mutations in presenilins result in loss of ER Ca^{2+} leak function. As discussed previously (Tu, Nelson et al. 2006), autosomal-dominant character of these mutations may potentially be explained by dominant negative effect of mutant PS allele on Ca^{2+} channel function of wild type alleles. Our results are in general agreement with the “loss of presenilin function” hypothesis of FAD (Saura, Choi et al. 2004; De Strooper 2007; Shen and Kelleher 2007) and provide further support for the contribution of disturbed Ca^{2+} homeostasis to AD pathogenesis (Khachaturian 1989; Mattson, LaFerla et al. 2000; LaFerla 2002;

Smith, Green et al. 2005). Additional studies will be required to investigate the

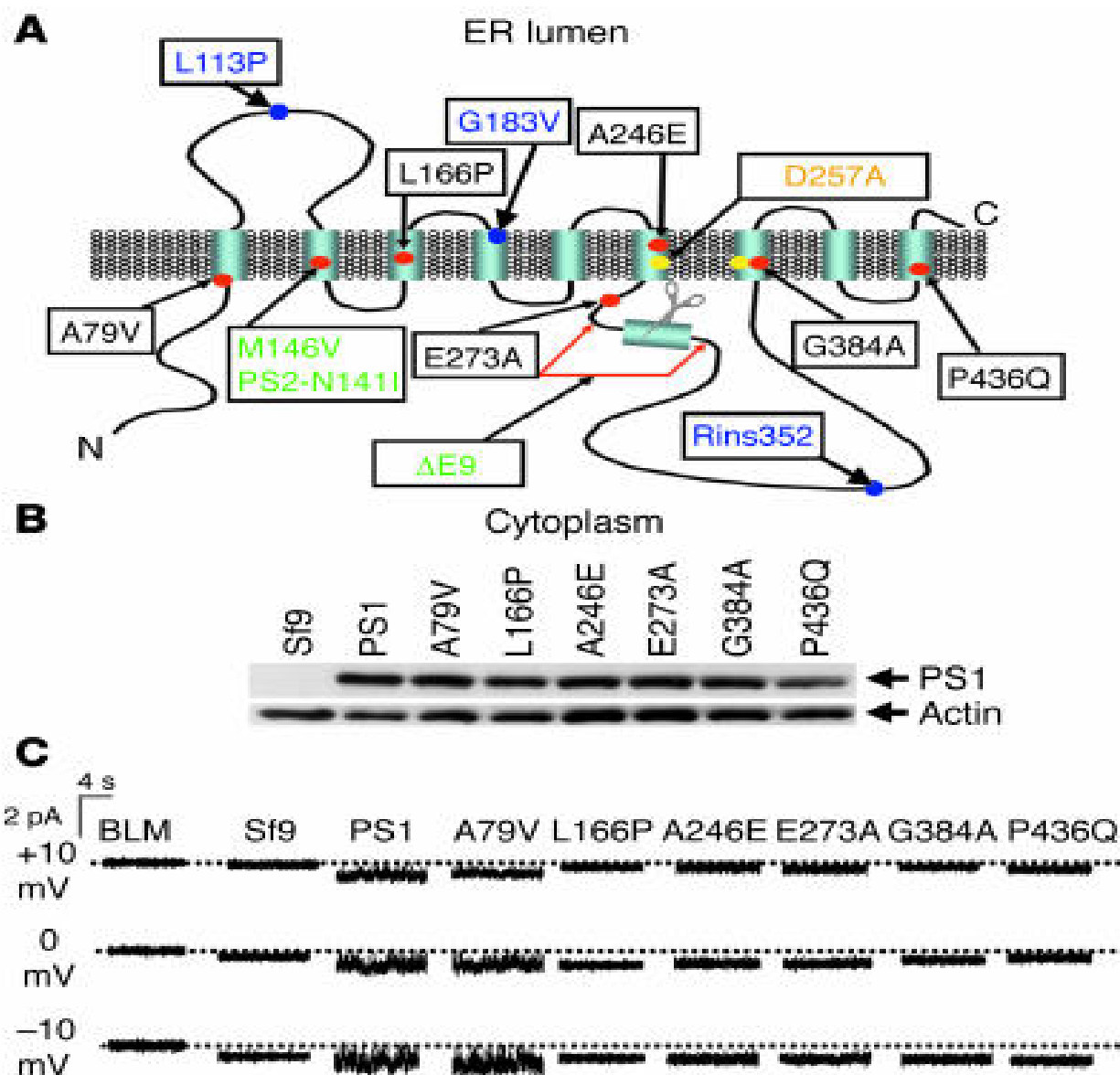


Fig 6. Recombinant presenilins form calcium channels in planar lipid bilayers.

a. Molecular model of presenilins (Laudon, Hansson et al. 2005; Spasic, Tolia et al. 2006). The nine transmembrane domains (TM1-TM9) of presenilins, the γ -secretase catalytic aspartate residues and the site of the endoproteolytic cleavage are shown. The positions of PS1 FAD mutants A79V, L166P, A246E, E273A, G384A and P436Q examined in our study are shown. Also shown are positions of PS1-M146V, PS2-N141I, PS1- Δ E9 and PS1-D257A mutations analyzed in the previous study (Tu, Nelson et al. 2006) and positions of PS1 FTD-associated mutants L113P, G183V, and Rins352.

b. The expression of PS1 and PS1 mutants in Sf9 cells. The ER microsomes from non-infected Sf9 cells (Sf9) and from Sf9 cells infected with wild type and FAD mutant PS1-encoding baculoviruses (as indicated) were analyzed by Western blotting with anti-PS1 monoclonal antibodies. The position of PS1 holoprotein is shown by an arrow. Actin was used as the loading control.

c. The Ba^{2+} currents recorded at +10 mV, 0 mV and -10 mV holding potentials are shown for the empty bilayer (BLM) and for BLM fused with ER microsomal preparations from Sf9 cells infected with wild type and FAD mutant PS1-encoding baculoviruses as indicated. Similar results were obtained in at least 5 independent BLM experiments with each PS1 mutant.

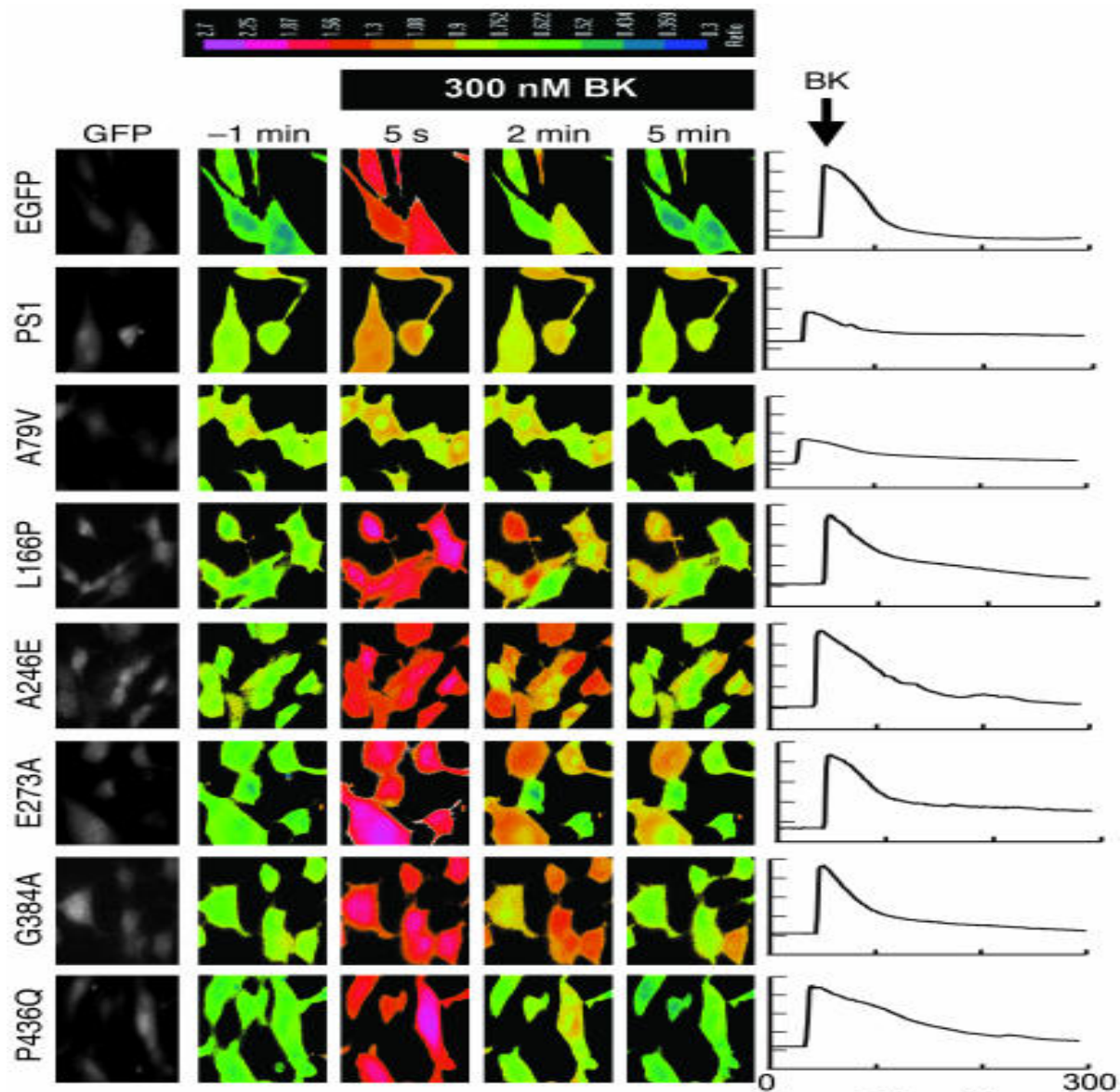


Fig 7. Rescue of Ca^{2+} signaling defects in DKO MEFs with PS1-FAD mutants. The representative images of BK-induced Ca^{2+} responses in DKO cells transfected with EGFP, EGFP+PS1, EGFP+PS1-A79V, EGFP+PS1-L166P, EGFP+PS1-A246E, EGFP+PS1-E273A, EGFP+PS1-G384A, and EGFP+PS1-P436Q expression plasmids. The 340:380 Fura-2 ratio images shown are prior to application of BK (-1 min) and 5 seconds, 2 minutes, and 5 minutes after BK application. The 340:380 Fura-2 ratios are presented using pseudocolor scale (the calibration bar is shown at top). The GFP images were used to identify transfected cells. The representative Ca^{2+} traces recorded in individual transfected DKO cells are shown at right for each expression

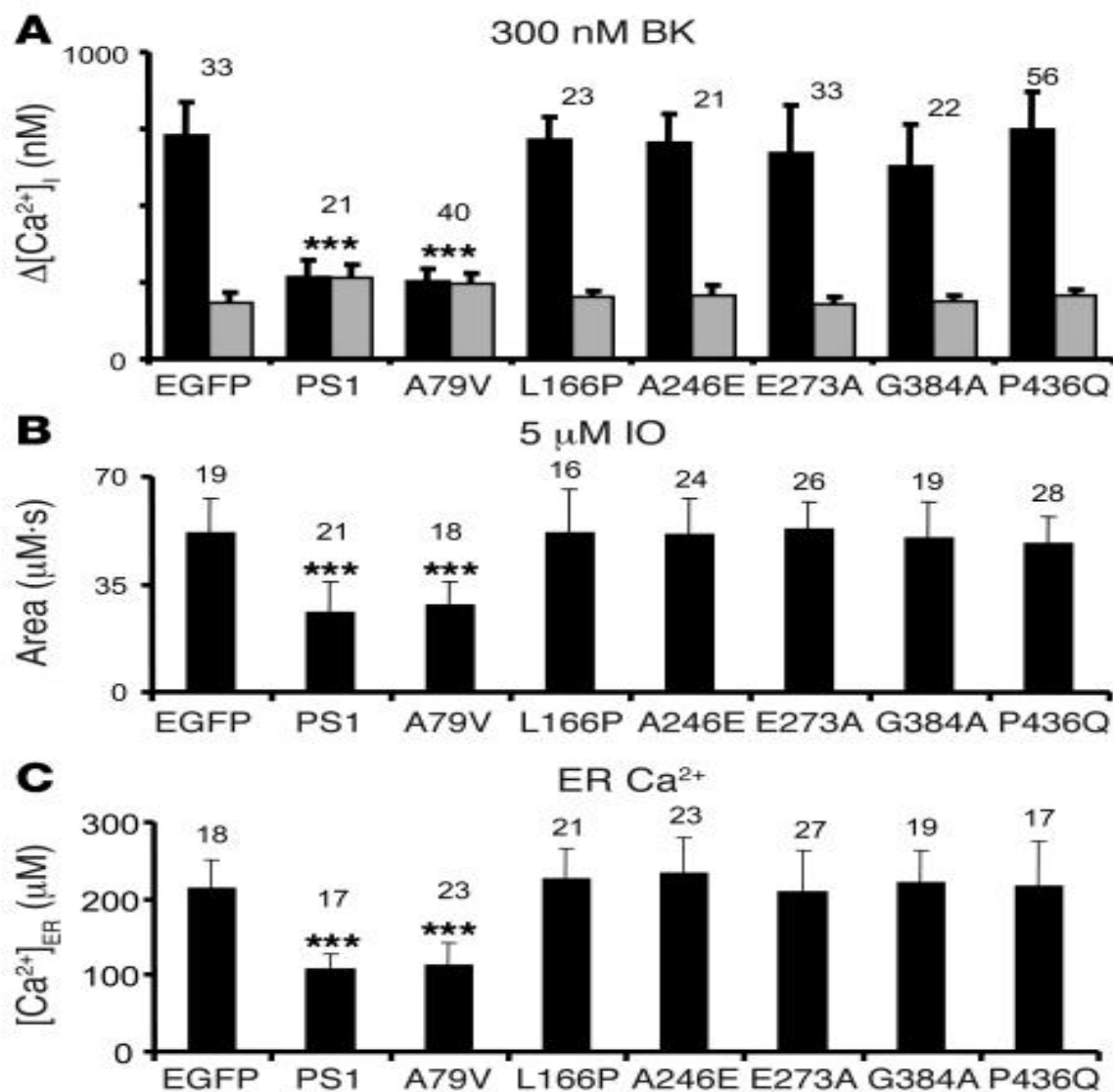


Fig 8. Summary of PS1-FAD rescue experiments. **a.** The average basal cytosolic Ca^{2+} levels (gray bars) and the amplitude of BK-induced Ca^{2+} responses (black bars) are shown as mean \pm SD for DKO cells transfected with EGFP and PS1 expression constructs (the number of cells analyzed is indicated above each set of bars). When compared with DKO cells transfected with EGFP alone, the basal Ca^{2+} levels were significantly higher and the amplitude of BK-induced Ca^{2+} responses was significantly smaller in DKO cells transfected with EGFP+PS1 and EGFP+PS1-A79V combinations. $[Ca^{2+}]_i$, intracellular Ca^{2+} concentration. **b.** The average size of IO-releasable Ca^{2+} pool is shown as mean \pm SD for DKO cells transfected with EGFP and PS1 expression constructs (the number of cells analyzed is shown above each bar). When compared with DKO cells transfected with EGFP alone, the size of IO-releasable Ca^{2+} pool was significantly smaller in DKO cells transfected with EGFP+PS1 and EGFP+PS1-A79V combinations. **c.** The average $[Ca^{2+}]_{ER}$ level is shown as mean \pm SD for DKO cells transfected with EGFP and PS1 expression constructs (the number of cells analyzed is shown above each bar). When compared with DKO cells transfected with EGFP alone, the $[Ca^{2+}]_{ER}$ levels were significantly smaller in DKO cells transfected with EGFP+PS1 and EGFP+PS1-A79V combinations. *** $P < 0.05$ by ANOVA.

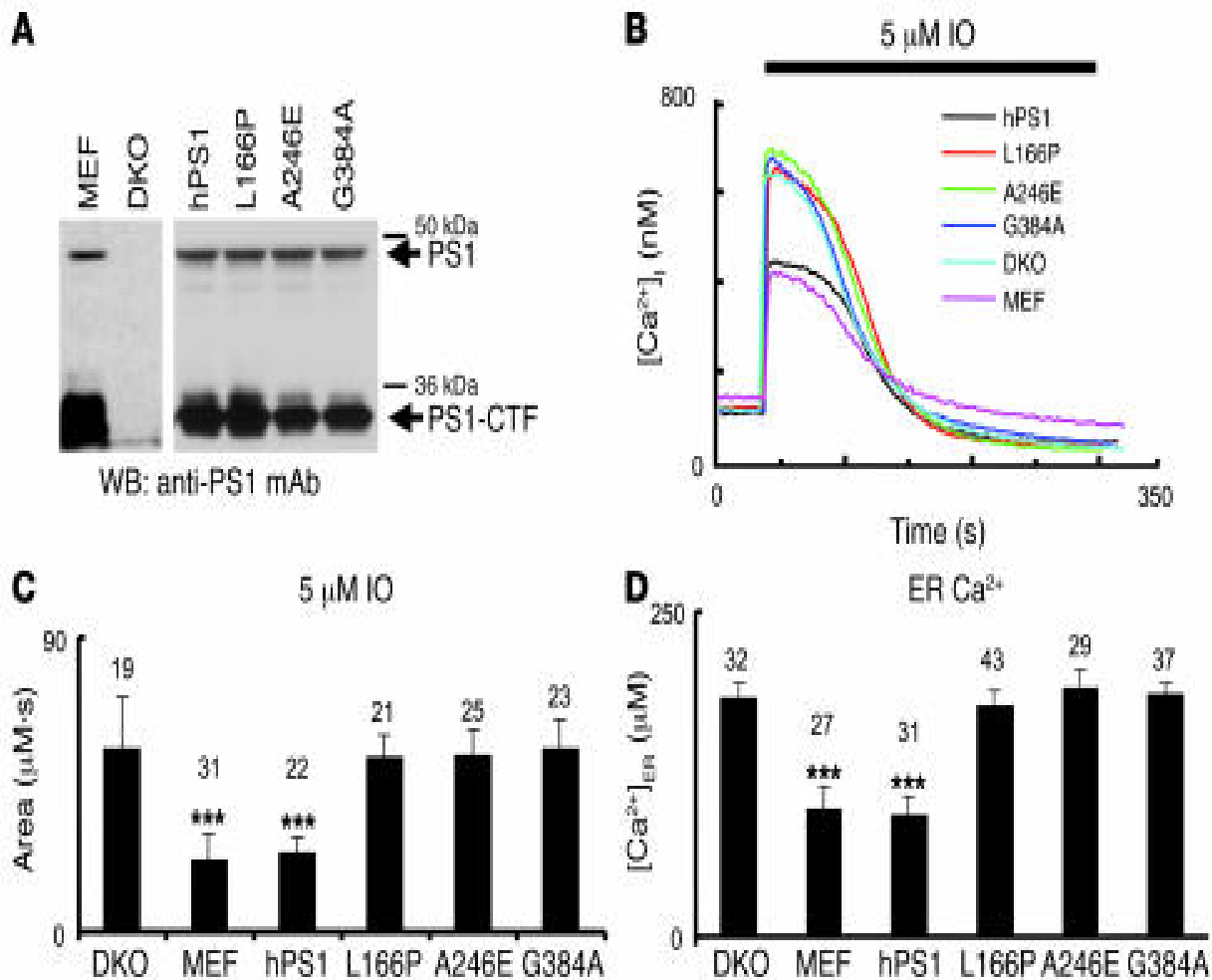


Fig 9. Ca²⁺ signals in stable DKO rescue lines. **a.** The lysates from WT MEFs, DKO cells, and stable DKO rescue lines hPS1, PS1-L166P, PS1-A246E, and PS1-G384A were prepared and analyzed by Western blotting with anti-PS1 monoclonal antibodies. The positions of PS1 holoprotein and PS1-CTF fragment are indicated. Longer exposure was used for MEF and DKO samples than for stable rescue lines. **b.** The representative IO-induced Ca²⁺ responses are shown for WT MEFs, DKO cells, and stable DKO rescue lines. **c.** The average size of IO-sensitive Ca²⁺ pool is shown as mean \pm SD for WT MEFs, DKO cells, and stable DKO rescue lines (the number of cells analyzed is shown above each bar). When compared with DKO cells, the size of IO-sensitive Ca²⁺ pool was significantly smaller in WT MEFs and hPS1 cells but not significantly different in FAD stable rescue lines. **d.** The average [Ca²⁺]_{ER} in WT MEFs, DKO cells, and stable DKO rescue lines is shown as mean \pm SD (the number of cells analyzed is shown above each bar). When compared with DKO cells, the [Ca²⁺]_{ER} was significantly smaller in WT MEFs and hPS1 cells but not significantly different in FAD stable rescue lines. ****P* < 0.05 by ANOVA.

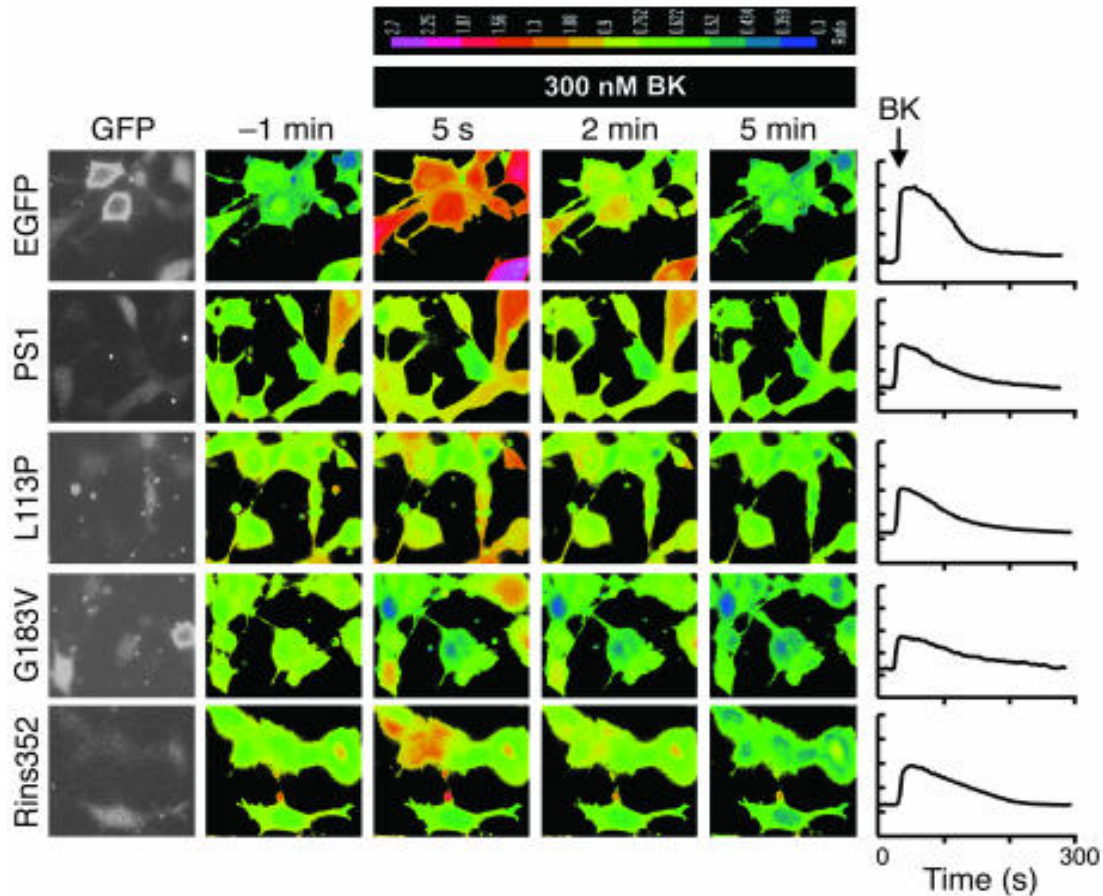


Fig 10. Rescue of Ca²⁺ signaling defects in DKO MEFs with PS1-FTD mutants. The representative images of BK-induced Ca²⁺ responses in DKO cells transfected with EGFP, EGFP+PS1, EGFP+PS1-L113P, EGFP+PS1-G183V, and EGFP+PS1-Rins352 expression plasmids. The 340:380 Fura-2 ratio images are shown prior to application of BK (-1 min) and 5 seconds, 2 minutes, and 5 minutes after BK application. The 340:380 Fura-2 ratios are presented using a pseudocolor scale (the calibration bar is shown at top). The GFP images were used to identify transfected cells. The representative Ca²⁺ traces recorded in individual transfected DKO cells are shown for each expression construct on the right.

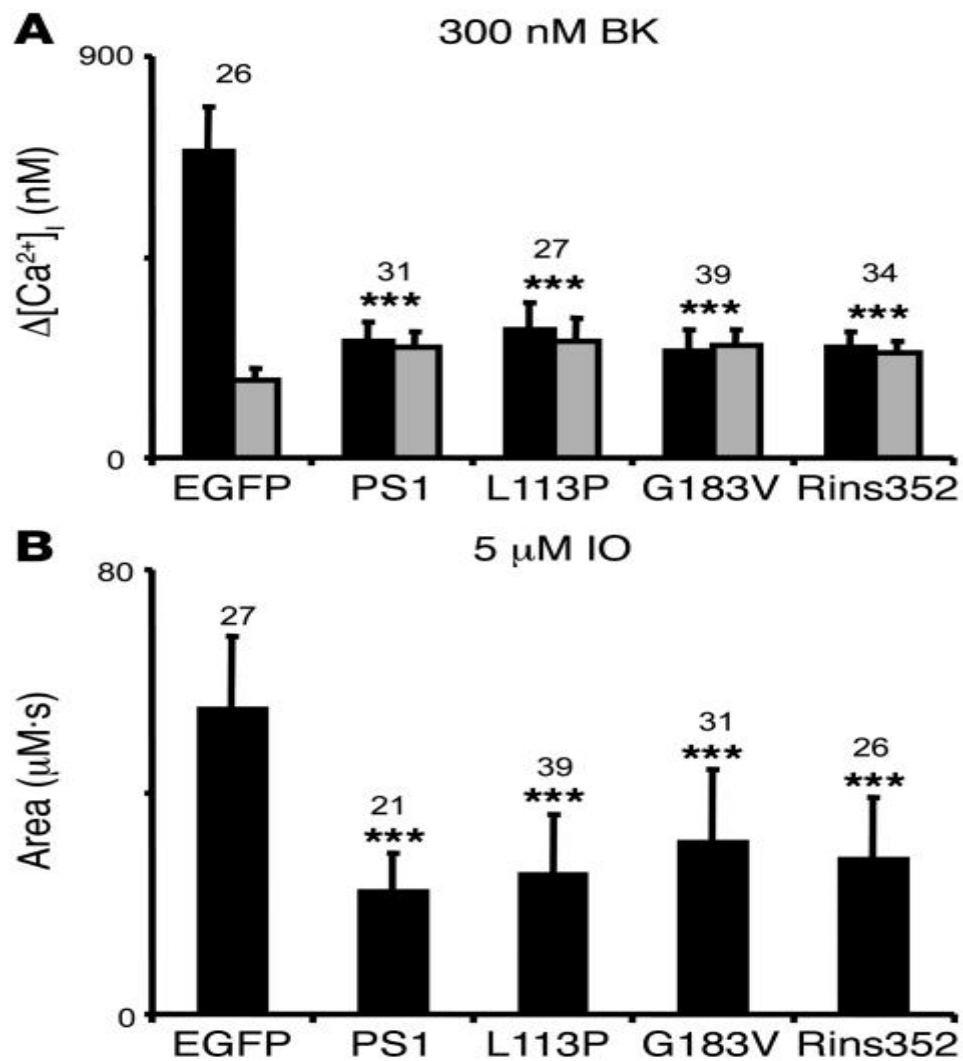


Fig 11. Summary of PS1-FTD rescue experiments. **a.** The average basal cytosolic Ca^{2+} levels (gray bars) and the amplitude of BK-induced Ca^{2+} responses (black bars) are shown as mean \pm SD for DKO cells transfected with EGFP and PS1 expression constructs (the number of cells analyzed is shown above each set of bars). When compared with DKO cells transfected with EGFP alone, the basal Ca^{2+} levels were significantly higher and the amplitude of BK-induced Ca^{2+} response was significantly smaller in DKO cells transfected with EGFP+PS1, EGFP+PS1-L113P, EGFP+PS1-G183V, and EGFP+PS1-Rins352. **b.** The average size of IO-releasable Ca^{2+} pool is shown as mean \pm SD for DKO cells transfected with EGFP and PS1 expression constructs (the number of cells analyzed is shown above each bar). When compared with DKO cells transfected with EGFP alone, the size of IO-releasable Ca^{2+} pool was significantly smaller in DKO cells transfected with EGFP+PS1, EGFP+PS1-L113P, EGFP+PS1-G183V, and EGFP+PS1-Rins352 combinations. *** $P < 0.05$ by ANOVA.

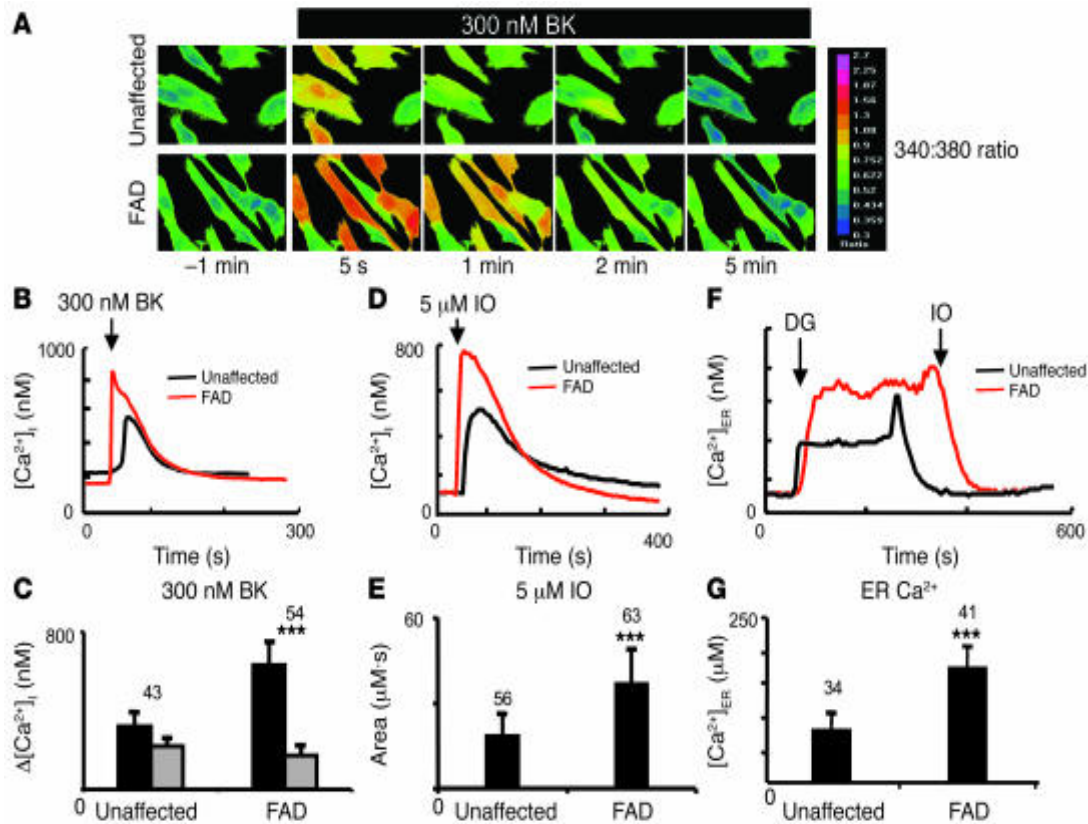


Fig 12. Ca²⁺ signals in human primary fibroblasts from the FAD patient. **a.** The representative Fura-2 images of BK-induced Ca²⁺ responses are shown for hFs from symptomatic PS1-A246E FAD patient and for hFs from the unaffected spouse. The Fura-2 340:380 ratios are presented as explained in the Figure 2 legend. **b.** The time course of BK-induced Ca²⁺ signals in representative experiments with hFs and hF-A246E cells. **c.** The average basal cytosolic Ca²⁺ levels (gray bars) and the amplitude of BK-induced Ca²⁺ responses (black bars) are shown as mean ± SD for hFs and hF-A246E cells (the number of cells analyzed is shown above each set of bars). When compared with hFs, the basal Ca²⁺ levels were significantly lower and the amplitude of BK-induced Ca²⁺ response was significantly larger in hF-A246E cells. **d.** The time course of IO-induced Ca²⁺ signals in representative experiments with hFs and hF-A246E cells. **e.** The average size of IO-sensitive Ca²⁺ pool is shown as mean ± SD for hFs and hF-A246E cells (the number of cells analyzed is shown above each bar). When compared with hFs, the size of IO-sensitive Ca²⁺ pool was significantly larger in hF-A246E cells. **f.** Representative ER Ca²⁺ traces recorded by ER-loaded Mag-Fura-2 in hFs and hF-A246E cells. The cells were loaded with Mag-fura-2 and permeabilized by 10 μM digitonin (DG) in a buffer containing 170 nM Ca²⁺ and 3 mM ATP. The ER membrane was permeabilized with 5 μM IO in Ca²⁺-free buffer at the end of the experiment. The Mag-Fura-2 340:380 ratios were converted to [Ca²⁺]_{ER} as described in Methods. **g.** The average [Ca²⁺]_{ER} determined for hFs and hF-A246E cells are shown as mean ± SD (the number of cells analyzed is shown above each bar). When compared with control hFs, the ER Ca²⁺ concentration was significantly higher in hF-A246E cells. ****P* < 0.05 by ANOVA.

	i (pA)	Transient			Stable		AAO	
		BK peak (nM)	IO area ($\mu\text{M}\cdot\text{sec}$)	ER Ca^{2+} (μM)	IO area ($\mu\text{M}\cdot\text{sec}$)	ER Ca^{2+} (μM)	range (years)	ref
MEF	NA	234 \pm 27	See stable	See stable	22 \pm 8	97 \pm 19	NA	
DKO	NA	752 \pm 141	See stable	See stable	56 \pm 16	183 \pm 42	NA	
PS1	0.04 \pm 0.01	271 \pm 53	33 \pm 9	108 \pm 21	24 \pm 5	93 \pm 15	NA	
A79V	0.035 \pm 0.003	253 \pm 39	31 \pm 14	114 \pm 28	ND	ND	53-58	(Larner and Doran 2006)
M146V	-	634 \pm 125	49 \pm 11	170 \pm 36	ND	ND	32-39	(Larner and Doran 2006)
L166P	-	714 \pm 73	52 \pm 14	227 \pm 39	53 \pm 9	178 \pm 19	24	(Bentahir, Nyabi et al. 2006)
A246E	-	706 \pm 92	51 \pm 12	234 \pm 47	54 \pm 11	191 \pm 23	53	(Larner and Doran 2006)
ΔE9	0.09 \pm 0.02	242 \pm 76	20 \pm 10	65 \pm 20	23 \pm 8	81 \pm 30	36-55	(Larner and Doran 2006)
E273A	-	674 \pm 154	53 \pm 9	210 \pm 53	ND	186 \pm 31	63	(Larner and Doran 2006)
D257A	0.06 \pm 0.01	219 \pm 99	23 \pm 5	70 \pm 10	25 \pm 11	ND	NA	
G384A	-	631 \pm 133	50 \pm 12	221 \pm 42	57 \pm 9	104 \pm 36	31-37	(Larner and Doran 2006)
P436Q	-	748 \pm 124	48 \pm 9	216 \pm 59	ND	ND	20-42	(Larner and Doran 2006)
PS2	0.03 \pm 0.01	343 \pm 58	ND	ND	34 \pm 10	104 \pm 36	NA	
N141I/L	-	617 \pm 169	ND	ND	48 \pm 19	211 \pm 55	50-65	(Mattson, Guo et al. 1998)
hF	NA	318 \pm 71	See stable	ND	19 \pm 7	84 \pm 19	NA	
hF-A246E	-	629 \pm 114	See stable	ND	37 \pm 12	169 \pm 27	53	(Mattson, Guo et al. 1998)

Table 1. The summary of results obtained in the present study with and in the previous publication (Tu, Nelson et al. 2006) is shown. The unitary size of Ba^{2+} currents estimated from “noise analysis” of BLM reconstitution experiments (i) is shown for PS1,

PS1-A79V, PS1-ΔE9, PS1-D257A, and PS2. No currents were observed in the experiments with other mutants tested. The average amplitude of bradykinin (BK)-induced Ca²⁺ response, the average content of ionomycin (IO)-sensitive Ca²⁺ pool and the mean ER Ca²⁺ concentrations [Ca²⁺]_{ER} are shown for wild type MEF cells, DKO cells, DKO cells transiently and stably transfected with PS rescue constructs, human hF fibroblasts and human PS1-A246E cells as indicated. The FAD onset age for cases resulting from the same mutations (AAO) is also shown. NA – not applicable. ND – not determined.

CHAPTER THREE

Calcium signaling defects in familial Alzheimer's disease patient. Relevance for

Alzheimer's disease

Abstract

Mutations in presenilin 1 (PS1) and presenilin 2 (PS2) are responsible for approximately 40% of all early onset familial Alzheimer's disease (FAD) cases in which a genetic cause has been identified. In addition, three mutations in PS1 have been associated with the occurrence of frontal temporal dementia (FTD) although a formal proof of their causal involvement has not been provided. PSs are highly conserved transmembrane proteins that support cleavage of the amyloid precursor protein (APP) by γ -secretase. The presence of senile plaques that is composed of the Amyloid β peptide ($A\beta$) serves as a key pathological hallmark for Alzheimer's disease. Most cases of AD with mutations in PS1 results in dense core senile plaques (classical plaques), however, there are certain PS1 mutations that are associated with a variant plaque, known as cotton wool plaques (CWP), which consist of a large round $A\beta$ deposits primarily positive for $A\beta$ 42 and usually devoided of a compact amyloid core. Recently, we discovered that presenilins also function as passive endoplasmic reticulum calcium (Ca^{2+}) leak channels and that most PSs FAD mutations tested affected their leak function. Contrary to these findings the FTD-associated mutations in PS1 did not affect ER Ca^{2+} leak function. In this study, we use Ca^{2+} imaging experiments to evaluate ER Ca^{2+} leak in lymphoblast from FAD patients harboring mutations in PS1, PS2, tau, APP and sporadic AD cases. In addition, ER Ca^{2+} rescue experiments with the PS1 FAD lymphoblast mutations, PS1 CWP FAD mutations; PS1-M292D (uncleavable PS1), PS1-D385A (γ -secretase dead mutant), PS1-dTAG (PS1 targeting construct used to generate PScDKO mice) and PS1-P284H a non-FAD mutation were performed in PS-null mouse embryonic fibroblasts (MEF) to evaluate ER Ca^{2+} leak function. We found that PS1 FAD mutations M139V, M146L, G217D, K239E, V261F, D385A, L420R,

A426P, A431E and PS2-N141I abolished ER Ca²⁺ leak, while PS1 mutations PS1-dTAG, L85P, ΔE8, ΔE9, P264L, R269G, E280G, P284H, T291P, M292D, C410Y and N405S had no apparent effect. Mutations in tau-R406W, APP-V717L and sporadic AD had no effect of ER Ca²⁺ leak in lymphoblast. From these results we concluded that most CWP PS1 mutations were functional for ER Ca²⁺ leak, while most of the other PS1 FAD mutation tested abolished ER Ca²⁺ leak.

Introduction

Alzheimer's disease (AD) is the most common form of age-related dementia in human beings over the age of 65 years. Recently we discovered that presenilins function as passive endoplasmic reticulum Ca²⁺ leak channels (Tu, Nelson et al. 2006). We further found that M146V/L, L166P, A246E, E273A, G384A, P436Q, PS1-ΔE9 and PS2-N141I FAD mutations in presenilins affected their ER Ca²⁺ leak function (Tu, Nelson et al. 2006) (Nelson, Tu et al. 2007), while FTD associated mutant, FAD A79V and PS1-D257A (γ-secretase mutant) did not. Based on these results and the vast number of mutations in PSs and APP, we wanted to further expand our studies and also examine FAD mutations in a human based model. Here we use Ca²⁺ imaging experiments to evaluate ER Ca²⁺ leak in lymphoblast from AD patients harboring mutations in PSs (M139V, M146L, K239E, V261F, P264L, R269G, C410Y, A426P, A431E, ΔE9 (Fig 13) and PS2-N141I), tau-R406W, APP-V717L and sporadic AD cases. In addition, Ca²⁺ rescue experiments were performed in PS-null MEF with the PS1 FAD mutations from the lymphoblast cell line, FAD PS1 (L85P, G217D, E280G, T291P, N405S, L420R and ΔE8), PS1-M292D, PS1-D385A, PS1-dTAG and PS1-P284H a non-FAD mutation. From the PS1 FAD mutation tested G217D, P264L, E280G, T291P, ΔE8, ΔE9, C410Y,

N405S and L420R caused an increase incidence of CWP in AD patient. From our results we conclude that most of the FAD PS1 mutation tested abolished ER Ca^{2+} and that most of the FAD mutation that were functional had the CWP phenotype in AD patients. PS1-M292D, PS1-D385A, PS1-dTAG, PS1-P284H, tau-R406W, APP-V717L and sporadic AD cases did not have any apparent effect on ER Ca^{2+} leak. These observations further suggest that PSs play a pivotal role in deranged Ca^{2+} in AD and they also provided further support for the contribution of disturbed Ca^{2+} homeostasis to AD pathogenesis (Khachaturian 1989; Mattson, LaFerla et al. 2000; LaFerla 2002; Smith, Green et al. 2005).

Results

Ca^{2+} signaling defects in human FAD lymphoblast

In our previous studies (Tu, Nelson et al. 2006), we showed that PSs function as ER Ca^{2+} leak channels and that most FAD mutations in PSs examined abolished its leak channel activity (Tu, Nelson et al. 2006). We also showed that a sample of FAD primary human fibroblasts derived from a 56-year-old symptomatic patient with A246E mutation in PS1 (AG06840) exhibited defects in ER Ca^{2+} leak. To further establish the relevance of our results in a human FAD context, we obtained lymphoblast from symptomatic AD patients harboring mutations in PSs, tau, APP and sporadic AD cases from the National Cell Repository for Alzheimer's disease (NCRAD). Human lymphoblast from healthy individuals were also obtained and used as controls. The function of ER Ca^{2+} leak pathway in these cells was evaluated in Ca^{2+} imaging experiments. The lymphoblasts were used in Fura-2 Ca^{2+} imaging experiments by following the procedures as described in methods. In these experiments we determined that application of 5 μM

ionomycin (IO) induced larger Ca^{2+} transients in PS1 FAD mutation M139V, M146L, K239E, V261F, A431E and PS2-N141I, compared to wild type (WT). When compared to the WT lymphoblast IO induced similar Ca^{2+} transients in PS1 (P264L, R269G, C410Y, A426P and Δ E9) Tau-R406W and APP-V717L lymphoblast, when we calculated the area under the IO-induced Ca^{2+} curve to quantify the content of IO-sensitive Ca^{2+} stores in these cells. A representative ionomycin (IO)-induced Ca^{2+} response is shown for wild type, PS1-M139V and PS1-P264L lymphoblast (Fig 14). We found that the average content of IO-sensitive Ca^{2+} stores was equal to $11 \pm 3 \mu\text{M}\cdot\text{sec}$ ($n = 12$) for WT lymphoblast, $19 \pm 4 \mu\text{M}\cdot\text{sec}$ ($n = 9$) for PS1-M139V, $24 \pm 4 \mu\text{M}\cdot\text{sec}$ ($n = 9$) for PS1-M146L ($n = 8$), $22 \pm 4 \mu\text{M}\cdot\text{sec}$ ($n = 10$) for PS1-K239E, $21 \pm 5 \mu\text{M}\cdot\text{sec}$ ($n = 10$) for PS1-V261F, $9 \pm 2 \mu\text{M}\cdot\text{sec}$ ($n = 9$) for PS1-P264L, $7 \pm 2 \mu\text{M}\cdot\text{sec}$ ($n = 6$) for PS1-R269G, $10 \pm 3 \mu\text{M}\cdot\text{sec}$ ($n = 5$) for PS1-C410Y, $17 \pm 3 \mu\text{M}\cdot\text{sec}$ ($n = 6$) for PS1-A426P, $20 \pm 3 \mu\text{M}\cdot\text{sec}$ ($n = 6$) for PS1-A431E $10 \pm 3 \mu\text{M}\cdot\text{sec}$ ($n = 5$) for PS1- Δ E9, $21 \pm 5 \mu\text{M}\cdot\text{sec}$ ($n = 6$) for PS2-N141I, $11 \pm 3 \mu\text{M}\cdot\text{sec}$ ($n = 4$) for tau-R406W and $16 \pm 4 \mu\text{M}\cdot\text{sec}$ ($n = 6$) for APP-V717L lymphoblast (Fig 15). From these experiments, we concluded that the intracellular Ca^{2+} stores were overfilled in lymphoblast from FAD patient with PS1 mutations M139V, M146L, K239E, V261F, A431E and PS2-N141I, while it was at a similar level compared to WT lymphoblast from patients with PS1 mutation P264L, R269G, C410Y, A426P, Δ E9 and tau-R406W and APP-V717L. From these results we concluded that PSs FAD mutations that affected ER Ca^{2+} signaling leads to a doubling of ER Ca^{2+} contents in the lymphoblast cell lines.

Rescue of Ca²⁺ signaling defects in PS DKO mouse embryonic fibroblasts with FAD PS1 mutations from Lymphoblast cell lines

To evaluate the ER Ca²⁺ leak function of wild type PS1 and selected PS1 FAD mutants, we performed a series of “rescue” experiments. In these experiments the DKO fibroblasts were transfected with EGFP plasmid alone (EGFP control) or EGFP plasmid together with the presenilin expression constructs and analyzed by Fura-2 Ca²⁺ imaging 48 hours after transfection. The transfected cells in these experiments were identified by GFP fluorescence (Tu, Nelson et al. 2006). The resting Ca²⁺ levels in the transfected DKO cells were estimated from the Fura-2 340/380 ratio measurements. We found that the average basal Ca²⁺ level in DKO cells transfected with EGFP plasmid was equal to 173 ± 32 nM (n = 56)(Fig. 16A, gray bar). The average basal Ca²⁺ levels in DKO cells co-transfected with EGFP and M139V, K239E, V261F, A426P and A431E mutant PS1 expression plasmids were not significantly different from DKO cells transfected with EGFP plasmid alone (data not shown). In contrast, the mean basal Ca²⁺ level in DKO cells transfected with (EGFP + PS1) plasmid combination was equal to 257 ± 39 nM (n = 61), significantly higher (p < 0.05) than in DKO cells transfected with EGFP alone (Fig. 16A, gray bars). The mean basal Ca²⁺ level in DKO cells co-transfected with EGFP and P264L, R269G and C410Y PS1 mutant plasmid was equal to 261 ± 34 nM (n =31), 264 ± 26 nM (n =38) and 248 ± 26 nM (n =30) respectively, also significantly higher (p < 0.05) than in DKO cells transfected with EGFP alone. To explain these results we reasoned that expression of wild type PS1, PS1-P264L, PS1-R269G and PS1-C410Y mutant plasmids, but not the other five FAD PS1 mutants tested in our study increases

passive Ca^{2+} leak from the ER and elevates basal cytosolic Ca^{2+} levels in transfected DKO cells.

When transfected DKO cells were challenged with 300 nM BK, large transient Ca^{2+} signals were observed in EGFP alone, (EGFP + M139V), (EGFP +K239E), (EGFP +V261F), (EGFP + A426P) and (EGFP + A431E) transfected cells. In contrast, a significantly smaller Ca^{2+} signal was induced by BK in DKO cells transfected with (EGFP + PS1), (EGFP + P264L), (EGFP + R269G) and (EGFP + C410Y) combinations. On average, the difference between peak and basal Ca^{2+} levels ($\Delta[\text{Ca}^{2+}]$) in BK-stimulated cells was equal to 693 ± 93 nM ($n = 37$) for EGFP-transfected cells, 221 ± 36 nM ($n = 37$) for (EGFP + PS1)-transfected cells, 231 ± 37 nM ($n = 31$) for (EGFP + P264L) and 314 ± 47 nM ($n = 38$) for (EGFP + R269G) 254 ± 33 nM ($n = 30$) for (EGFP + C410Y)-transfected cells(Fig. 16A). The peak responses in DKO cells transfected with the other FAD mutants were not significantly different from the peak Ca^{2+} responses in cell transfected with EGFP plasmid alone (Fig 16A, black bars). Thus, transfection of DKO cells with wild type PS1, P264L, R269G and C410Y expression constructs reduced the amplitude of BK-induced Ca^{2+} responses to levels observed in experiments with WT MEFs (Tu, Nelson et al. 2006) whereas expression of M139V, K239E, V261F, A426P and A431E FAD mutants had no significant effect on the amplitude of BK-induced responses.

In the next series of experiments we evaluated the size of ionomycin-sensitive Ca^{2+} pool in PS1- transfected DKO cells. Ionomycin is an ionophore that induces formation of Ca^{2+} -permeable pores in cellular membranes, leading to complete emptying of ER Ca^{2+} stores independently from the InsP_3R activation. In agreement with the previous findings (Tu, Nelson et al. 2006), we found that addition of 5 μM ionomycin (IO) induced

large and long-lasting elevation of cytosolic Ca^{2+} levels in EGFP-transfected DKO cells, but smaller in amplitude and shorter in duration Ca^{2+} elevation in (EGFP + PS1)-transfected cells (data not shown). To estimate the size of IO-sensitive Ca^{2+} pool, we calculated the area under the IO-induced Ca^{2+} curve. On average, the area under the IO-induced Ca^{2+} curve was equal to $50 \pm 9 \mu\text{M}\cdot\text{sec}$ ($n = 33$) for EGFP-transfected DKO cells, $22 \pm 7 \mu\text{M}\cdot\text{sec}$ ($n = 26$) for (EGFP + PS1)-transfected DKO cells, $48 \pm 11 \mu\text{M}\cdot\text{sec}$ ($n = 27$) for (EGFP + M139V)-transfected DKO cells, $54 \pm 9 \mu\text{M}\cdot\text{sec}$ ($n = 33$) for (EGFP + K239E)-transfected DKO cells, $26 \pm 7 \mu\text{M}\cdot\text{sec}$ ($n = 29$) for (EGFP + R269G)-transfected DKO cells, $52 \pm 11 \mu\text{M}\cdot\text{sec}$ ($n = 24$) for (EGFP + V261F)-transfected DKO cells, $23 \pm 7 \mu\text{M}\cdot\text{sec}$ ($n = 18$) for (EGFP + P264L)-transfected DKO cells, $27 \pm 6 \mu\text{M}\cdot\text{sec}$ ($n = 21$) for (EGFP + C410Y)-transfected DKO cells, $49 \pm 10 \mu\text{M}\cdot\text{sec}$ ($n = 34$) for (EGFP + A426P)-transfected DKO cells and $53 \pm 13 \mu\text{M}\cdot\text{sec}$ ($n = 29$) for (EGFP + A431E)-transfected DKO (Fig 16B). Thus, transfection of DKO cells with wild type PS1, P264L, R269G and C410Y expression constructs reduced the IO releasable Ca^{2+} pool to levels observed in experiments with WT MEFs (Tu, Nelson et al. 2006) or DKO MEF transfected with WT-PS1; (Nelson, Tu et al. 2007), whereas expression of M139V, K239E, V261F, A426P and A431E FAD mutants had no significant effect on the IO releasable Ca^{2+} pool. From these results we concluded that FAD P264L, R269G and C410Y could rescue ER Ca^{2+} leak while M139V, K239E, V261F, A426P and A431E FAD mutants could not.

Rescue of Ca²⁺ signaling defects in PS DKO mouse embryonic fibroblasts with FAD PS1 CWP mutations

From previously results reported in (Tu, Nelson et al. 2006), $\Delta E9/S290C$ was a gain of function mutation for ER calcium leak. Upon examination PS1-P264L and C410Y in lymphoblast (Fig 6A and Fig 13) and in Ca²⁺ rescue experiments they had no apparent effect on ER Ca²⁺ leak function. PS1-P264L, PS1-C410Y and $\Delta E9/S290C$ resulted in the formation of CWP in AD patients (Fig 2). In PS1 FAD patients with CWP the clinical phenotype spastic paraparesis (SP) is often (but not always) present. From these observations we wanted to examine the effects of CWP PS1 FAD mutations on ER calcium leak. In the next set of experiments we examined PS1 FAD mutations with clinical phenotype SP only, CWP/SP, CWP only and PS1-P284H (non-FAD mutation) in Ca²⁺ rescue experiment in DKO-MEF. In these experiments DKO MEF were transfected by EGFP plasmid alone (EGFP control) or EGFP plasmid together with the presenilin expression constructs and analyzed by Fura-2 Ca²⁺ imaging 48 hours after transfection. When transfected DKO cells was challenged with 300 nM BK, large transient Ca²⁺ signals were observed in EGFP alone, (EGFP + G217D) and (EGFP + L420R) transfected cells. In contrast, a significantly smaller Ca²⁺ signal was induced by BK in DKO cells transfected with (EGFP + PS1), (EGFP + L85P), (EGFP + $\Delta E8$), (EGFP + E280G), (EGFP + T291P), (EGFP + N405S) and (EGFP + P284H) combinations. On average, the difference between peak and basal Ca²⁺ levels ($\Delta[Ca^{2+}]$) in BK-stimulated cells was equal to 689 ± 87 nM (n = 41) for EGFP-transfected cells, 249 ± 43 nM (n = 33) for (EGFP + PS1)-transfected cells, 219 ± 27 nM (n = 27) for (EGFP + L85P), 231 ± 35 nM (n = 21) for (EGFP + $\Delta E8$), 698 ± 139 nM (n = 29) for (EGFP + G217D), 287 ± 41 nM (n = 38) for (EGFP + E280G), 263 ± 52 nM (n = 21) for (EGFP + P284H), 254 ± 29

nM (n =32) for (EGFP + T291P), 239 ± 31 nM (n = 34) for (EGFP + N405S) and 674 ± 91 nM (n = 39) for (EGFP + L420R -transfected cells(Fig 17A, black bars). The average basal Ca^{2+} level in DKO cells transfected with EGFP plasmid was equal to 173 ± 32 nM (n = 41)(Fig. 17A, gray bar). The average basal Ca^{2+} levels in DKO cells co-transfected with EGFP + G217D and EGFP + L420R PS1 mutant expression plasmids were not significantly different from DKO cells transfected with EGFP plasmid alone (data not shown). In contrast, the mean basal Ca^{2+} level in DKO cells transfected with (EGFP + PS1) plasmid combination was equal to 257 ± 39 nM (n = 33), significantly higher ($p < 0.05$) than in DKO cells transfected with EGFP alone (Fig. 17A, gray bars). The mean basal Ca^{2+} level in DKO cells co-transfected with EGFP and L85P, $\Delta E8$, E280G, P284H, T291P and N405S PS1 mutant plasmid was equal to 261 ± 33 nM (n =27), 258 ± 41 nM (n =21), 263 ± 39 nM (n =38), 229 ± 27 nM (n =32), 248 ± 32 nM (n =38) and 274 ± 34 nM (n =34), respectively, also significantly higher ($p < 0.05$) than in DKO cells transfected with EGFP alone (Fig 17A, gray bars).

In the next series of experiments we evaluated the size of ionomycin-sensitive Ca^{2+} pool in PS1- transfected DKO cells. To estimate the size of IO-sensitive Ca^{2+} pool, we calculated the area under the IO-induced Ca^{2+} curve. On average, the area under the IO-induced Ca^{2+} curve was equal to 49 ± 11 μ M.sec (n = 43) for EGFP-transfected DKO cells, 23 ± 7 μ M.sec (n = 37) for (EGFP + PS1)-transfected DKO cells, 21 ± 7 μ M.sec (n = 20) for (EGFP + $\Delta E8$)-transfected DKO cells, 21 ± 5 μ M.sec (n = 29) for (EGFP + L85P)-transfected DKO cells, 54 ± 13 μ M.sec (n = 30) for (EGFP + G217D)-transfected DKO cells, 25 ± 7 μ M.sec (n = 27) for (EGFP + E280G)-transfected DKO cells, 29 ± 6 μ M.sec (n = 33) for (EGFP + P284H)-transfected DKO cells, 29 ± 6 μ M.sec (n = 33) for (EGFP + T291P)-transfected DKO cells, 26 ± 7 μ M.sec (n = 34) for (EGFP + N405S)-

transfected DKO cells and $48 \pm 9 \mu\text{M}\cdot\text{sec}$ ($n = 32$) for (EGFP + L420R)-transfected DKO cells (Fig 17B). Thus, transfection of DKO cells with wild type PS1, L85P, P284H, ΔE8 , E280G, T291P and N405S expression constructs reduced the IO releasable Ca^{2+} pool to levels observed in experiments with WT MEF (Tu, Nelson et al. 2006) or DKO MEF transfected with WT-PS1 (Tu, Nelson et al. 2006); (Nelson, Tu et al. 2007).

Ca^{2+} rescue experiment with uncleavable PS1 and γ -secretase PS1 mutation

To evaluate the ER Ca^{2+} leak function of uncleavable PS1-M292D and PS1-D385A, we performed a series of “rescue” experiments in DKO MEF. In these experiments DKO fibroblasts were transfected by EGFP plasmid alone (EGFP control) or EGFP plasmid together with the presenilin expression constructs and analyzed by Fura-2 Ca^{2+} imaging 48 hours after transfection. The transfected cells in these experiments were identified by GFP fluorescence (Tu, Nelson et al. 2006). PS1-M292D a point mutation located within the motif required for endoproteolytic cleavage of PS1 (Fig 18A), accumulates as a holoprotein (Steiner 1999). When transfected DKO cells was challenged with 300 nM BK, large transient Ca^{2+} signals were observed in EGFP alone, in contrast, a significantly smaller Ca^{2+} signal was induced by BK in DKO cells transfected with (EGFP + PS1) and (EGFP + M292D) combinations (Fig 18B). Since PS1-M292D was able to rescue DKO Ca^{2+} levels back to WT-PS1; we reasoned that PS1-M292D is capable of functioning as an ER Ca^{2+} leak channel.

PS1-D385 is located in transmembrane domain (TM7)(Fig 18A), whenever aspartate is substituted by alanine it diminished aspartyl protease activity and physiological endoproteolysis (Wolfe, Xia et al. 1999); (Kimberly WT 2000). The other γ -secretase

mutant D257 is shown in TM 6. D257A is known to function as an ER Ca^{2+} leak channel (Tu, Nelson et al. 2006). To test whether D385A function as ER Ca^{2+} leak channels, rescue experiments were performed in DKO MEF as described above. When transfected DKO cells were challenged with 5 μM IO, large transient Ca^{2+} signals were observed in EGFP alone and (EGFP + D385A) transfected cells. In contrast, a significantly smaller Ca^{2+} signal was induced by DKO cells transfected with (EGFP + PS1) combinations (Fig 18C). Thus, transfection of DKO cells with PS1-D385A expression constructs could not reduce the IO releasable Ca^{2+} pool to levels observed in experiments in WT MEFs (Tu, Nelson et al. 2006) or DKO MEF transfected with WT-PS1 (Tu, Nelson et al. 2006); (Nelson, Tu et al. 2007).

Ca^{2+} signals in PS1 targeting construct (dTAG)

Our collaborator Bart De Strooper generated the floxed PS1 (fPS1) mice in which the first exon of the PS1 gene is surrounded by loxP sites (unpublished, Bart De Strooper). Very similar approach has been taken previously to achieve conditional inactivation of PS1 gene in mice (Feng, Rampon et al. 2001; Yu, Saura et al. 2001). Indeed, preliminary results from Bart De Strooper's laboratory indicated that expression of Cre recombinase in the brains of fPS1/fPS1 mice caused excision of floxed PS1 alleles and abolished expression of PS1 (Bart De Strooper, personal communication). It has then been shown that expression of Cre recombinase in cultured hippocampal and cortical neuron can lead to excision of PS1 (unpublished Hua Zhang). Bart De Strooper's laboratory then crossed the generated fPS1 mice with PS2^{-/-} mice that his laboratory previously produced (Herreman, Hartmann et al. 1999). The resulting fPS1/fPS1; PS2^{-/-} mice was provided to us by Bart De Strooper for studies of neuronal Ca^{2+}

signaling. Working with this mice is not apart of my project, however, I tested the targeting construct (dTAG) used to generate this mice. dTAG consist of a CBP tag followed by a linker and three FLAG tag sequence followed by PS1. To evaluate ER Ca^{2+} leak function of wild type PS1 and dTAG I performed a series of “rescue” experiments. In these experiments DKO fibroblasts were transfected by EGFP plasmid alone (EGFP control) or EGFP plasmid together with the dTAG construct and analyzed by Fura-2 Ca^{2+} imaging 48 hours after transfection.

When transfected DKO cells were challenged with 300 nM BK and 5 μM IO, large transient Ca^{2+} signals were observed in EGFP alone transfected cells. In contrast, a significantly smaller Ca^{2+} signal was induced by BK (Fig 19A) and IO in DKO cells transfected with (EGFP + PS1) and (EGFP + dTAG) combinations (Fig 19 B and D). Quantification of BK and IO responses, also showed that both WT-PS1 and PS1-dTAG had significantly small calcium pools compare to EGFP only(Fig 19 C and E). Thus, transfection of DKO cells with wild type PS1 and dTAG expression constructs reduced the IO releasable Ca^{2+} pool to levels observed in experiments with WT MEFs (Tu, Nelson et al. 2006) or DKO MEF transfected with WT-PS1(Tu, Nelson et al. 2006);(Nelson, Tu et al. 2007).

Discussion

In the present study we use lymphoblast from FAD patients to examine ER Ca^{2+} signaling in a human context. In addition, we used Ca^{2+} rescue experiments in DKO MEF to confirm our observations in lymphoblast. Does PSs function as ER Ca^{2+} leak channel in lymphoblast? Deletion of PSs in B cells has been reported to cause deficits in both lipopolysaccharide and B cell antigen receptor-induced proliferation and signal transduction events, including a deficit in anti-IgM-mediated calcium influx (Yagi,

Giallourakis et al. 2008). Mutations in PSs accounts for the majority of all known FAD cases (Tandon and Fraser 2002). Many FAD mutations in PSs result in deranged calcium (Ca^{2+}) signaling, but the mechanistic explanation to these finding has been controversial (reviewed in(Smith, Green et al. 2005). Our recent discovery that presenilins function as ER Ca^{2+} leak channels (Tu, Nelson et al. 2006) provided a direct link between presenilins and Ca^{2+} signaling. In addition to PSs, a polymorphism in CALHM1 was shown to influence Ca^{2+} homoeostasis and $\text{A}\beta$ levels (Ute Dreses-Werringloer, Ankit Jain et al. 2008). CALHM1 was shown to be a risk gene for the onset of Alzheimer's disease. The results in the present report and in the previous studies (Tu, Nelson et al. 2006) indicate that most FAD mutations in presenilins have dramatic effect on their ability to function as ER Ca^{2+} leak channels. In our combined Ca^{2+} imaging experiments we tested 23 FAD mutations in PS1, 1 FAD mutation in PS2, PS1-M292D, PS1-D385A and dTAG. In addition we tested FAD mutations in APP-V717L, mutation in tau-R406W, three FTD-associated PS1 mutations and in sporadic AD cases. From the 26 FAD mutations tested 14 mutations (M139V, M146V/L, L166P, G217D, K239E, A246E, V261F, E273A, G384A, L420R, A426P, A431E, P436Q mutations in PS1 and N141I/L mutation in PS2) abolished ER Ca^{2+} leak function of PSs. This conclusion was based on the lack of channel activity in BLM experiments with the FAD mutants (Tu, Nelson et al. 2006), by failure of these mutants to rescue Ca^{2+} signaling defects in PS DKO cells, the ability of these mutations to enhance ER Ca^{2+} contents in fibroblast from a FAD patient and the ability of these mutations to increase ER Ca^{2+} contents in lymphoblast from FAD patients. One FAD mutation (PS1- Δ E9) appear to be a "gain of function" mutation which enhanced Ca^{2+} channel activity of presenilins in BLM experiments (Tu, Nelson et al. 2006). Interestingly, ER Ca^{2+} leak function was not

affected by D257A mutation that abolishes γ -secretase function of PS1 (Tu, Nelson et al. 2006), while another γ -secretase mutation PS1-D385A abolished ER Ca^{2+} leak function. Based on work by Bart De Strooper's laboratory PS1-D385 is exposed to water, while PS1-D257 was not, these results may explain why these γ -secretase affect Ca^{2+} signaling differently. These data also suggest that D385 is more important in maintain the integrity of the channel. As discussed in our previous publication (Tu, Nelson et al. 2006), "ER Ca^{2+} leak function" appear to be independent from their " γ -secretase function". In addition, ER Ca^{2+} leak function was not affected in AD patients harboring mutations in tau or APP. Surprisingly, there was a slight increase in ER Ca^{2+} pool in lymphoblast from FAD APP-V717L patients and old AD sporadic cell lines, however it was not significant compared to WT control lymphoblast cell line. More experiments with APP-V717L mutation need to carry out to determine whether FAD mutations in APP affect Ca^{2+} signaling. If APP FAD mutations does affect Ca^{2+} signaling it would imply that mutated genes that are involve in FAD are acting through a similar pathway to cause AD.

From the FAD mutations tested in the present study and previous publications, (PS1-A79V, L85P, Δ E8, P264L, R269G, E280G, T291P, N405S and C410Y) had no apparent effect on ER Ca^{2+} leak function in our experiments. Interestingly, most of the FAD mutations that were functional in our experiments segregated with the CWP phenotype. This may suggest that PS1 mutations that are functional in our assay cause APP to be processed differently from LOF PS1 mutations for ER Ca^{2+} leak.

Not surprising, both the uncleavable for of PS1 (M292D) and dTAG (PS1 targeting construct) were able to function as ER Ca^{2+} leak channel. We hypothesized that it's PS1 holoprotein that function as ER Ca^{2+} channel and not the cleave form (Tu, Nelson et al.

2006). The dTAG data suggest that the targeting construct used to generate PS-cDKO was able to facilitate ER leak.

The mutations analyzed in the present paper and in the previous studies are spread across the sequence of presenilins and correspond to FAD cases with variable ages of onset (Larner and Doran 2006). From our results we could not detect any particular “hot spot” region or pattern that can be used to predict which mutations influence ER Ca^{2+} leak function of presenilins; however, we did notice that most PSs FAD mutations that affected ER Ca^{2+} leak were mainly located in transmembrane domains (Fig 20). In conclusion, from the results obtained so far we can conclude that many FAD point mutations in presenilins result in loss of ER Ca^{2+} leak function. As discussed previously (Tu, Nelson et al. 2006), autosomal-dominant character of these mutations may potentially be explained by dominant negative effect of mutant PS allele on Ca^{2+} channel function of wild type alleles. Our results are in general agreement with the “loss of presenilin function” hypothesis of FAD (Saura, Choi et al. 2004; De Strooper 2007; Shen and Kelleher 2007) and provide further support for the contribution of disturbed Ca^{2+} homeostasis to AD pathogenesis (Khachaturian 1989; Mattson, LaFerla et al. 2000; LaFerla 2002; Smith, Green et al. 2005). Additional studies will be required to investigate the connection between defective Ca^{2+} signaling and neurodegeneration in neurons.

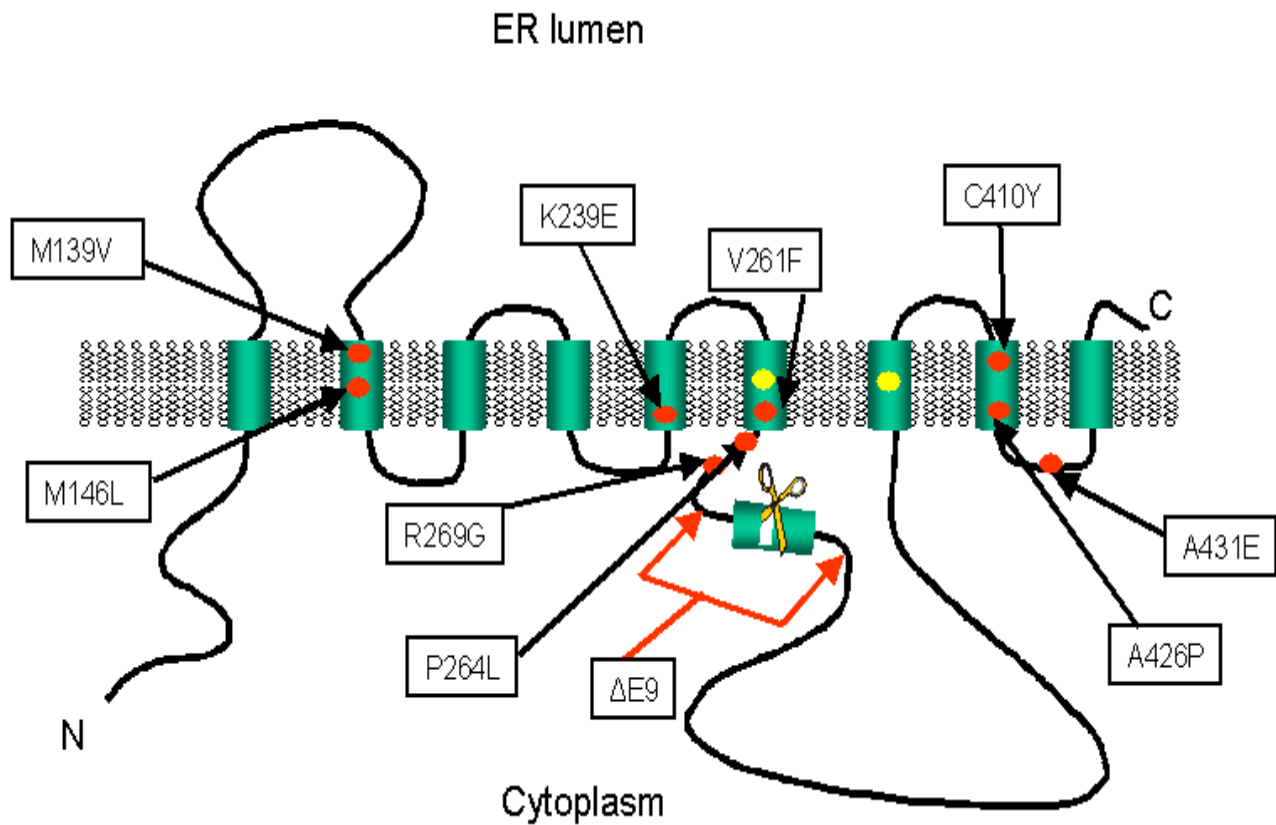


Fig 13. Molecular model of presenilins. (Laudon, Hansson et al. 2005; Spasic, Tolia et al. 2006). The nine transmembrane domains (TM1-TM9) of presenilins, the γ -secretase catalytic aspartate residues (yellow circle) and the site of the endoproteolytic cleavage are shown. The positions of PS1 FAD mutants M139V, M146L, K239E, V261F, P264L, R269G, Δ E9, A426P and A431E examined in our study are shown.

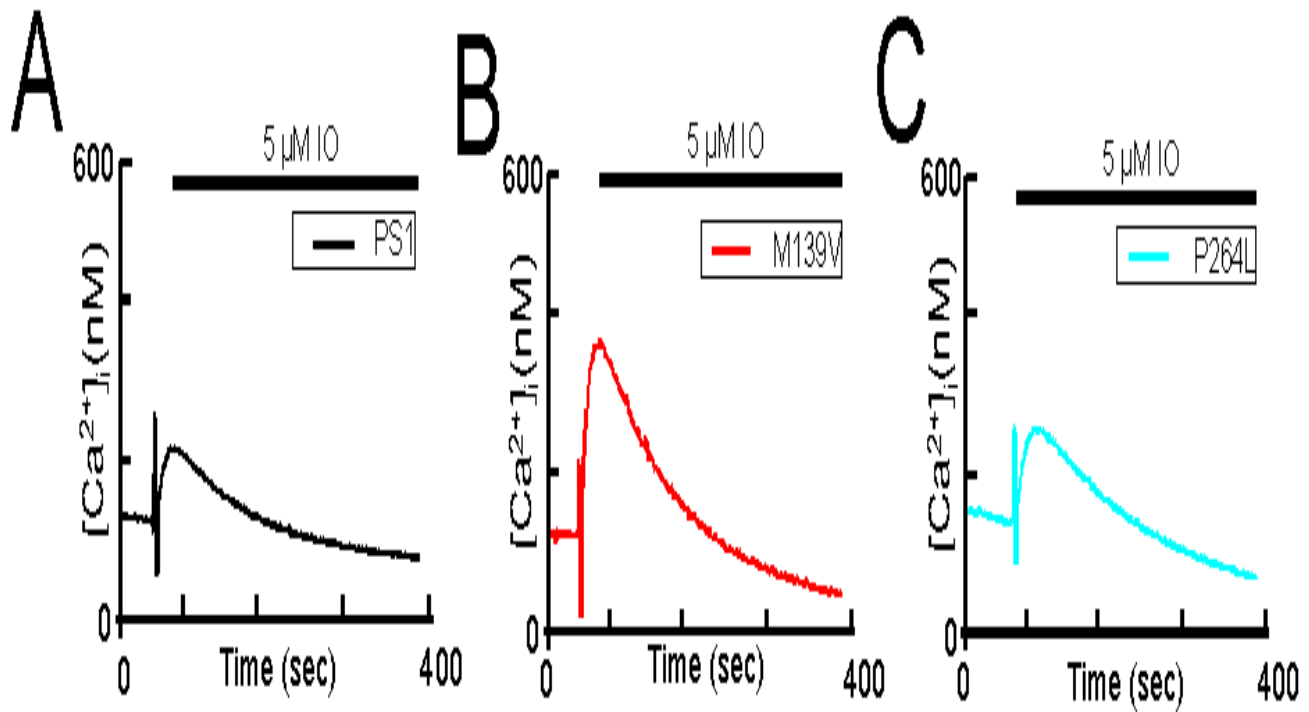


Figure 14. Ca^{2+} signals in lymphoblast from the FAD patient. a. The time course of ionomycin (IO)-induced Ca^{2+} signals in representative experiments with wild type lymphoblast. b. The time course of ionomycin (IO)-induced Ca^{2+} signals in representative experiments with lymphoblast from FAD patient harboring PS1-M139V mutation. c. The time course of ionomycin (IO)-induced Ca^{2+} signals in representative experiments with lymphoblast from FAD patient harboring PS1-P264L mutation

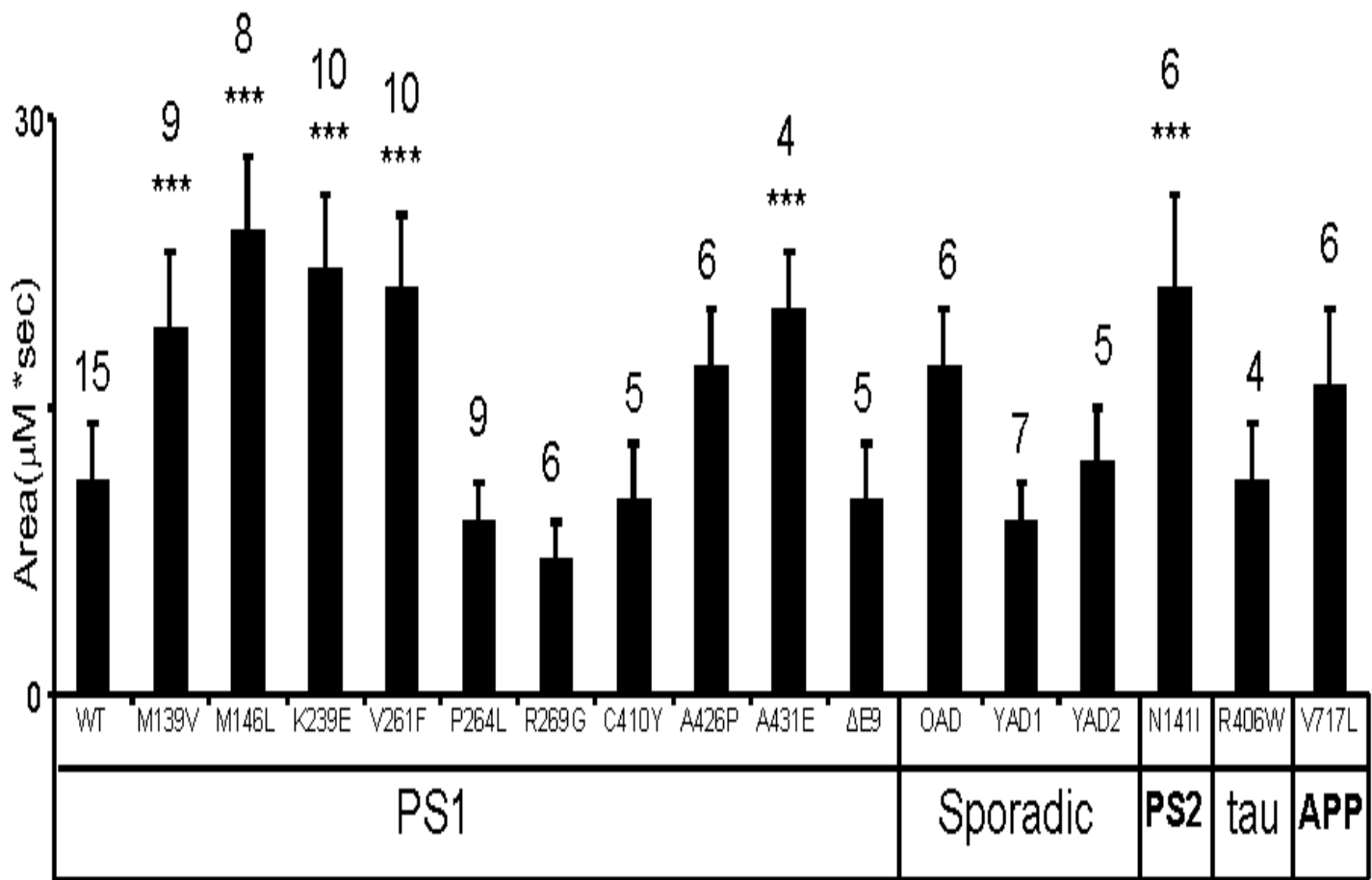


Figure 15. Ca²⁺ signals in human lymphoblast from FAD patients. The average size of ionomycin (IO)-releasable Ca²⁺ pool is shown for human FAD lymphoblast, data is shown as mean ± S.D. (n = number of experiments done). When compared to WT lymphoblast, the size of IO-releasable Ca²⁺ pool is significantly (***, p < 0.05 by ANOVA) larger in FAD lymphoblast with PS1 mutation M139V, M146L, K239E, V261F, A431E and PS2-N141I. There were no significant differences in the IO-releasable Ca²⁺ pool of PS1-P264L, R269G, C410Y, A426P, DE9, tau-R406W, APP-V717L, young (YAD) or old(OAD) sporadic cases when compared to WT. Even though the IO-releasable Ca²⁺ pool was more elevated in FAD lymphoblast PS1-A426P, APP-V717L and OAD there were no significant difference compared to WT lymphoblast.

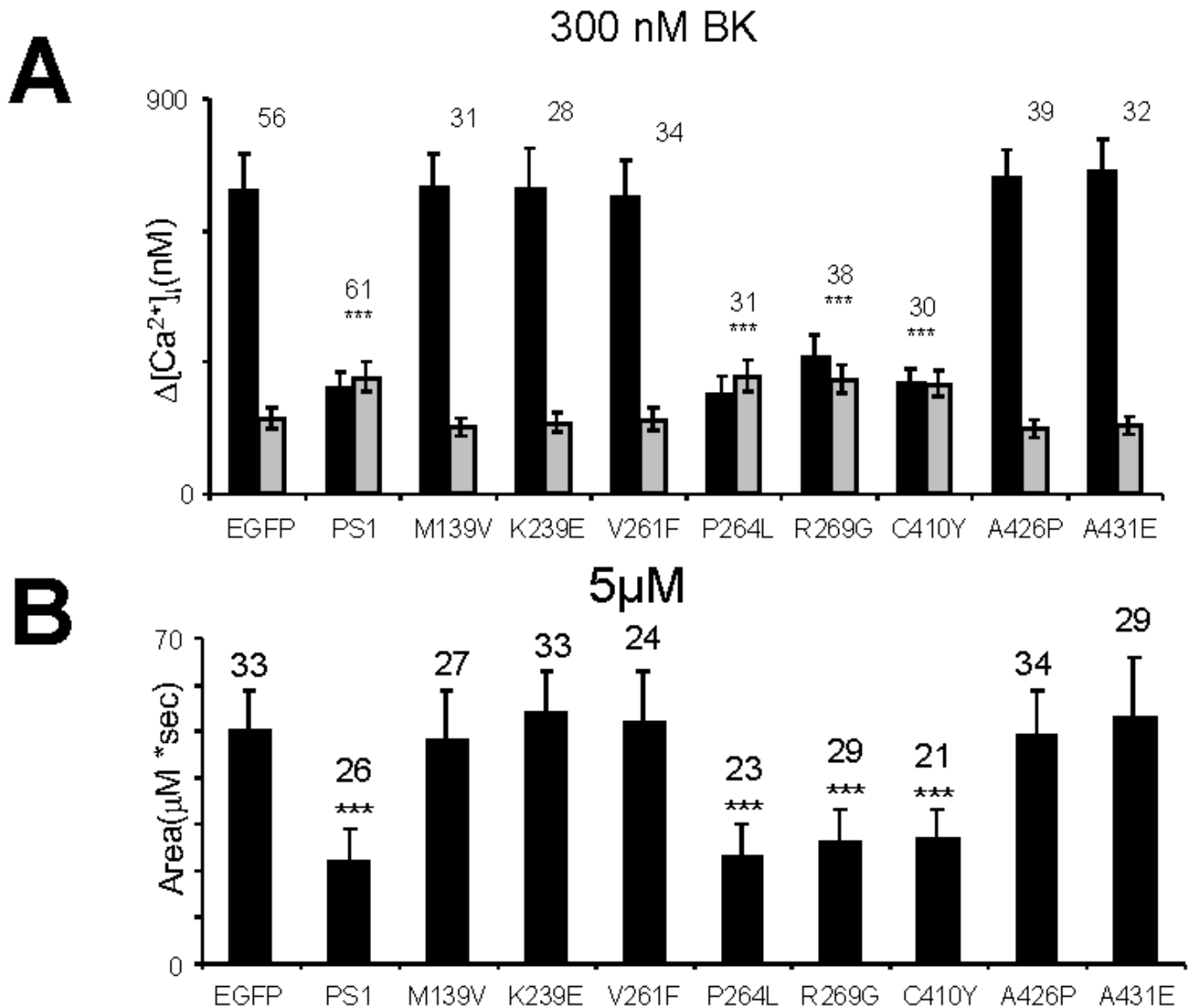


Fig 16. Summary of PS1-FAD rescue experiments. **a.** The average basal cytosolic Ca^{2+} levels (gray bars) and amplitude of BK-induced Ca^{2+} responses (black bar) is shown for DKO cells transfected with EGFP and PS1 expression constructs as mean \pm S.D. (n = number of cells analyzed). When compared to DKO cells transfected with EGFP alone, the basal Ca^{2+} levels are significantly higher (***, $p < 0.05$ by ANOVA) and the amplitude of BK-induced Ca^{2+} response is significantly smaller (***, $p < 0.05$ by ANOVA) in DKO cells transfected with EGFP + PS1, EGFP + PS1-P264L, EGFP + PS1-R269G and EGFP + C410Y combinations. There were no differences between EGFP alone and the PS1 mutations (M139V, K239E, V261F, A426P and A431E). **b.** The average size of ionomycin (IO)-releasable Ca^{2+} pool is shown for DKO cells transfected with EGFP and PS1 expression constructs as mean \pm S.D. (n = number of cells analyzed). When compared to DKO cells transfected with EGFP alone, the size of IO-releasable Ca^{2+} pool is significantly (***, $p < 0.05$ by ANOVA) smaller in DKO cells transfected with EGFP + PS1 and EGFP + PS1-P264L, EGFP + PS1-R269G and EGFP + C410Y combinations when compared to DKO cells transfected with EGFP plasmid alone.

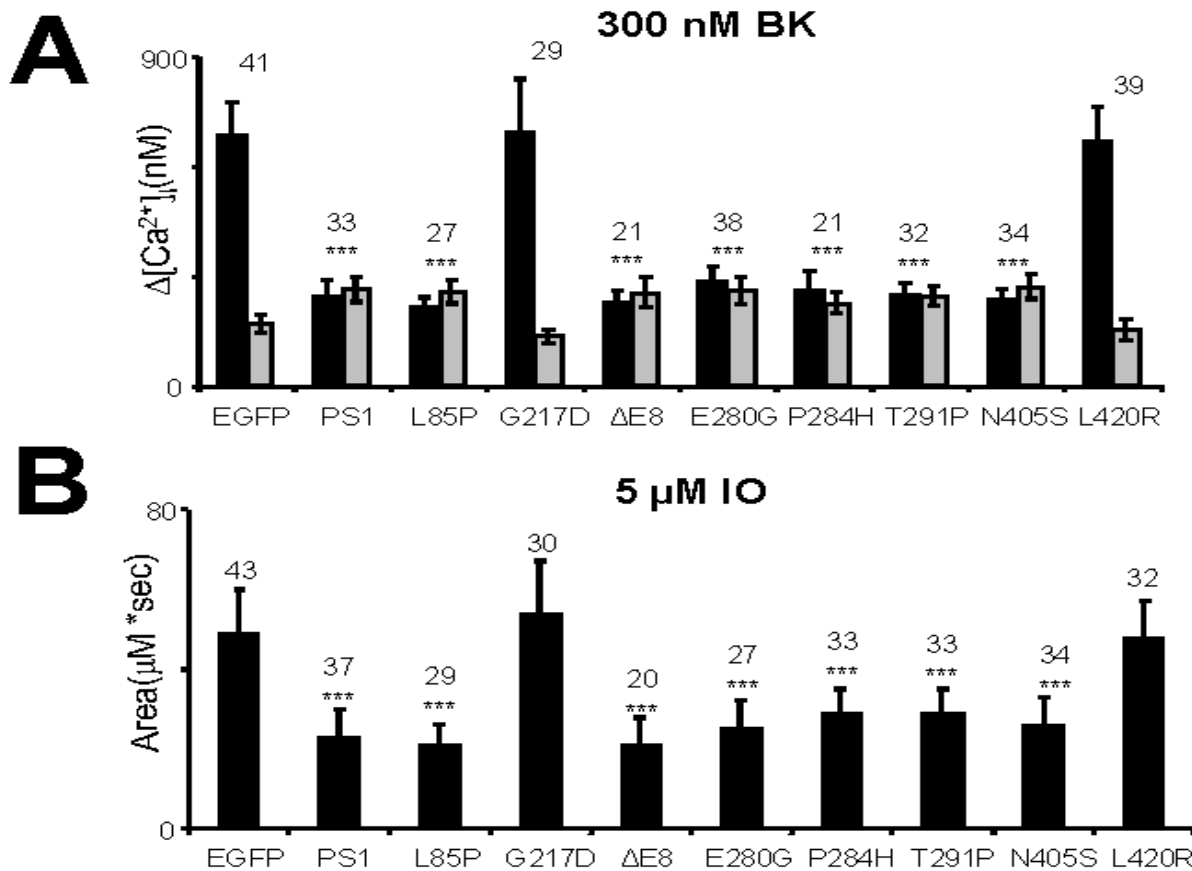


Figure 17. Summary of CWP PS1-associated rescue experiments.

a. The average basal cytosolic Ca^{2+} levels (gray bars) and amplitude of BK-induced Ca^{2+} responses (black bar) is shown for DKO cells transfected with EGFP and PS1 expression constructs as mean \pm S.D. (n = number of cells analyzed). When compared to DKO cells transfected with EGFP alone, the basal Ca^{2+} levels are significantly higher (***, $p < 0.05$ by ANOVA) and the amplitude of BK-induced Ca^{2+} response is significantly smaller (***, $p < 0.05$ by ANOVA) in DKO cells transfected with EGFP + PS1, EGFP + PS1-P85L, EGFP + PS1-P264L, EGFP + PS1-E280G, EGFP + PS1-P284H, EGFP + PS1-T291P, EGFP + PS1-N405S and EGFP + $\Delta E8$ combinations. There was no significant difference with EGFP alone compared to EGFP + PS1-G217D and EGFP + PS1-L420R. **b.** The average size of ionomycin (IO)-releasable Ca^{2+} pool is shown for DKO cells transfected with EGFP and PS1 expression constructs is shown as mean \pm S.D. (n = number of cells analyzed). When compared to DKO cells transfected with EGFP alone, the size of IO-releasable Ca^{2+} pool is significantly (***, $p < 0.05$ by ANOVA) smaller in DKO cells transfected with EGFP + PS1 and EGFP + PS1-P85L, EGFP + PS1-E280G, EGFP + PS1-P284H, EGFP + PS1-T291P, EGFP + PS1-N405S and EGFP + $\Delta E8$ combinations when compared to DKO cells transfected with EGFP plasmid alone. There was no significant difference with EGFP alone compared to EGFP + PS1-G217D and EGFP + PS1-L420R.

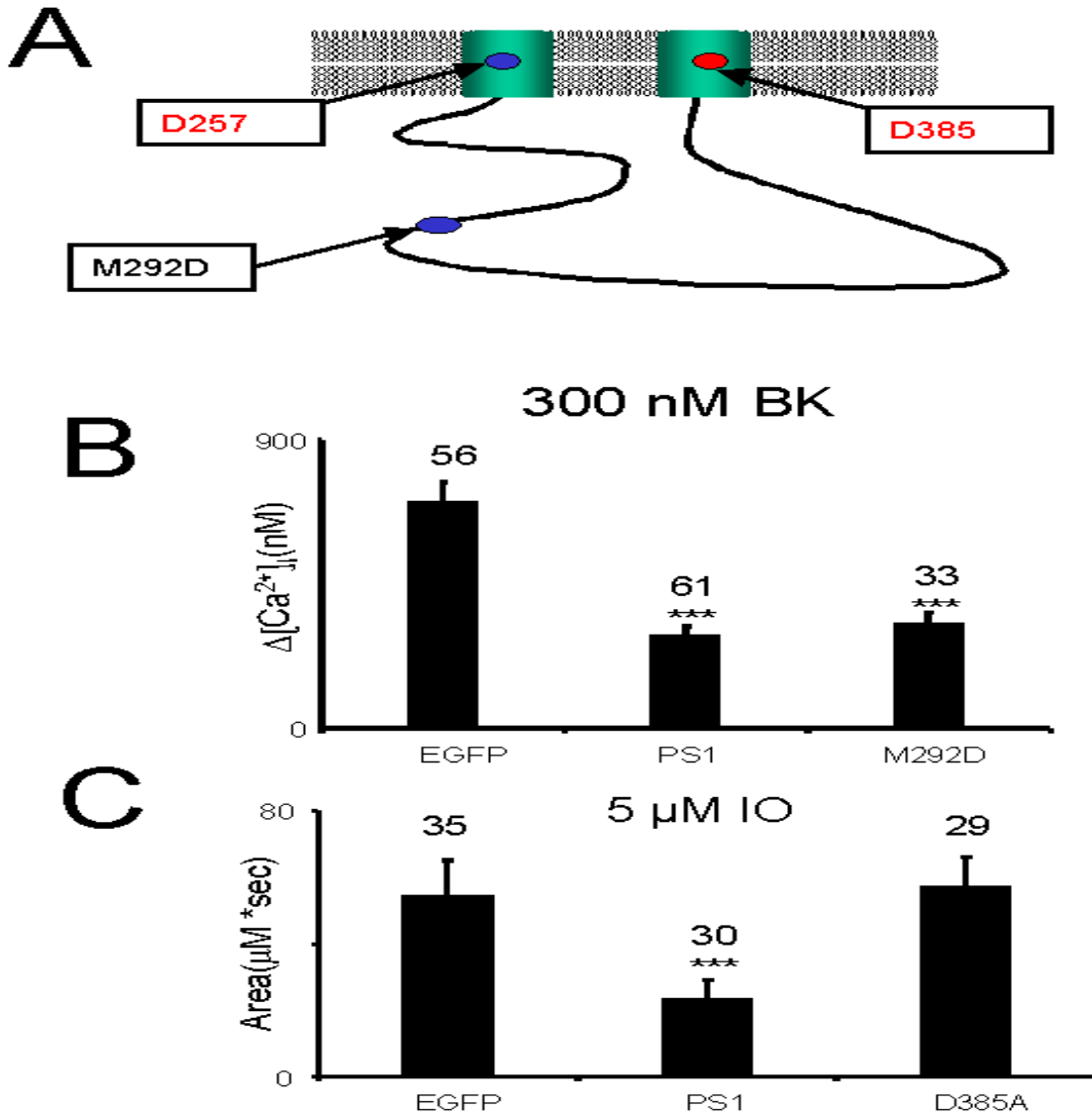


Fig 18. Effect of Uncleavable PS1-M292D and γ -secretase mutant on ER Ca²⁺ leak.

a. PS1 TM 6 and 7 showing the location of D257(blue circle) and D385(red circle) respectively. Uncleavable PS1 mutant M292D (blue circle) is shown in the hydrophilic loop between TM 6 and 7. **b.** The amplitude of BK-induced Ca²⁺ responses are shown for DKO cells transfected with EGFP only, EGFP +WT-PS1 and EGFP + M292D expression constructs as mean \pm S.D. (n = number of cells analyzed). When compared to DKO cells transfected with EGFP alone, the amplitude of BK-induced Ca²⁺ response is significantly smaller (***, p < 0.05 by ANOVA) in DKO cells transfected with EGFP + PS1 and EGFP + M292D combinations. **c.** The average size of ionomycin (IO)-releasable Ca²⁺ pool is shown for DKO cells transfected with EGFP only, EGFP+ WT-PS1and EGFP + D385A expression constructs is shown as mean \pm S.D. (n = number of cells analyzed). When compared to DKO cells transfected with EGFP alone, the size of IO-releasable Ca²⁺ pool is significantly (***, p < 0.05 by ANOVA) smaller in DKO cells transfected with EGFP + PS1, while there were no significant difference between EGFP + PS1-D385A combinations.

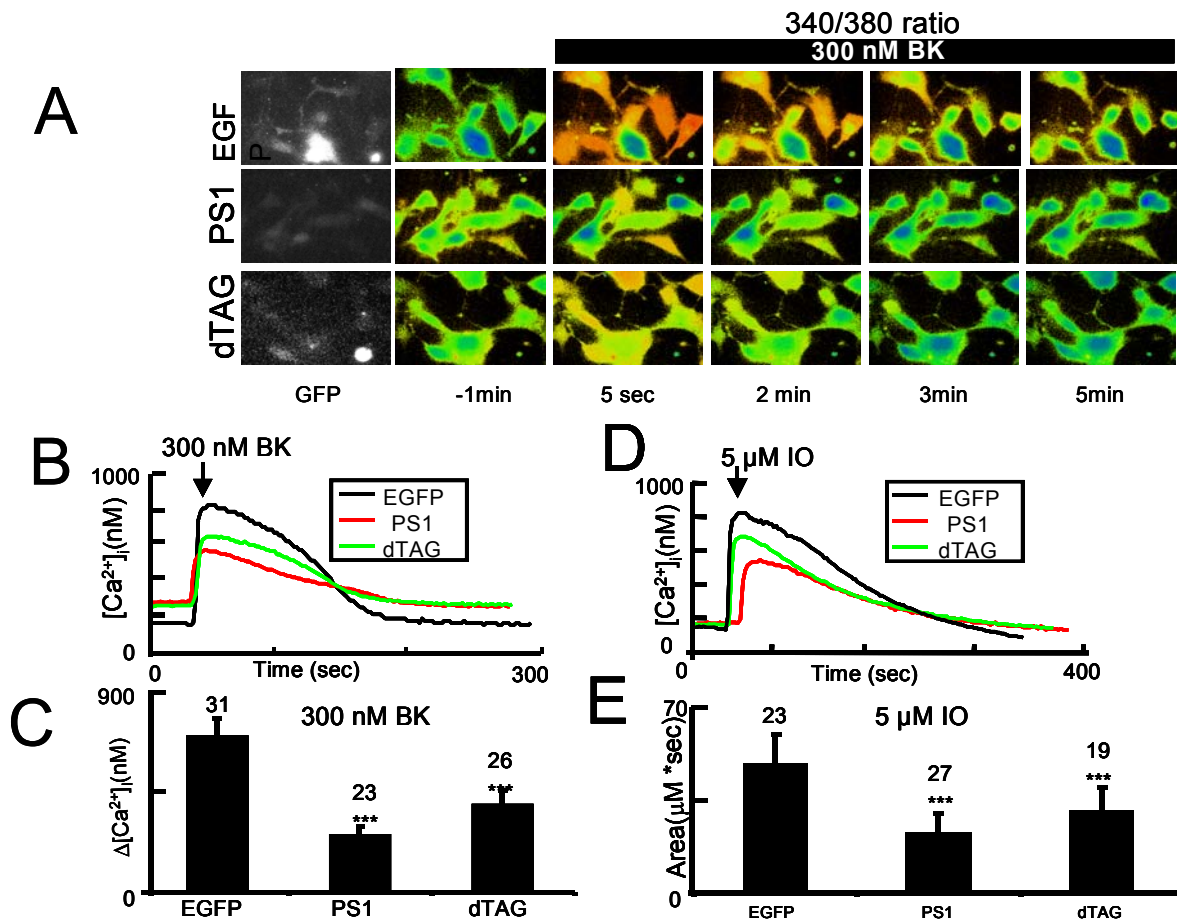


Figure 19. Ca²⁺ signals in PS1 targeting construct (dTAG)

a. The representative images of Bradykinin (BK)-induced Ca²⁺ responses in DKO MEF transfected with EGFP, EGFP + WT-PS1 and EGFP + dTAG expression plasmid as indicated. The 340/380 Fura-2 ratio images are shown prior to application of BK (-1 min) and 5sec, 2 min, and 5 min after BK application as indicated. The 340/380 Fura-2 ratios are presented using pseudocolor scale (the calibration bar is shown below). The GFP images (first column) were used to identify transfected cells. The representative Ca²⁺ traces recorded in individual transfected DKO cells are shown for each expression construct on the right.

b. The time course of BK-induced Ca²⁺ signals in representative experiments with EGFP, EGFP + WT-PS1 and EGFP + dTAG expression plasmid as indicated.

c. The average amplitude of BK-induced Ca²⁺ release is shown as mean ± S.D. (n = number of cells analyzed) for EGFP, EGFP + WT-PS1 and EGFP + dTAG expression plasmid in DKO cells. When compared to EGFP only, the amplitude of BK-induced Ca²⁺ response is significantly (***, p < 0.05) smaller in EGFP + WT-PS1 and EGFP + dTAG in DKO.

d. The time course of ionomycin (IO)-induced Ca²⁺ signals in representative experiments with EGFP, EGFP + WT-PS1 and EGFP + dTAG expression plasmid as indicated.

e. The average size of IO-sensitive Ca²⁺ pool is shown as mean ± S.D. (n = number of cells analyzed) for EGFP, EGFP + WT-PS1 and EGFP + dTAG expression plasmid as indicated. When compared to EGFP only, the size of IO-sensitive Ca²⁺ pool is significantly (***, p < 0.05) smaller in EGFP + WT-PS1 and EGFP + dTAG expression plasmid in DKO.

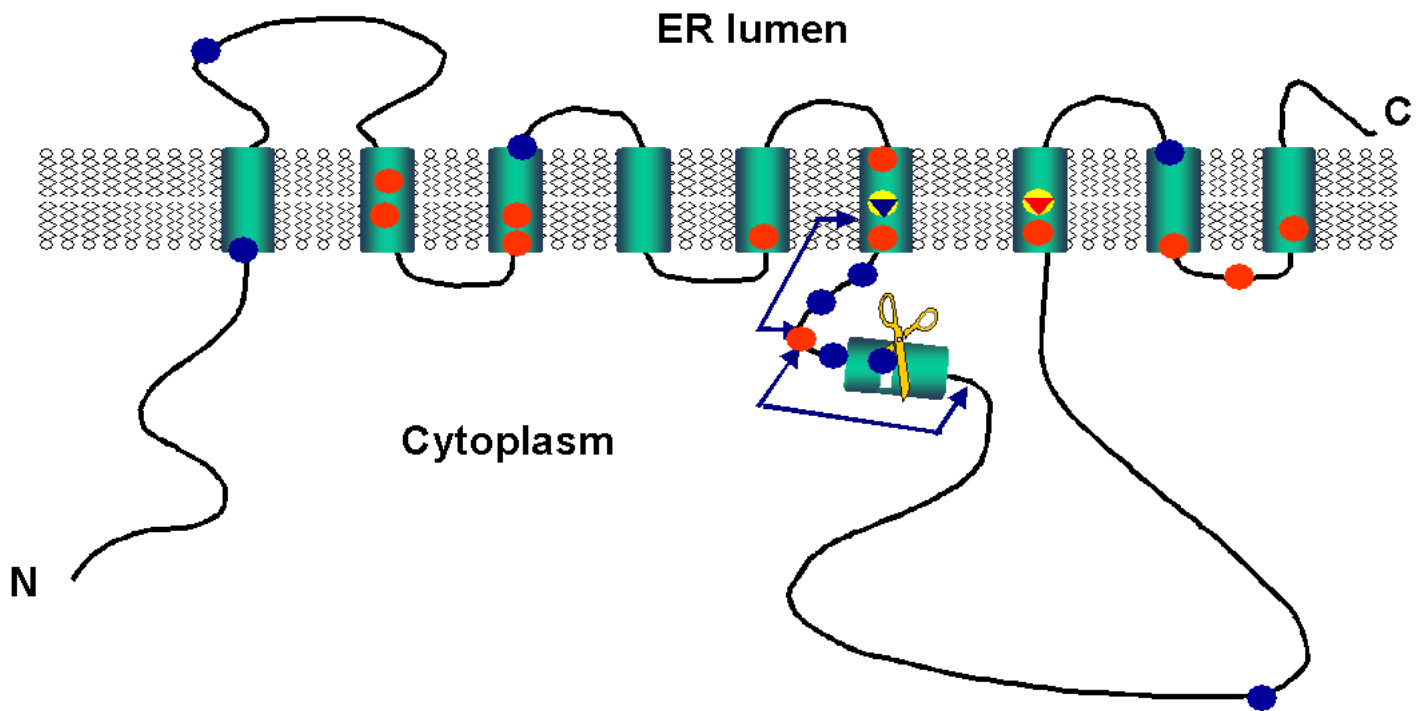


Fig 20. Molecular model of presenilins with mutations. Mutations examined are listed as red, yellow and blue dots. Loss of function(red)- M139V, M146V(L), H163Y, L166P, G217D, K239E, A246E, V261F, E273A, G384A, A426P, A431E, P436Q, Functional (blue)- A79V, L85P, L113P, G183V, P264L, R269G, Δ E8, Δ E9, E280G, T291P, Rins352, N405S, C410Y and γ -Secretase mutants(yellow)-D257A, D385A.

CHAPTER FOUR

The role of Presenilin 1 transmembrane domain 6, 7 and 9 in Endoplasmic Reticulum

Calcium leak.

Abstract

The multi-protein complex γ -secretase consists of four distinct proteins that play different roles in its ability to recognize and cleave its substrates. The γ -secretase complex is responsible for the cleavage of the amyloid precursor protein (APP) and other type I transmembrane proteins. It is known that among the subunits of γ -secretase; nicastrin, Aph-1, pen-2 and PSs, that the presenilins (PS1 and PS2) function as the catalytic subunit. Presenilins are multi-spanning membrane proteins that depend on two aspartate residues (D257 and D385) in transmembrane 6 and 7 to carry out their proteolytic activity. Substitution of D257 and D385 or knock out of presenilins inhibits the substrate cleavage of the γ -secretase complex. However, the mechanism of carrying out such a function is not completely understood. We recently discovered that presenilins also function as passive endoplasmic reticulum calcium (Ca^{2+}) leak channels and that most PSs Familial Alzheimer's disease (FAD) mutations tested affected their ability to function as an ER Ca^{2+} leak channel. The machinery that drives PSs to function as an ER leak channel is poorly understood. However, it has been shown that the catalytic core of presenilin between TM 6 and 7 is filled with water and that this is important for its ability to function as a protease. In addition, it has been shown that TM 9 of PS1 determines the dynamic conformation of the catalytic site for the γ -secretase complex. These observations are suggestive of PSs to function as a channel because the water cavity may aid in the passage of ion across its conductance pore and TM 9 may function as a gating mechanism for the conductance pore. Here we will use Ca^{2+} imaging experiments to examine the effects of cysteine-substituted residues in TM 6,7 and 9, so that we can evaluate if these TM are important in aiding ion passage through the conductance pore of the PSs. Also we will be able to decipher which residues in

each TMs are important for ion conductance depending on whether they affect ER Ca²⁺ leak or not. From our result we observed that cysteine-less mPS1 was able to function as an ER Ca²⁺ leak channel. T245C, S254 and A260C of TM6 abolished ER Ca²⁺ leak, while the other TM 6 residues did not affect ER Ca²⁺ leak. E376C, G382C, G384C, D385C, I387C, and Y389C of TM7 abolished ER Ca²⁺ leak, the other residues had no effect on ER Ca²⁺ leak. L435C, P436C, I439C, F441C, F455C, Y446C, F447C and T449C of TM 9 abolished ER Ca²⁺ leak, the other residues did not have any effect on ER Ca²⁺ leak.

Introduction

Presenilins (PSs) belong to the aspartic protease family of proteins and they are involved in the regulation of transmembrane proteolysis, a mechanism that is used to cleave peptide bonds within the lipid bilayer (Urban S. 2002), (Brown 2000). Presenilins are 50 kD proteins that contain 9 transmembrane domains (Laudon, Hansson et al. 2005; Spasic, Tolia et al. 2006) and reside in the endoplasmic reticulum (ER) membrane (Annaert, Levesque et al. 1999) with its N terminus oriented towards the cytosol and the C terminus toward the extra cellular space. Mutation of either D257 or D385 in TM 6 and 7, respectively, abolishes the catalytic activity of PSs as well as binding to the transition state of inhibitors of γ -secretase (Wolfe, Xia et al. 1999) (Esler WP 2000) (Li YM 2000). The complex of presenilins with nicastrin, aph-1 and pen-2 subunits is transported to cell surface and endosomal structures; and functions as γ -secretase, which cleaves the amyloid precursor protein (APP) and releases the amyloid β -peptide (A β), the principal constituent of the amyloid plaques in the brains of AD patients. Consistent with the role of presenilins as the catalytic subunits of γ -secretase

(De Strooper, Saftig et al. 1998; Wolfe, Xia et al. 1999), FAD mutations in presenilins affect APP processing. Currently there are 156 mutation in PS1 and 10 in PS2 that result in FAD with early onset. FAD-linked mutations are missense mutations that are mostly located within transmembrane domains of presenilins (Fig 1A). The PS1 and PS2 holoproteins undergo endoproteolysis in the cytosolic loop between TM domains 6 and 7, resulting in the generation of a 35 kD amino-terminal fragment (PS-NTF) and a 18-20 kD carboxy-terminal fragment (PS-CTF), which remain associated with each other (Thinakaran, Borchelt et al. 1996; De Strooper, Beullens et al. 1997; Yu, Chen et al. 1998). Cleavage of presenilins occurs only after incorporation into a ~440 kDa complex which also contains nicastrin, aph-1 and pen-2 subunits (Edbauer, Winkler et al. 2003; Kimberly, LaVoie et al. 2003; Takasugi, Tomita et al. 2003; Lazarov, Fraering et al. 2006). Following assembly, the “mature” complex of PS-NTF: PS-CTF, nicastrin, aph-1 and pen-2 travel towards the cell surface and get incorporated into the plasma membrane.

In addition to changes in APP processing and other type 1 transmembrane proteins, many FAD mutations in presenilins result in deranged calcium (Ca^{2+}) signaling (reviewed in (Smith, Green et al. 2005)). Although the connection between FAD mutations in presenilins and abnormal Ca^{2+} signaling has been known for over a decade (Ito, Oka et al. 1994), the mechanistic explanation to these finding has been controversial (Smith, Green et al. 2005). Recently, we discovered that presenilins function as passive endoplasmic reticulum Ca^{2+} leak channels (Tu, Nelson et al. 2006). We further found that M146V/L, L166P, A246E, E273A, G384A, P436Q, PS1- Δ E9 and PS2-N141I FAD mutations in presenilins affected their ER Ca^{2+} leak function (Tu, Nelson et al. 2006), while FTD associated mutant and FAD A79V did not. We also used

Ca²⁺ imaging experiments in lymphoblast from AD patients to evaluate ER Ca²⁺ leak in (PS1-M139V, M146L, K239E, V261F, P264L, R269G, C410Y, A426P, A431E, ΔE9 and PS2-N141I), tau-R406W, APP-V717L and sporadic AD cases. In addition, Ca²⁺ rescue experiments were performed in PS-null MEF with the PS1 FAD mutations from the lymphoblast cell line, FAD PS1 (L85P, G217D, E280G, T291P, N405S, L420R and ΔE8) and PS1-P284H a non-FAD mutation. From the PS1 FAD mutation tested G217D, P264L, E280G, T291P, ΔE8, ΔE9, C410Y, N405S and L420R resulted in CWP from patient studies. We showed that PS1 (M139V, M146L, G217D, K239E, V261F, L420R, A426P, A431E and PS2-N141I abolished ER Ca²⁺ leak, while PS1 mutations L85P, ΔE8, ΔE9, P264L, R269G, E280G, P284H, T291P, C410Y and N405S had no apparent effect. Mutations in tau-R406W, APP-V717L and sporadic AD had no effect of ER Ca²⁺ leak in lymphoblast (Nelson et al., unpublished). From our results we conclude that most of the FAD PS1 mutation tested abolished ER Ca²⁺ and that most of the FAD mutation that were functional had the CWP phenotype in AD patients. PS1-P284H, tau-R406W, APP-V717L and sporadic AD cases did not have any apparent effect on ER Ca²⁺ leak. These observations suggest that PSs play a pivotal role in deranged Ca²⁺ in AD and they also provided further support for the contribution of disturbed Ca²⁺ homeostasis to AD pathogenesis (Khachaturian 1989; Mattson, LaFerla et al. 2000; LaFerla 2002; Smith, Green et al. 2005).

However, these results do not explain how PSs are able to function as a channel and what TMs are important for forming the conductance pore of PSs. It has been shown by Bart De Strooper's group that TM 6 and 7 of PS1 contributes to the water-containing cavity in the γ-secretase complex (Tolia, Chavez-Gutierrez et al. 2006). His group also showed that TM 9 of PS1 determines the dynamic confirmation of the catalytic site for

the γ -secretase complex (Alexandra Tolia 2008). Here we set out to examine the effects of cysteine-substituted residues in TM 6,7 and 9. These results will help us to understand which TM is important in aiding ion passage through the conductance pore of the PSs. They will also provide informative data on which residues in each TMs are important for ion conductance depending on whether they affect ER Ca^{2+} leak or not. We observed that cysteine-less mPS1 was able to function as an ER Ca^{2+} leak channel. T245C, S254 and A260C of TM6 abolished ER Ca^{2+} leak, while the other TM 6 residues did not affect ER Ca^{2+} leak. E376C, G382C, G384C, D385C, I387C, and Y389C of TM7 abolished ER Ca^{2+} leak, the other residues had not effect on ER Ca^{2+} leak. L435C, P436C, I439C, F441C, F455C, Y446C, F447C and T449C of TM 9 abolished ER Ca^{2+} leak, the other residues did not have any effect on ER Ca^{2+} leak.

Results

Model of Mouse Presenilin 1 (mPS1)

According to the latest topological data, presenilins spans the membrane 9 times with the amino-terminus in the cytosol and carboxy-terminus in the ER lumen (Laudon, Hansson et al. 2005; Oh and Turner 2005; Spasic, Tolia et al. 2006)(Fig 21A). Previously, an 8 transmembrane (TM) domain model was widely used (Tandon and Fraser 2002). FAD-linked mutations are missense mutations are mostly located within transmembrane domains of the presenilins (Fig 1). The location of TM 6, 7 and 9 (highlighted in blue) that were examined in this study is shown in Fig 21A. The cysteine residues examined in each TM is highlighted in Fig 21B. The PS1 and PS2 holoproteins undergo endoproteolysis in the cytosolic loop (yellow circle) between TM domains 6 and 7 (Fig 21A), resulting in the generation of a 35 kD amino-terminal fragment (PS-NTF)

and a 18-20 kD carboxy-terminal fragment (PS-CTF), which remain associated with each other (Thinakaran, Borchelt et al. 1996; De Strooper, Beullens et al. 1997; Yu, Chen et al. 1998).

Effects of cysteine-less mPS1 on ER Ca²⁺ leak

In our experiments we will use the cysteine-substituted residues in TM 6, 7 and 9 to identify the residues lining ion permeation pore of PS1 holoprotein. In designing our experiments we will capitalize on recent application of cysteine mutants to study γ -secretase function of PS1 in Bart De Strooper's laboratory (Tolia, Chavez-Gutierrez et al. 2006) (Alexandra Tolia 2008). These investigators generated Cys-less mPS1 by mutating the 5 endogenous cysteines in the mouse PS1 sequence to alanines (Tolia, Chavez-Gutierrez et al. 2006). They further demonstrated that Cys-less mPS1 was able to support γ -secretase function in DKO MEF stable transfection experiments, similar to wild type mPS1 (Tolia, Chavez-Gutierrez et al. 2006). Is the ER Ca²⁺ leak function also intact in Cys-less mPS1? To answer this question we evaluated the ability of Cys-less mPS1 construct to rescue ER Ca²⁺ leak pathway deficiency in DKO cells. Our collaborator Bart De Strooper provided us with wild type mPS1 and Cys-less mPS1 constructs and stable DKO rescue lines (Tolia, Chavez-Gutierrez et al. 2006) to facilitate these experiments. In agreement with the previous studies of hPS1 rescue lines (Tu, Nelson et al. 2006) we found that the application of 5 μ M ionomycin (IO) resulted in high amplitude and long lasting Ca²⁺ signals in DKO cells and attenuated Ca²⁺ signals in mPS1 DKO cell line (Fig 22A). The IO-induced Ca²⁺ signals in Cys-less PS1 rescue line were similar to Ca²⁺ signals in mPS1 rescue line (Fig 22A). On average, the area under the IO-induced Ca²⁺ signals were equal to $56 \pm 11 \mu\text{M}\cdot\text{sec}$ (n = 19) in DKO cells, $23 \pm 6 \mu\text{M}\cdot\text{sec}$ (n = 53) in mPS1 rescue cells, and $26 \pm 8 \mu\text{M}\cdot\text{sec}$ (n =

47) in Cys-less mPS1 rescue cells (Fig 22B, 22D). From these results we reasoned that expression of Cys-less mPS1 construct restored ER Ca²⁺ leak pathway deficiency in DKO cells and restored the content of ER Ca²⁺ stores to wild type levels. These conclusions were further supported by direct measurements of ER Ca²⁺ concentrations using Mag-Fura-2 (Tu, Nelson et al. 2006) (Nelson, Tu et al. 2007). We found that the [Ca²⁺]_{ER} concentration was equal to 183 ± 42 μM (n = 32) in DKO cells, 107 ± 23 μM (n = 39) in mPS1 rescue cells, and 91 ± 17 μM (n = 42) in Cys-less mPS1 rescue cells (Fig 22C, 22D). From these stable rescue experiments we concluded that Cys-less mPS1 protein is able to support ER Ca²⁺ leak function similar to the wild type mPS1.

Effects of cysteine-substitution in mPS1 TM 6, 7 and 9 on ER Ca²⁺ leak

It has been shown by Bart De Strooper's group that TM 6 and 7 of PS1 contributes to the water-containing cavity in the γ-secretase complex (Tolia, Chavez-Gutierrez et al. 2006). His group also showed that TM 9 of PS1 determines the dynamic confirmation of the catalytic site for the γ-secretase complex and that Hydrophobic domain VII, plays an important role in allowing water entry in the water cavity of PS1 (Alexandra Tolia 2008). In addition they showed that by using the substituted-cysteine-accessibility method that W247 of TM 6, G382, G384, D385, F388, Y389 and K395 of TM 7 and all the residues of TM 9 were exposed to water. These results did not explain how PSs are able to function as a channel or what TMs are important for forming the conductance pore of PSs. The conservation of ER Ca²⁺ leak function in Cys-less mPS1 protein provides a basis for application of for TM 6, 7 and 9. Bart De Strooper and his colleagues already generated a series of cysteine mutants in TM 6, 7 and 9 of Cys-less mPS1 (Fig 21) (Tolia, Chavez-Gutierrez et al. 2006) (Alexandra Tolia 2008). In order to

evaluate which residues abolished ER Ca^{2+} leak, we use Ca^{2+} imaging experiments to measure the ionomycin releasable pool in MEF stable cell lines carrying a cysteine mutation in each TM. When compared to wild type MEF, IO induced high amplitude and long lasting Ca^{2+} signals in T245C, S254 and A260C of TM6, while there were no difference seen in the curves of W247C, L250C, V255C, D257C, L258C, V259C, V261C, L262C and P264C (data not shown). From these results we reason that T245C, S254 and A260C abolished ER Ca^{2+} leak and lead to higher Ca^{2+} in the ER stores. On average the area under the IO curves was two times higher in T245C, S254 and A260C compared to W247C, L250C, V255C, D257C, L258C, V259C, V261C, L262C and P264C (Fig 23A and table 2). On average the area under the IO curves was two times higher in E376C, G382C, G384C, D385C, I387C, and Y389C of TM7 compared to G378C, K380C, L381C, L383C, F388C, S390C, L392C, G394C and K395C (Fig 23B and table 2). On average the area under the IO curves was two times higher in L435C, P436C, I439C, F441C, F445C, Y446C, F447C and T449C compared to P433C, A434C, I437C, S438C, T440C, G442C, V444C, Y451C, L452C, V253C, Q454C and P455C (Fig 23C and Table 2).

Effect of PS1 hydrophilic loop deletion on ER Ca^{2+} leak

From our previous data we found that PS1- Δ E8 (Nelson et al., unpublished) and PS1- Δ E9 (Tu, Nelson et al. 2006) were functional for ER Ca^{2+} leak. These FAD mutations are deletions of exon 8 and 9 respectively. Both PS1- Δ E8 and Δ E9 results in partial deletion of the hydrophobic domain VII (HDVII-yellow circle Fig 21A), that is thought to regulation water entry into the water cavity between TM6 and 7 (Alexandra Tolia 2008). From these data we wanted to test whether deletion of the hydrophilic loop between TM

6 and 7 affected ER Ca^{2+} leak. Bart de Strooper provided use with the stable cell line expressing mPS1- Δ loop (D302-E372). When compared to wild type MEF, IO induced high amplitude and long lasting Ca^{2+} signals in mPS1- Δ loop, while there were no differences seen in the curves of DKO-MEF (data not shown). On average, the area under the IO-induced Ca^{2+} signals were equal to $56 \pm 11 \mu\text{M}\cdot\text{sec}$ ($n = 45$) in DKO cells, $20 \pm 5 \mu\text{M}\cdot\text{sec}$ ($n = 41$) in mPS1 rescue cells, and $55 \pm 12 \mu\text{M}\cdot\text{sec}$ ($n = 57$) in mPS1- Δ loop rescue cells (Fig 24A). From these data we reasoned that mPS1- Δ loop was a loss of function for ER Ca^{2+} leak.

It was very interesting to note that Bart's groups discovered a proline at position 433 of the PAL domain of PS1 was pivotal in the flexibility of TM 9. They showed that mutation of P443 to either Ala or leu caused the mutated protein to be in an open confirmation, and this rendered the water cavity more accessible to water and γ -secretase substrates, however, cleavage of substrate did not occur. With these observations we tested the effects of P433A and P433L on ER Ca^{2+} leak in stable MEFs. On average, the area under the IO-induced Ca^{2+} signals were equal to $56 \pm 11 \mu\text{M}\cdot\text{sec}$ ($n = 45$) in DKO cells, $20 \pm 5 \mu\text{M}\cdot\text{sec}$ ($n = 41$) in mPS1 rescue cells, $25 \pm 6 \mu\text{M}\cdot\text{sec}$ ($n = 39$) in P433A and $19 \pm 6 \mu\text{M}\cdot\text{sec}$ ($n = 44$) in P433L (Fig 24B).

Discussion

In the present study we use Ca^{2+} Imaging experiments to investigate the effect of cysteine substitution in TM 6, 7 and 9 of PS1 on ER Ca^{2+} leak. In addition we examined PS1 mutants that are know to affect γ -secretase activity. We found that several of the mutants that were examined affected PS1 ability to function as an ER Ca^{2+} leak

channel. We also observed that a number of substitutions that were exposed to water based on the work of (Tolia, Chavez-Gutierrez et al. 2006) (Alexandra Tolia 2008) affected PS1 ability to function as an ER leak Ca^{2+} channel. Interestingly, the cys-less mPS1 construct was able to maintain γ -secretase (Tolia, Chavez-Gutierrez et al. 2006) and ER Ca^{2+} leak (Fig 22). From the constructs tested T245C, S254 and A260C of TM6, E376C, G382C, G384C, D385C, I387C, and Y389C of TM7 and L435C, P436C, I439C, F441C, F445C, Y446C, F447C and T449C of TM9 where loss of function for ER Ca^{2+} leak (Fig 25, red circles). From the cys-mutants examined that were loss of function E376C, G384C, D385C, I387C, Y389C, L435C, P436C, I439C, F441C, F445C, Y446C, F447C and T449C were exposed to water based on the work from Tolia et al. W247C, L381C, L383C, F388C, K395C, P433C, A434C, I437C, S438C, T440C, G382C, V444C, Y451C, L452C, V253C, Q454C and P445C were exposed to water and functional in our assay. Where is the conductance pore of PS1 and how is it regulated? What insight does the Ca^{2+} data gives us about pore regulation? It has been shown by Bart De Strooper's group that TM 6 and 7 of PS1 contributes to the water-containing cavity in the γ -secretase complex (Tolia, Chavez-Gutierrez et al. 2006). His group also showed that TM 9 of PS1 determines the dynamic confirmation of the catalytic site for the γ -secretase complex (Alexandra Tolia 2008). The data from this study does not tell us exactly where is the conductance pore, that would have to be validated with the crystal structure of PS1. The "loss of function" cys-mutants from our study do point to key residues that are important for maintaining the integrity of the conductance pore of PS1. In addition, we do observe that either exposed or none-exposed residues to water can affect ion conductance and that these amino acids range from bulky to small residues (Fig 25, table 2). How does PSs function as a leak channel? Is the mechanism

of the catalytic site regulation similar to the ion channel regulation of PS1? Based on (Alexandra Tolia 2008) in their experiments they were able to cross link TM6 and 9, but not TM 7 and 9, because of their distance of separation and from the fact that HDVII (site of endoproteolysis by presenilinase) (Thinakaran, Borchelt et al. 1996) that is embedded in the water cavity inhibits such an interaction. The cross linking results indicate the arrangement of the TMs in the catalytic cavity; in addition, it could also serve as a topology for the conductance pore for PSs. As a γ -secretase, TM 6 and 7 are oppose to each other in the water cavity, with D257 and D385 facing each other, TM9 is located close to TM6 and HDVII is deep within the water cavity (Alexandra Tolia 2008). Once substrate binds in the vicinity of TM9, HDVII exits the catalytic site and by some molecular motion TM 9 moves and allows the substrate to enter the catalytic site (Alexandra Tolia 2008). From our results, TM9 had the most mutations that affected ER Ca^{2+} leak (Fig 25, table 2); this is very interesting because TM 9 is known to modulate the dynamics of the catalytic site of the γ -secretase complex. One can infer that the loss of function Ca^{2+} leak cys-mutations is inhibiting conformational changes that would allow pore opening. Cys-mutations may affect key residues that are involved in inter/intra-molecular interactions that are essential for allowing ions to pass through the conductance pore of PS1. This can be seen with Y389, which is known to form a hydrogen bond with D385 (Tolia, Chavez-Gutierrez et al. 2006); hence replacing Y with C at 389 disrupts such interaction and renders the pore inactive (Fig 25, table 2). From the helical wheel plot (Fig 4) we see that substitution of residues that are bulky and buried deep within the cavity to Cys had adverse effects on PS1 ability to function as channel (Y389, F441, F445, Y449). On the other hand we see where substitution of less bulky residues such a Gly to Cys in TM7 leads to loss of function, this maybe a

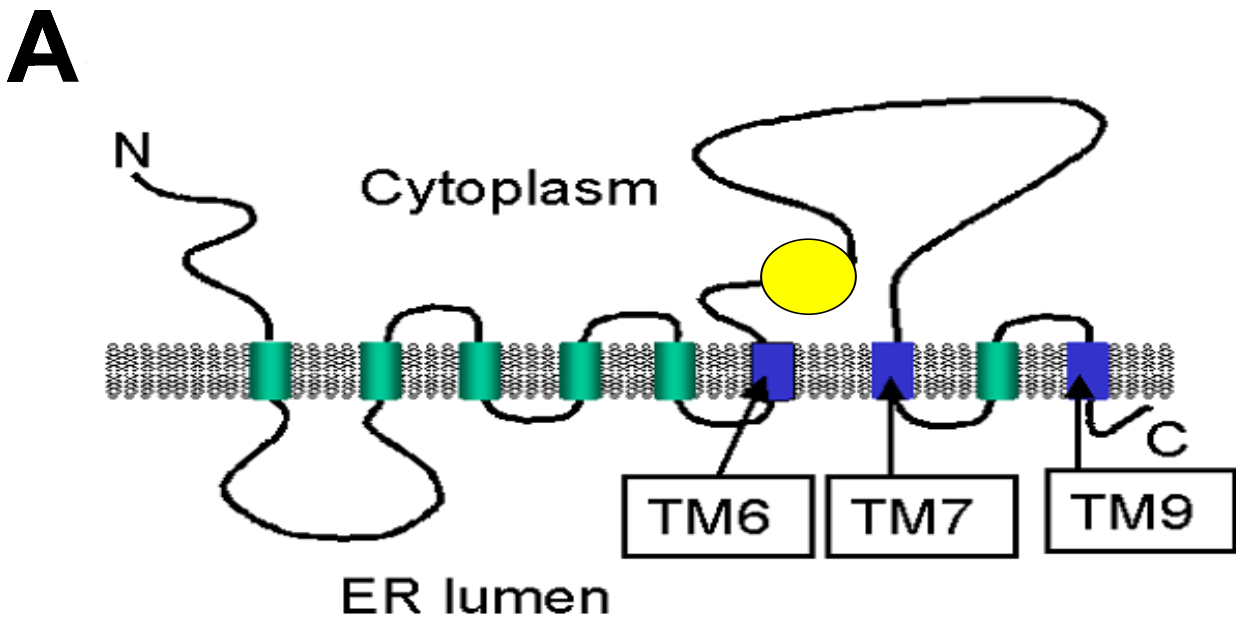
result of introducing a somewhat less flexible residue. This would have a big effect of PSs to leak ions because it is a low conductance channel (Tu, Nelson et al. 2006).

We can also speculate that loss of function Cys-mutations may not allow HDVII to exit the cavity so that water or ions may enter. We do see where truncation of HDVII (PS1- Δ E9) (Tu, Nelson et al. 2006) or PS1- Δ E8 (unpublished) leads to gain of function for Ca^{2+} leak or functional PS1, respectively. This may occur because truncation of HDVII reduces its hydrophobicity; hence water and ions are free to enter the conductance pore because its gating mechanism is abolished.

Both P433A and P433L that are known to cause PS1 to be in an open conformation for water entry (Alexandra Tolia 2008) were functional based on Ca^{2+} imaging experiments, while the deletion of the hydrophilic loop of PS1 results in a loss of function channel. From these observations we reasoned that both P433A/L allow the conductance pore of PS1 to be open and HDVII exits the water cavity. This in turn allowed the passage of ions across the channel more readily. On the other hand the hydrophilic loop deletion was a loss of function because the channel did not take on a conformation that allow ions to cross the conductance pore or HDVII got embedded in the pore and hindered ions/water entry.

In conclusion, we have provided experimental evidence for Cys-mutants in TM 6, 7 and 9 that leads to overloaded ER Ca^{2+} stores. The data from this study provided some insight into the mechanism of how the conductance pore of PSs is regulated as an ER Ca^{2+} leak channel. In addition, we have a better understanding of the role of HDVII and the hydrophilic loop of PS1 regulates ER Ca^{2+} leak. Further experiments with other TM that may be involved in the formation of the conductance pore of PSs should be tested. However, not until the crystal structure of PSs is solved most experiments will be based

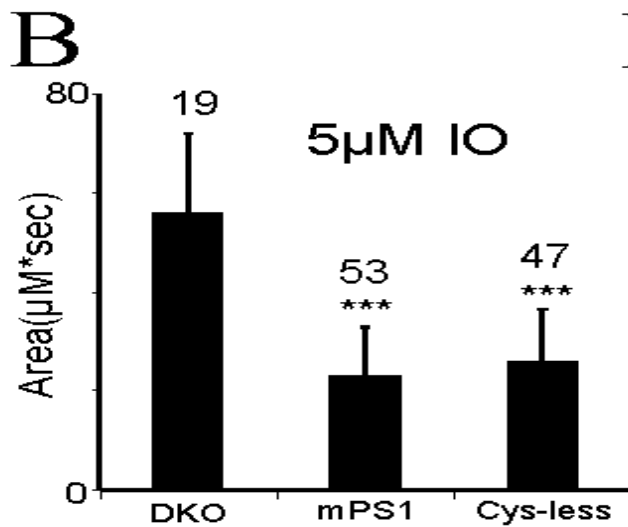
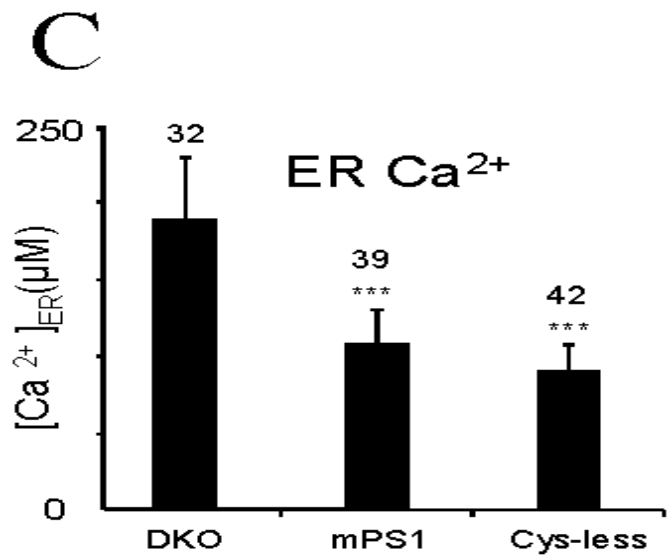
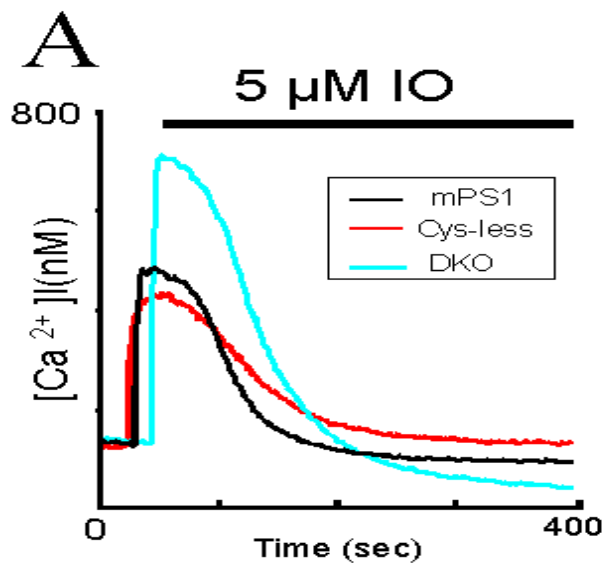
on speculation; nevertheless, they will give us key data on how PSs function as an ER Ca^{2+} leak.



B

<u>TM6</u>	<u>TM7</u>	<u>TM9</u>	<u>Control</u>
T245C	E376C	P433L	mPS1-WT
W247C	G378C	P433A	Cys-less
L250C	K380C	P433C	
S254C	L381C	A434C	
V255C	G382C	L435C	
D257C	L383C	P436C	
L258C	G384C	I437C	
V259C	D385C	S438C	
A260C	I387C	I439C	
V261C	F388C	T440C	
L262C	Y389C	F441C	
P264C	S390C	G442C	
mPS1-loop	L392C	V444C	
	G394C	F445C	
	K395C	Y446C	
		F447C	
		T449C	
		Y451C	
		L452C	
		V253C	
		Q454C	
		P445C	

Fig 21. Cys-less mPS1 and cysteine mutants. a. The individual TM that had its endogenous residues mutated to Cys is shown (blue TM). Yellow circle represents HDVII. b. All the cys mutants, control construct and mPS1- Δ loop examine in the study is shown



D

	Area IO ($\mu\text{M}\cdot\text{sec}$)	ER Ca ²⁺ (μM)
DKO	56 \pm 11	183 \pm 42
mPS1	23 \pm 6	107 \pm 23
Cys-less	26 \pm 8	91 \pm 17

Fig 22. Cys-less mPS1 rescues ER Ca²⁺ leak pathway in stably transfected DKO cells

a. IO-induced Ca²⁺ signals curves in DKO cells (blue line), DKO cells stably transfected with mPS1 (black line) and Cys-less mPS1 (red line) constructs. **b.** The average size of the ionomycin (IO)-releasable Ca²⁺ pool is shown for DKO, DKO cells stably transfected with mPS1 and Cys-less mPS1 constructs are shown as mean \pm S.D. (n = number of cells analyzed). When compared to DKO MEF, the size of IO-releasable Ca²⁺ pool is significantly (***, p < 0.05 by ANOVA) smaller in cys-less mPS1 and WT-mPS1 stable. **c.** The average ER Ca²⁺ concentrations [Ca²⁺]_{ER} are shown for DKO-MEF and DKO-MEF stably expressing mPS1 and Cys-less mPS1 cells as mean \pm S.D. (n = number of cells analyzed). When compared to DKO MEF, the [Ca²⁺]_{ER} size is significantly (***, p < 0.05 by ANOVA) smaller in cys-less mPS1 and WT-mPS1 stable. **d.** The summary of DKO-MEF, WT-mPS1 and Cys-less mPS1 stable DKO rescue experiments.

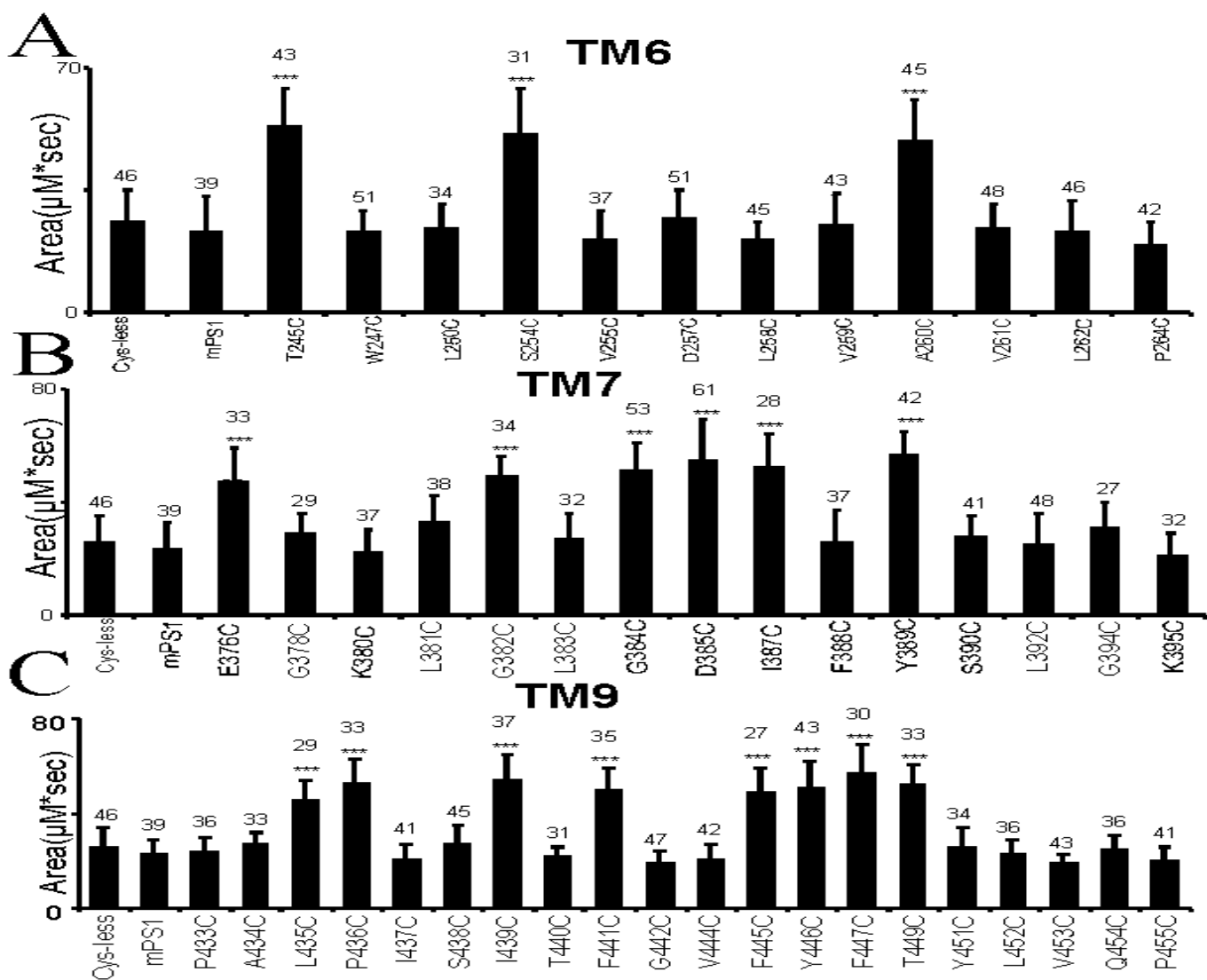


Fig 23. Summary of TM 6, 7 and 9 IO releasable Ca²⁺ ER pool. **a.** The average size of the ionomycin (IO)-releasable Ca²⁺ pool is shown for DKO cells stably expressing cysteine mutants in TM 6 are shown as mean ± S.D. (n = number of cells analyzed). When compared to cys-less mPS1 and WT-mPS1 stable, the size of IO-releasable Ca²⁺ pool is significantly (***, p < 0.05 by ANOVA) larger in T245C, S254 and A260C of TM6, while the other TM 6 residues did not shown any significant difference. **b.** The average size of the ionomycin (IO)-releasable Ca²⁺ pool is shown for DKO cells stably expressing cysteine mutants in TM 7 are shown as mean ± S.D. (n = number of cells analyzed). When compared to cys-less mPS1 and WT-mPS1 stable, the size of IO-releasable Ca²⁺ pool is significantly (***, p < 0.05 by ANOVA) larger in E376C, G382C, G384C, D385C, I387C, and Y389C of TM7, while the other TM 6 residues did not shown any significant difference. **c.** The average size of the ionomycin (IO)-releasable Ca²⁺ pool is shown for DKO cells stably expressing cysteine mutants in TM 9 is shown as mean ± S.D. (n = number of cells analyzed). When compared to cys-less mPS1 and WT-mPS1 stable, the size of IO-releasable Ca²⁺ pool is significantly (***, p < 0.05 by ANOVA) larger in L435C, P436C, I439C, F441C, F455C, Y446C, F447C and T449C of TM 9, while the other TM 6 residues did not shown any significant difference.

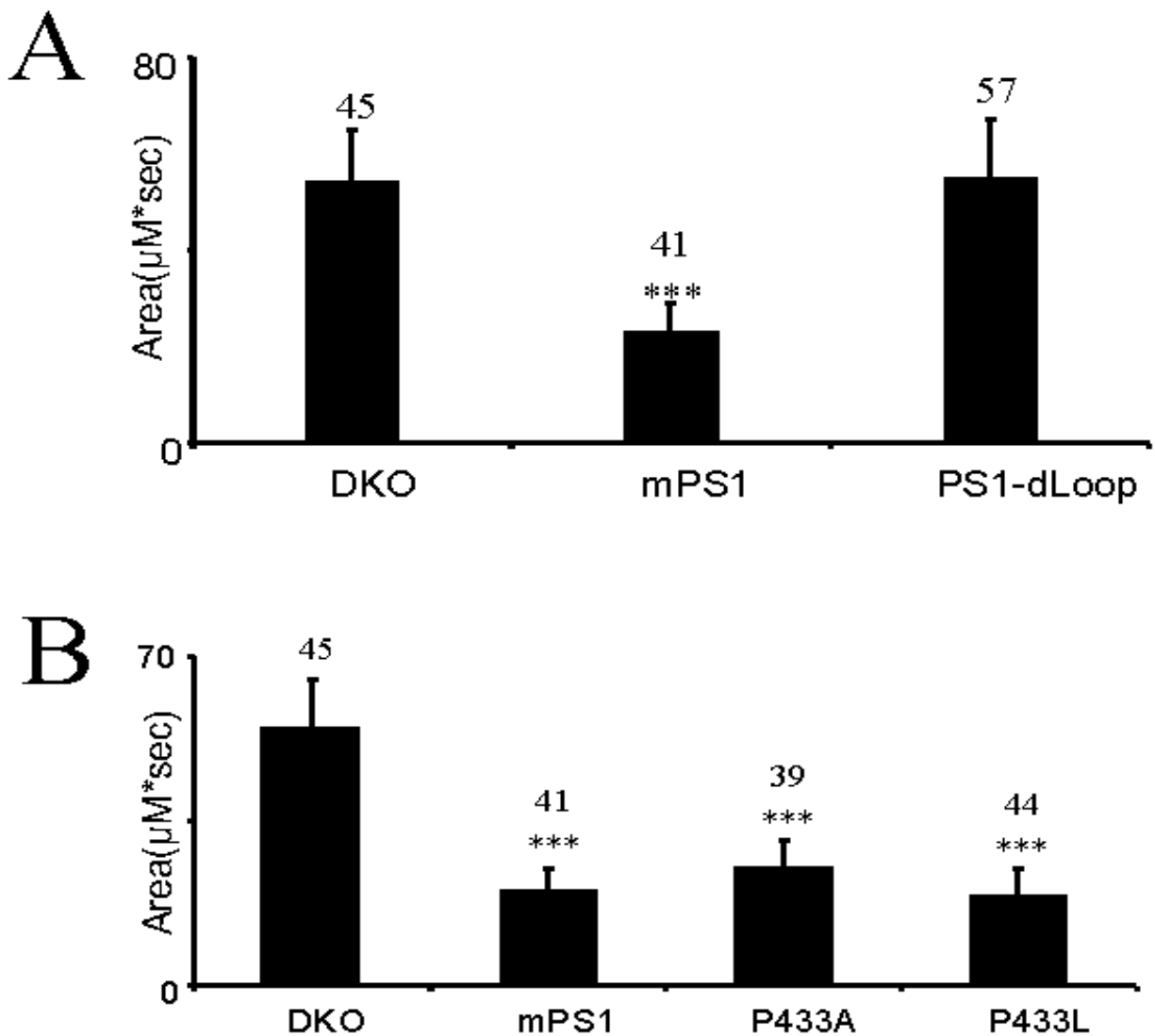


Fig 24. mPS1- Δ loop does not ER Ca^{2+} leak pathway in stably transfected DKO cells.

a. The average size of the ionomycin (IO)-releasable Ca^{2+} pool is shown for DKO-MEF, DKO cells stably transfected with mPS1 and mPS1- Δ loop constructs are shown as mean \pm S.D. (n = number of cells analyzed). When compared to DKO MEF, the size of IO-releasable Ca^{2+} pool is significantly (***, $p < 0.05$ by ANOVA) smaller in WT-mPS1 stable; however, there were no significant difference between DKO-MEF and mPS1- Δ loop.

b. The average size of the ionomycin (IO)-releasable Ca^{2+} pool is shown for DKO-MEF, DKO cells stably transfected with mPS1, mPS1-P433A and mPS1- P433L constructs are shown as mean \pm S.D. (n = number of cells analyzed). When compared to DKO MEF, the size of IO-releasable Ca^{2+} pool is significantly (***, $p < 0.05$ by ANOVA) smaller in WT-mPS1, mPS1-P433A and mPS1- P433L stable.

Control		TM6		TM7		TM9	
Construct	$\mu\text{M}\cdot\text{sec}$	Construct	$\mu\text{M}\cdot\text{sec}$	Construct	$\mu\text{M}\cdot\text{sec}$	Construct	$\mu\text{M}\cdot\text{sec}$
mPS1-WT	20 \pm 5	T245C	53 \pm 11	E376C*	47 \pm 12	P433C	24 \pm 6
Cys-less	26 \pm 8	W247C	23 \pm 6*	G378C	29 \pm 7	A434C	27 \pm 5
P433L	19 \pm 6	L250C	24 \pm 7	K380C	22 \pm 8	L435C	46 \pm 8
P443A	25 \pm 6	S254C	51 \pm 13	L381C	33 \pm 9*	P436C	53 \pm 10
mPS1- Δ loop	55 \pm 12	V255C	21 \pm 8	G382C	49 \pm 14	I437C	21 \pm 4
		D257C	27 \pm 11	L383C	27 \pm 9*	S438C	27 \pm 8
		L258C	21 \pm 5	G384C	51 \pm 10*	I439C	54 \pm 11
		V259C	25 \pm 9	D385C	55 \pm 14*	T440C	22 \pm 4
		A260C	49 \pm 12	I387C	52 \pm 12	F441C	50 \pm 9
		V261C	24 \pm 7	F388C	26 \pm 11*	G442C	19 \pm 5
		L262C	23 \pm 9	Y389C	57 \pm 15*	V444C	21 \pm 6
		P264C	19 \pm 7	S390C	28 \pm 10	F445C	49 \pm 10
				L392C	25 \pm 11	Y446C	51 \pm 11
				G394C	31 \pm 9	F447C	57 \pm 12
				K395C	21 \pm 8*	T449C	52 \pm 9
						Y451C	26 \pm 8
						L452C	23 \pm 6
						V453C	19 \pm 4
						Q454C	25 \pm 6
						P445C	20 \pm 6

Table 2. The average size of ionomycin (IO)-releasable Ca²⁺ pool is shown for cys-less mPS1, WT-mPS1, mPS1- Δ loop, P433A, P433L and TM 6, 7 and 9 cys-mutant. Cell lines that have a significant increase in ER Ca²⁺ compare to WT-mPS1 is shown in red. * denotes residues in TM 6 and 7 that are exposed to water (Tolia, Chavez-Gutierrez et al. 2006). All residues in TM 9 are exposed to water (Alexandra Tolia 2008).

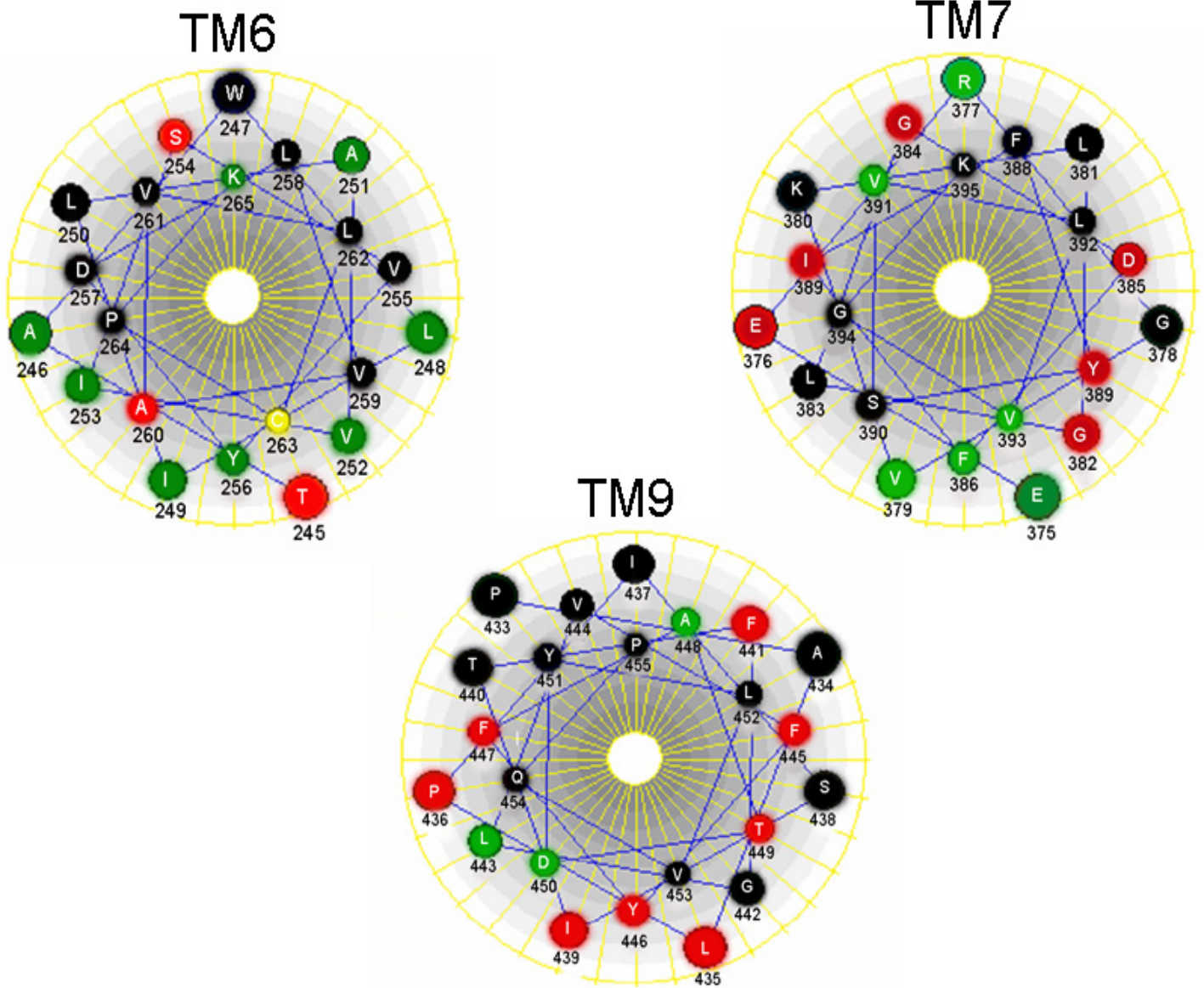


Fig 25. Helical representation of TMs 6, 7 and 9. Amino acids are represented by a single letter code. Helical wheel model is viewed from the N-terminus (DNASTAR). Red circle-loss of function, black circle-functional, green circle-not tested and yellow circle-endogenous cysteine.

CHAPTER FIVE

Conclusions and Future Experiments

Conclusions

In our recent studies (Tu, Nelson et al. 2006) (Nelson, Tu et al. 2007) and unpublished work, we discovered that PSs function as an ER Ca^{2+} leak channels, most FAD PSs mutations affects ER Ca^{2+} leak channels, most functional FAD PS1 mutations segregate with the CWP phenotype, cysteine mutants in TM 6, 7 and 9 affected ER Ca^{2+} leak and that deletion of the hydrophilic loop between TM 6 and 7 abolished ER Ca^{2+} leak. In order to obtain these data we relied on the lipid bilayer reconstitution technique and Ca^{2+} imaging experiments in MEF cell lines, fibroblast and lymphoblast from AD patients. From these data we showed that PSs function as ER Ca^{2+} leak channels, PSs DKO-MEF cell had a doubling of ER Ca^{2+} levels, FAD PS1-M146V and FAD PS2-N141I abolished ER Ca^{2+} leak, PS1-D257A (γ -secretase mutant) and ApHtko (γ -secretase knockout) MEF line had ER Ca^{2+} leak and that FAD PS1- Δ E9 enhanced ER Ca^{2+} leak activity (Tu, Nelson et al. 2006). We further found that FAD PS- L166P, A246E, E273A, G384A and P436Q abolished ER Ca^{2+} leak function, while FAD PS1-A79V and FTD PS1 associated mutant (L113P, G183V and Rins352) did not affect ER Ca^{2+} leak (Nelson, Tu et al. 2007). From our unpublished data using Ca^{2+} imaging in lymphoblast from AD patients harboring mutations in PSs (M139V, M146L, K239E, V261F, P264L, R269G, C410Y, A426P, A431E, Δ E9 and PS2-N141I), tau-R406W, APP-V717L and sporadic AD cases. From these data we learned that PS1-M139V, M146L, K239E, V261F, A426P, A431E and PS2-N141I abolished ER Ca^{2+} leak, while FAD PS1-P264L, R269G, C410Y and Δ E9 did not affect ER Ca^{2+} leak. The tau-R406W, APP-V717L and sporadic AD cases did not have any apparent effect on ER Ca^{2+} leak based on Ca^{2+} imaging experiments. From our data we noticed that most FAD mutants that were functional for Ca^{2+} leak segregated with the CWP/SP phenotype, so we tested

FAD SP only (L85P), FAD CWP/SP (G217D, E280G, T291P, N405S) and FAD CWP only (L420R and $\Delta E8$) on ER leak. From these experiments G217D and L420R abolished ER leak, while L85P, E280G, T291P, N405S and $\Delta E8$ did not.

To test the idea whether PSs holoprotein function as an ER Ca^{2+} leak channel we test PS1-M292D, an uncleavable form of PS1. As expected, PS1-M292D was able to rescue DKO-MEF, hence PS1 holoprotein functions as an ER Ca^{2+} leak channels. From our previous studies, we discovered that PS1-D257A (γ -secretase mutant) did not affect ER Ca^{2+} leak, so we tested whether the other aspartate at 385 that is critical for γ -secretase function affected ER Ca^{2+} leak. Surprisingly, the D385A mutant abolished ER Ca^{2+} leak in our assay. We also tested whether the targeting construct (dTAG) that was used to develop the PScDKO mice was able to function as an ER Ca^{2+} leak. Based on our data dTAG was about to rescue DKO-MEK, hence dTAG was able to function as an ER Ca^{2+} leak channel. From our results we conclude that most of the FAD PS1 mutation tested abolished ER Ca^{2+} and that most of the FAD mutation that were functional had the CWP/S phenotype in AD patients. So far we have not observe a “hot Spot” for mutations that affect ER Ca^{2+} leak; however, most FAD mutations that were loss of function we localize in the TM domains. These observations further suggest that PSs play a pivotal role in deranged Ca^{2+} in AD and they also provided further support for the contribution of disturbed Ca^{2+} homeostasis to AD pathogenesis (Khachaturian 1989; Mattson, LaFerla et al. 2000; LaFerla 2002; Smith, Green et al. 2005).

In the next series of experiments we used Ca^{2+} imaging experiments to examine the effects of cysteine mutants in TM6, 7 and 9 on ER Ca^{2+} leak. In addition, we tested a PS1 mutant that had its hydrophilic loop (PS1- Δ loop) deleted. We also tested PS1-P433A/L that is known to keep PS1 in an open conformation. We found that several of

the mutants that were examined affected PS1 ability to function as an ER Ca^{2+} leak channel. We also observed that a number of substitutions that were exposed to water based on the work of Tolia et al affected PS1 ability to function as an ER leak Ca^{2+} channel. Interestingly, the cys-less mPS1 construct was able to maintain γ -secretase (Tolia, Chavez-Gutierrez et al. 2006) and ER Ca^{2+} leak. From the constructs tested T245C, S254 and A260C of TM6, E376C, G382C, G384C, D385C, I387C, and Y389C of TM7 and L435C, P436C, I439C, F441C, F445C, Y446C, F447C and T449C of TM9 where loss of function for ER Ca^{2+} leak. From the cys-mutants examined that were loss of function E376C, G384C, D385C, I387C, Y389C, L435C, P436C, I439C, F441C, F445C, Y446C, F447C and T449C were exposed to water based on the work from Tolia et al. W247C, L381C, L383C, F388C, K395C, P433C, A434C, I437C, S438C, T440C, G382C, V444C, Y451C, L452C, V253C, Q454C and P445C were exposed to water and functional in our assay. These data suggest that both residues that are exposed and not exposed to water can affect channel activity by affecting how the channel is gated by a conformational change. Both P433A and P433L that are known to cause PS1 to be in an open conformation for water entry were functional based on Ca^{2+} imaging experiments, while the deletion of the hydrophilic loop of PS1 results in a loss of function channel.

Currently, the dominant model for the cause of AD is the “amyloid hypothesis”(Fig 3), which states that the increase in amyloidogenic $\text{A}\beta_{42}$ peptide (or an increase in $\text{A}\beta_{42}$: $\text{A}\beta_{40}$ ratio) is the major cause of neuronal and synaptic loss (Hardy and Selkoe 2002). As a result most AD therapies have been geared at targeting the amyloid plaques in the brain of AD patients. Most recently clinical trials have suggested that additional targets other than amyloid should be exploited if we should combat this devastating

neurological disorder (Seabrook 2007). Is there a place for the “Ca²⁺ hypothesis” in the AD field? What is the role of ER Ca²⁺ leak in the pathogenesis of FAD? This is the million-dollar question. Does the “amyloid hypothesis” and “Ca²⁺ hypothesis” exert synergistic effects on AD pathology or do they function independently? There are surmounting evidence implicating Ca²⁺ dysregulation and/or dyshomeostais both in the cell body and at the synapse. However, they differ by their proposed mechanism of how Ca²⁺ is mishandled. The general consensus in the Ca²⁺ /AD field, is that many PSs FAD mutations result in excessive Ca²⁺ release from the ER through the InsP₃R and RyanR. To best explain and understand the role of Ca²⁺ in AD pathology, please refer to Fig 26 and the excerpt taken from Bezprovanny review in Trends of Molecular medicine.

“Sequential cleavages of β -amyloid precursor protein (APP) by β -secretase (β) and γ -secretase (γ) generate amyloid β -peptide (A β). A β forms oligomers, which can insert into the plasma membrane and form Ca²⁺-permeable pores. The association of A β oligomers with the plasma membrane is facilitated by binding to surface phosphatidylserine (PtdS); age and Ca²⁺-related mitochondrial impairment leads to ATP depletion and might trigger flipping of PtdS from the inner portion of the plasma membrane to the cell surface. Reduction in ATP levels and loss of membrane integrity causes membrane depolarization, which leads to facilitation of Ca²⁺ influx through NMDAR and VGCC. A β oligomers can also affect activity of NMDAR, AMPAR and VGCC directly. Glutamate stimulates activation of mGluR1/5 receptors, production of InsP₃ and InsP₃-mediated Ca²⁺ release from the ER. Presenilins (PS) function as an ER Ca²⁺-leak channel and many FAD mutations impair Ca²⁺-leak-channel function of PS, resulting in excessive accumulation of Ca²⁺ in the ER. Increased ER Ca²⁺ levels result in enhanced Ca²⁺ release through InsP₃-gated InsP₃R1 and Ca²⁺-gated RyanR2. PS

might also modulate activity of InsP₃R, RyanR and SERCA pump directly. Elevated cytosolic Ca²⁺ levels result in the activation of calcineurin (CaN) and calpains and lead to facilitation of LTD, inhibition of LTP, modification of neuronal cytoskeleton, synaptic loss and neuritic atrophy. Excessive Ca²⁺ is taken up by mitochondria through mitochondrial Ca²⁺ uniporter (MCU), eventually leading to opening of mitochondrial permeability-transition pore (mtPTP) and apoptosis. The NMDAR inhibitor memantine (MMT) is approved for the treatment of AD and the NR2B-specific antagonist EVT-101 was recently developed for AD treatment. 'CNS-optimized' L-type VGCC inhibitor MEM-1003, putative 'mitochondrial agent' Dimebon and 'mitochondrial energizer' Ketasyn are in clinical trials for AD". Lets cure Alzheimer's disease before we forget...

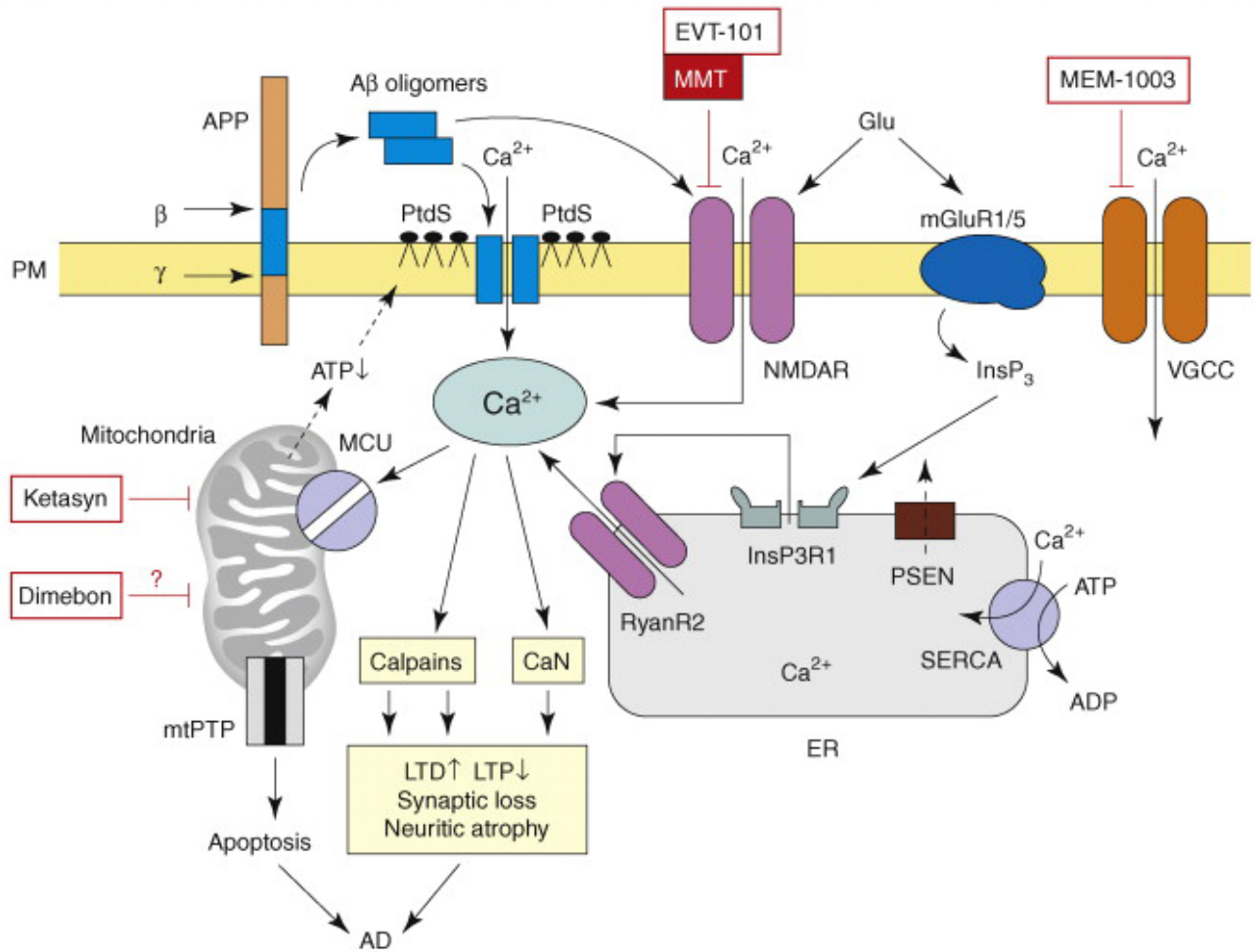


Fig 26. The model of Ca²⁺ dysregulation in AD. (Bezprozvanny 2009), in press

Future Experiments

1. Measure A-beta 42/40 ratio

In our combine studies we have examine over 25 PSs(PS1-A79V, L85P, M139V, M146L, H163Y, L166P, G217D, K239E, A246E, V261F, P264L, R269G, E280G, P284H, T291P, G384A, N405S, C410Y, L420R, A426P, A431E, P436Q, ΔE8, ΔE9 and PS2-N141I) mutation and we currently have the Ca²⁺ data for all the construct we have made, hence it would also be interesting to examine the A-beta 42/40 ratio for each constructs. For these experiments we would explore the sandwich ELISA technique that is widely used to measure A-beta-42/40 ratio. As a model system we would develop stable cell line for each construct and infect them with lenti-sweAPP. A-beta 42/40 ratios would be measured 24hour post lenti-viral infection. Alternatively, we could use hippocampal or cortical neurons from the PScDKO mice; the cultures would be subject to CRE, followed by lenti-viral infection of individual PS construct and sweAPP.

2. Examine the effects of MTS reagents on TM 6, 7 and 9 cysteine mutant in the BLM

Our electrophysiological and Ca²⁺ imaging experiments indicated that presenilins function as Ca²⁺ permeable ER channels (Tu, Nelson et al. 2006). Presenilins are transmembrane proteins which contain 9 transmembrane domains (Laudon, Hansson et al. 2005). Where is the ion permeation pore in presenilin-1? To answer this question more directly we will capitalize on the fact that we have the Ca²⁺ data from the cysteine mutants in TM6, 7 and 9 that are functional and we also know most of the cys residues that are exposed to water in a cell base assay (Tolia, Chavez-Gutierrez et al. 2006) (Alexandra Tolia 2008). We will employ the substituted-cysteine-accessibility method

(SCAM). The SCAM method is widely used to study secondary structure of membrane proteins (Akabas, Stauffer et al. 1992; Stauffer and Karlin 1994; Karlin and Akabas 1998). This method is particularly suited for mapping pore-lining residues in ion channels and transporters. BLM experiments will be performed with functional cysteine point mutants in TM, 6, 7 and 9 domains of PS1, cys-less mPS1 will be used as a negative control. The surface accessibility of the introduced cysteine residues will be tested by applying thiol-specific modifying methanethiosulfonate (MTS) reagents (Fig 27B). MTS reagents selectively and rapidly react with cysteine side chain to form a permanent disulfide bond (Fig 27A). The three charged MTS reagents, MTSET (2-(trimethylammonium)ethyl methanethiosulfonate bromide), MTSEA (2-aminoethyl methanethiosulfonate hydrobromide), and MTSES [sodium(2-sulfonatoethyl) methanethiosulfonate] are most widely used in SCAM studies (Fig 27B). Chemical reaction of these agents with a side-chain of the cysteine residue introduces a positive (for MTSEA and MTSET) or negative (for MTSES) charge at the position of a previously neutral cysteine residue. The introduction of the charge often leads to changes in ion channel function, which can be detected by electrical recordings in the BLM. Only –SH group exposed to water will be able to react with MTS reagents (Fig 28A). I have already made microsomal preps from a few functional cys-residues (Fig 28B). The MTSEA, MTSET and MTSES molecules fit into a cylinder 6 Å in diameter and 10 Å in length. Because of their small size MTS reagents can access even Cys residues located in the narrow selectivity filter of ion channels (Akabas, Stauffer et al. 1992; Stauffer and Karlin 1994; Karlin and Akabas 1998). The MTSET and MTSES are not membrane permeable and can be used to determine which side of the membrane cysteine residues are exposed to. The data from these experiments will tell us which

cys-residues are exposed to water in the BLM and it will also inform us on how MTS reagents affect PS1 conductance.

3. Evaluate ER Ca²⁺ leak in neurons

The ultimate goal of our study is to examine ER Ca²⁺ leak in neurons, mainly hippocampal (HP) and cortical (CTX) neurons because they are the cell types that are mainly affected during AD pathogenesis. For these experiments we will use the PScDKO mice that were provided by our collaborator Bart De Strooper. They developed the PScDKO mice in which the first exon of PS1 is flanked by loxp sites, they then cross this mice with a PS2^{-/-} mice to develop the fPS1/fPS1; PS2^{-/-}. They also showed that CRE recombinase expression in this mice resulted in a PS null mice (unpublished). Similar to De Strooper we could treat HP and CTX cultures with CRE (Lenti-NLS-GFP-Cre) and examine GFP positive neuron using Ca²⁺ imaging experiments. Control cultures will be infected with Lenti-NLS-GFP virus. See preliminary data from Hua Zhang (Fig 29). We could then introduce our PSs FAD mutants via Calcium phosphate infection or lenti-viral infection. These cultures could then be subjected to Ca²⁺ imaging experiment. To stimulate InsP₃R-mediated Ca²⁺ release in these experiments, we will challenge Fura-2 loaded PS-null neurons with 100 μM 3,5-dihydroxyphenylglycine (DHPG), a specific mGluR1/5 receptor agonist (Schoepp, Jane et al. 1999; Mao and Wang 2002). To study RyanR-mediated Ca²⁺ release we will apply 5 mM caffeine, a potent activator of RyanR (Ehrlich, Kaftan et al. 1994). The physiological response will be evaluated by application of 100 μM glutamate as we previously described for striatal neurons (Tang, Slow et al. 2005). The size of intracellular Ca²⁺ pool will be determined based on response to ionomycin as we described previously for MEF cells (Tu, Nelson et al. 2006). The ER Ca²⁺ concentrations will be determined in our experiments with

Mag-Fura-2 which will be performed and analyzed as described for MEF cells (Tu, Nelson et al. 2006). If presenilins play a significant role in neuronal ER Ca^{2+} leak pathway, we expect that ER Ca^{2+} stores will be overfilled in PS-null neurons when compared to control neurons, resulting in enhanced InsP_3R - and RyanR -mediated Ca^{2+} responses and increased $[\text{Ca}^{2+}]_{\text{ER}}$ levels.

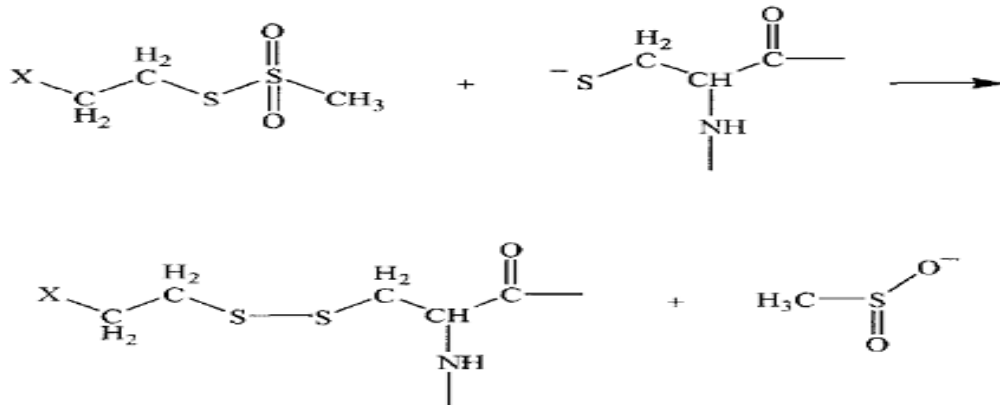
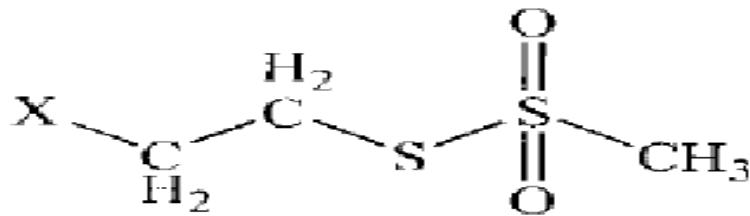
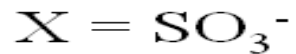
A**B****MTSET****MTSEA****MTSES**

Fig 27. Chemical reaction of cysteine side-chain modification with MTS reagent. a. General structure of three charged MTS reagents. **b.** Adapted from (Karlin and Akabas 1998).

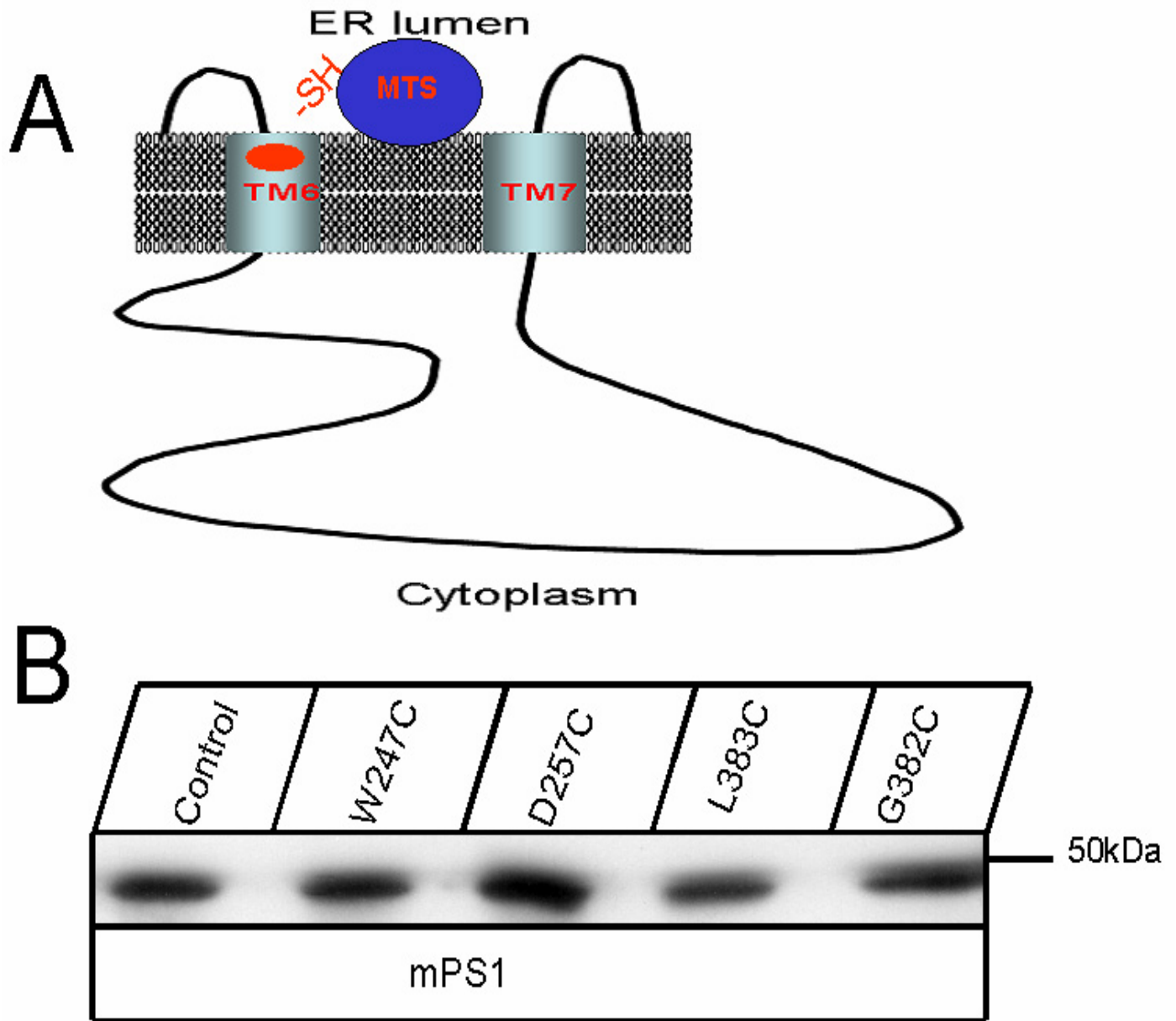
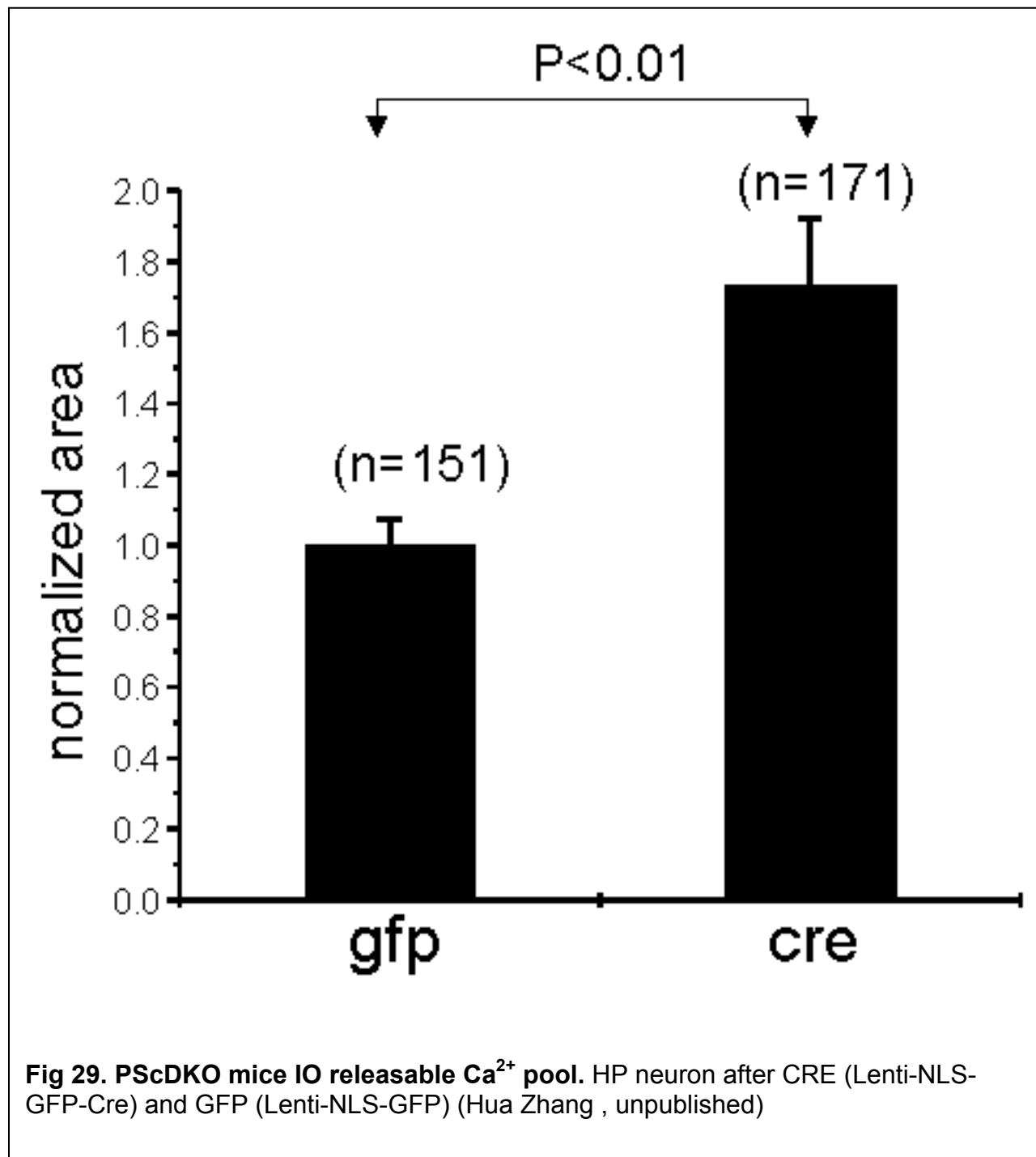


Fig 28. Substituted-cysteine-accessibility method (SCAM) a. Water exposed -SH group reacting with MTS reagent. b. Microsomal prep blots from cys mutant.



Bibliography

- Akabas, M. H., D. A. Stauffer, et al. (1992). "Acetylcholine receptor channel structure probed in cysteine-substitution mutants." Science **258**(5080): 307-10.
- Alexandra Tolia, K. H., and Bart De Strooper (2008). "Transmembrane Domain 9 of Presenilin Determines the Dynamic Conformation of the Catalytic Site of - Secretase." J. Biol. Chem. **Vol. 283**(Issue 28): 19793-19803.
- Amtul, Z., P. A. Lewis, et al. (2002). "A presenilin 1 mutation associated with familial frontotemporal dementia inhibits gamma-secretase cleavage of APP and notch." Neurobiol Dis **9**(2): 269-73.
- Annaert, W. G., L. Levesque, et al. (1999). "Presenilin 1 controls gamma-secretase processing of amyloid precursor protein in pre-golgi compartments of hippocampal neurons." J Cell Biol **147**(2): 277-94.
- Begley, J. G., W. Duan, et al. (1999). "Altered calcium homeostasis and mitochondrial dysfunction in cortical synaptic compartments of presenilin-1 mutant mice." J Neurochem **72**(3): 1030-9.
- Bentahir, M., O. Nyabi, et al. (2006). "Presenilin clinical mutations can affect gamma-secretase activity by different mechanisms." J Neurochem **96**(3): 732-42.
- Bezprozvanny, I. (2009). "Calcium signaling and neurodegenerative diseases." Trends in Molecular Medicine.
- Boeve, B. F., M. Baker, et al. (2006). "Frontotemporal dementia and parkinsonism associated with the IVS1+1G->A mutation in progranulin: a clinicopathologic study." Brain **129**(Pt 11): 3103-14.
- Brown, M. S., Ye, J., Rawson, R.B., and Goldstein, J.L (2000). "Regulated Intramembrane Proteolysis: A Control Mechanism Conserved from Bacteria to Humans." cell **100**: 315-323.
- Corder, E. H., A. M. Saunders, et al. (1993). "Gene dose of apolipoprotein E type 4 allele and the risk of Alzheimer's disease in late onset families." Science **261**(5123): 921-3.
- Crook, R., A. Verkkoniemi, et al. (1998). "A variant of Alzheimer's disease with spastic paraparesis and unusual plaques due to deletion of exon 9 of presenilin 1." Nat Med **4**(4): 452-5.
- Cruts, M., H. Backhovens, et al. (1995). "Genetic and physical characterization of the early-onset Alzheimer's disease AD3 locus on chromosome 14q24.3." Hum Mol Genet **4**(8): 1355-64.
- Cruts, M., C. M. van Duijn, et al. (1998). "Estimation of the genetic contribution of presenilin-1 and -2 mutations in a population-based study of presenile Alzheimer disease." Hum Mol Genet **7**(1): 43-51.
- De Strooper, B. (2007). "Loss-of-function presenilin mutations in Alzheimer disease." EMBO repts **8**(2): 141-146.
- De Strooper, B., W. Annaert, et al. (1999). "A presenilin-1-dependent gamma-secretase-like protease mediates release of Notch intracellular domain." Nature **398**(6727): 518-22.
- De Strooper, B., M. Beullens, et al. (1997). "Phosphorylation, subcellular localization, and membrane orientation of the Alzheimer's disease-associated presenilins." J Biol Chem **272**(6): 3590-8.
- De Strooper, B., P. Saftig, et al. (1998). "Deficiency of presenilin-1 inhibits the normal cleavage of amyloid precursor protein." Nature **391**(6665): 387-90.

- Dempster, J. (2001). The laboratory computer: a practical guide for neuroscientists and physiologists, Academic Press.
- Dermaut, B., M. Cruts, et al. (1999). "The Glu318Gly substitution in presenilin 1 is not causally related to Alzheimer disease." Am J Hum Genet **64**(1): 290-2.
- Dermaut, B., S. Kumar-Singh, et al. (2004). "A novel presenilin 1 mutation associated with Pick's disease but not beta-amyloid plaques." Ann Neurol **55**(5): 617-26.
- Edbauer, D., E. Winkler, et al. (2003). "Reconstitution of gamma-secretase activity." Nat Cell Biol **5**(5): 486-8.
- Ehrlich, B. E., E. Kaftan, et al. (1994). "The pharmacology of intracellular Ca²⁺-release channels." **15**: 145-149.
- Esler WP, K. W., Ostaszewski BL, Diehl TS, Moore CL, Tsai J-Y, Rahmati T, Xia W, Selkoe DJ, and Wolfe MS (2000). "Transition-State Analogue inhibitors of gamma-secretase bind directly to presenilin-1." nature cell biology: 2720-2725.
- Etcheberrigaray, R., N. Hirashima, et al. (1998). "Calcium responses in fibroblasts from asymptomatic members of Alzheimer's disease families." Neurobiol Dis **5**(1): 37-45.
- Feng, R., C. Rampon, et al. (2001). "Deficient neurogenesis in forebrain-specific presenilin-1 knockout mice is associated with reduced clearance of hippocampal memory traces." Neuron **32**(5): 911-26.
- Garlind, A., R. F. Cowburn, et al. (1995). "Diminished [3H]inositol(1,4,5)P3 but not [3H]inositol(1,3,4,5)P4 binding in Alzheimer's disease brain." Brain Res **681**(1-2): 160-6.
- Glenner, G. G. and C. W. Wong (1984). "Alzheimer's disease and Down's syndrome: sharing of a unique cerebrovascular amyloid fibril protein." Biochem Biophys Res Commun **122**(3): 1131-5.
- Goate, A., M. C. Chartier-Harlin, et al. (1991). "Segregation of a missense mutation in the amyloid precursor protein gene with familial Alzheimer's disease." Nature **349**(6311): 704-6.
- Goldman, J. S., J. K. Johnson, et al. (2005). "Presenilin 1 Glu318Gly polymorphism: interpret with caution." Arch Neurol **62**(10): 1624-7.
- Grynkiewicz, G., M. Poenie, et al. (1985). "A new generation of Ca²⁺ indicators with greatly improved fluorescence properties." J Biol Chem **260**(6): 3440-3450.
- Haass, C. (1997). "Presenilins: genes for life and death." Neuron **18**(5): 687-90.
- Hardy, J. and D. J. Selkoe (2002). "The amyloid hypothesis of Alzheimer's disease: progress and problems on the road to therapeutics." Science **297**(5580): 353-6.
- Herms, J., I. Schneider, et al. (2003). "Capacitive calcium entry is directly attenuated by mutant presenilin-1, independent of the expression of the amyloid precursor protein." J Biol Chem **278**(4): 2484-9.
- Herreman, A., D. Hartmann, et al. (1999). "Presenilin 2 deficiency causes a mild pulmonary phenotype and no changes in amyloid precursor protein processing but enhances the embryonic lethal phenotype of presenilin 1 deficiency." Proc Natl Acad Sci U S A **96**(21): 11872-7.
- Herreman, A., L. Serneels, et al. (2000). "Total inactivation of gamma-secretase activity in presenilin-deficient embryonic stem cells." Nat Cell Biol **2**(7): 461-2.
- Hofer, A. M. (1999). "Measurement of free [Ca²⁺] changes in agonist-sensitive internal stores using compartmentalized fluorescent indicators." Methods Mol Biol **114**: 249-65.

- Hofer, A. M., S. Curci, et al. (1996). "ATP regulates calcium leak from agonist-sensitive internal calcium stores." Faseb J **10**(2): 302-8.
- Hutton, M. (2004). "Presenilin mutations associated with fronto-temporal dementia." Ann Neurol **55**(5): 604-6.
- Ito, E., K. Oka, et al. (1994). "Internal Ca²⁺ mobilization is altered in fibroblasts from patients with Alzheimer disease." Proc Natl Acad Sci U S A **91**(2): 534-8.
- Karlin, A. and M. H. Akabas (1998). "Substituted-cysteine accessibility method." Methods Enzymol **293**: 123-45.
- Kelliher, M., J. Fastbom, et al. (1999). "Alterations in the ryanodine receptor calcium release channel correlate with Alzheimer's disease neurofibrillary and beta-amyloid pathologies." Neuroscience **92**(2): 499-513.
- Khachaturian, Z. S. (1989). "Calcium, membranes, aging, and Alzheimer's disease. Introduction and overview." Ann N Y Acad Sci **568**: 1-4.
- Kimberly, W. T., M. J. LaVoie, et al. (2003). "Gamma-secretase is a membrane protein complex comprised of presenilin, nicastrin, Aph-1, and Pen-2." Proc Natl Acad Sci U S A **100**(11): 6382-7.
- Kimberly WT, X. W., Rahmati T, Wolfe MS, Selkoe DJ (2000). "The transmembrane aspartates in presenilin 1 and 2 are obligatory for gamma-secretase activity and amyloid beta-protein generation." J Biol Chem **275**: 3173-3178.
- Kurumatani, T., J. Fastbom, et al. (1998). "Loss of inositol 1,4,5-trisphosphate receptor sites and decreased PKC levels correlate with staging of Alzheimer's disease neurofibrillary pathology." Brain Res **796**(1-2): 209-21.
- LaFerla, F. M. (2002). "Calcium dyshomeostasis and intracellular signalling in Alzheimer's disease." Nat Rev Neurosci **3**(11): 862-72.
- Larner, A. J. and M. Doran (2006). "Clinical phenotypic heterogeneity of Alzheimer's disease associated with mutations of the presenilin-1 gene." J Neurol **253**(2): 139-58.
- Laudon, H., E. M. Hansson, et al. (2005). "A nine-transmembrane domain topology for presenilin 1." J Biol Chem **280**(42): 35352-60.
- LaVoie, M. J., P. C. Fraering, et al. (2003). "Assembly of the gamma-secretase complex involves early formation of an intermediate subcomplex of Aph-1 and nicastrin." J Biol Chem **278**(39): 37213-22.
- Lazarov, V. K., P. C. Fraering, et al. (2006). "Electron microscopic structure of purified, active gamma-secretase reveals an aqueous intramembrane chamber and two pores." Proc Natl Acad Sci U S A **103**(18): 6889-94.
- Lee, P., L. Medina, et al. (2006). "The Thr354Ile substitution in PSEN1:: disease-causing mutation or polymorphism?" Neurology **66**(12): 1955-6.
- Leissring, M. A., F. M. LaFerla, et al. (2001). "Subcellular mechanisms of presenilin-mediated enhancement of calcium signaling." Neurobiol Dis **8**(3): 469-78.
- Leissring, M. A., I. Parker, et al. (1999). "Presenilin-2 mutations modulate amplitude and kinetics of inositol 1, 4,5-trisphosphate-mediated calcium signals." J Biol Chem **274**(46): 32535-8.
- Leissring, M. A., B. A. Paul, et al. (1999). "Alzheimer's presenilin-1 mutation potentiates inositol 1,4,5-trisphosphate-mediated calcium signaling in *Xenopus* oocytes." J Neurochem **72**(3): 1061-8.
- Levy, E., M. D. Carman, et al. (1990). "Mutation of the Alzheimer's disease amyloid gene in hereditary cerebral hemorrhage, Dutch type." Science **248**(4959): 1124-6.

- Levy-Lahad, E., W. Wasco, et al. (1995). "Candidate gene for the chromosome 1 familial Alzheimer's disease locus." Science **269**(5226): 973-7.
- Li YM, X. M., Lai MT, Huang Q, Castro JL, DiMuzio-Mower J, Harrison T, Lellis C, Nadin A, Neduvellil JG, Register RB, Sardana MK, Shearman MS, Smith AL, Shi XP, Yin KC, Shafer JA, Gardell SJ. (2000). "Photoactivated gamma-secretase inhibitors directed to the active site covalently label presenilin 1." Nature: 689-694.
- Mao, L. and J. Q. Wang (2002). "Glutamate cascade to cAMP response element-binding protein phosphorylation in cultured striatal neurons through calcium-coupled group I metabotropic glutamate receptors." Mol Pharmacol **62**(3): 473-84.
- Masters, C. L., G. Simms, et al. (1985). "Amyloid plaque core protein in Alzheimer disease and Down syndrome." Proc Natl Acad Sci U S A **82**(12): 4245-9.
- Mattila, K. M., C. Forsell, et al. (1998). "The Glu318Gly mutation of the presenilin-1 gene does not necessarily cause Alzheimer's disease." Ann Neurol **44**(6): 965-7.
- Mattson, M. P., Q. Guo, et al. (1998). "Presenilins, the endoplasmic reticulum, and neuronal apoptosis in Alzheimer's disease." J Neurochem **70**(1): 1-14.
- Mattson, M. P., F. M. LaFerla, et al. (2000). "Calcium signaling in the ER: its role in neuronal plasticity and neurodegenerative disorders." Trends Neurosci **23**(5): 222-9.
- Nelson, O., H. Tu, et al. (2007). "Familial Alzheimer disease-linked mutations specifically disrupt Ca²⁺ leak function of presenilin 1." J Clin Invest **117**(5): 1230-9.
- Oh, Y. S. and R. J. Turner (2005). "Topology of the C-terminal fragment of human presenilin 1." Biochemistry **44**(35): 11821-8.
- O'Neill, C., R. F. Cowburn, et al. (2001). "Dysfunctional intracellular calcium homeostasis: a central cause of neurodegeneration in Alzheimer's disease." Biochem Soc Symp **67**: 177-94.
- Raux, G., R. Gantier, et al. (2000). "Dementia with prominent frontotemporal features associated with L113P presenilin 1 mutation." Neurology **55**(10): 1577-8.
- Ris, L., I. Dewachter, et al. (2003). "Capacitative calcium entry induces hippocampal long term potentiation in the absence of presenilin-1." J Biol Chem **278**(45): 44393-9.
- Rogaev, E. I., R. Sherrington, et al. (1995). "Familial Alzheimer's disease in kindreds with missense mutations in a gene on chromosome 1 related to the Alzheimer's disease type 3 gene." Nature **376**(6543): 775-8.
- Rogaeva, E. A., K. C. Fafel, et al. (2001). "Screening for PS1 mutations in a referral-based series of AD cases: 21 novel mutations." Neurology **57**(4): 621-5.
- Saunders, A. M., W. J. Strittmatter, et al. (1993). "Association of apolipoprotein E allele epsilon 4 with late-onset familial and sporadic Alzheimer's disease." Neurology **43**(8): 1467-72.
- Saura, C. A., S. Y. Choi, et al. (2004). "Loss of presenilin function causes impairments of memory and synaptic plasticity followed by age-dependent neurodegeneration." Neuron **42**(1): 23-36.
- Schneider, I., D. Reverse, et al. (2001). "Mutant presenilins disturb neuronal calcium homeostasis in the brain of transgenic mice, decreasing the threshold for excitotoxicity and facilitating long-term potentiation." J Biol Chem **276**(15): 11539-44.

- Schoepp, D. D., D. E. Jane, et al. (1999). "Pharmacological agents acting at subtypes of metabotropic glutamate receptors." Neuropharmacology **38**(10): 1431-76.
- Seabrook, G. R. (2007). "Beyond amyloid:the next generation of Alzheimer's disease therapeutics." Mol. Interv **7**: 261-270.
- Selkoe, D. J. (2002). "Alzheimer's disease is a synaptic failure." Science **298**(5594): 789-91.
- Shen, J. and R. J. Kelleher, 3rd (2007). "The presenilin hypothesis of Alzheimer's disease: Evidence for a loss-of-function pathogenic mechanism." Proc Natl Acad Sci U S A **104**(2): 403-409.
- Sherrington, R., E. I. Rogaeve, et al. (1995). "Cloning of a gene bearing missense mutations in early-onset familial Alzheimer's disease." Nature **375**(6534): 754-60.
- Smith, I. F., K. N. Green, et al. (2005). "Calcium dysregulation in Alzheimer's disease: recent advances gained from genetically modified animals." Cell Calcium **38**(3-4): 427-37.
- Spasic, D., A. Tolia, et al. (2006). "Presenilin-1 maintains a nine-transmembrane topology throughout the secretory pathway." J Biol Chem **281**(36): 26569-77.
- Stauffer, D. A. and A. Karlin (1994). "Electrostatic potential of the acetylcholine binding sites in the nicotinic receptor probed by reactions of binding-site cysteines with charged methanethiosulfonates." Biochemistry **33**(22): 6840-9.
- Steiner, H. (1999). "Amyloidogenic function of the Alzheimer's disease associated presenilin-1 in the absence of endoproteolysis." Biochemistry **38**: 14600-14605.
- Steiner, H., T. Revesz, et al. (2001). "A pathogenic presenilin-1 deletion causes aberrant Abeta 42 production in the absence of congophilic amyloid plaques." J Biol Chem **276**(10): 7233-9.
- Struhl, G. and I. Greenwald (1999). "Presenilin is required for activity and nuclear access of Notch in Drosophila." Nature **398**(6727): 522-5.
- Stutzmann, G. E., A. Caccamo, et al. (2004). "Dysregulated IP3 signaling in cortical neurons of knock-in mice expressing an Alzheimer's-linked mutation in presenilin1 results in exaggerated Ca²⁺ signals and altered membrane excitability." J Neurosci **24**(2): 508-13.
- Takasugi, N., T. Tomita, et al. (2003). "The role of presenilin cofactors in the gamma-secretase complex." Nature **422**(6930): 438-41.
- Takeda, T., M. Asahi, et al. (2005). "Presenilin 2 regulates the systolic function of heart by modulating Ca²⁺ signaling." Faseb J **19**(14): 2069-71.
- Tandon, A. and P. Fraser (2002). "The presenilins." Genome Biol **3**(11): reviews3014.
- Tang, T.-S., E. J. Slow, et al. (2005). "Disturbed Ca²⁺ signaling and apoptosis of medium spiny neurons in Huntington's disease." Proc Natl Acad Sci U S A **102**: 2602-2607.
- Tang-Wai, D., P. Lewis, et al. (2002). "Familial frontotemporal dementia associated with a novel presenilin-1 mutation." Dement Geriatr Cogn Disord **14**(1): 13-21.
- Tanzi, R. E. and L. Bertram (2005). "Twenty years of the Alzheimer's disease amyloid hypothesis: a genetic perspective." Cell **120**(4): 545-55.
- Thinakaran, G., D. R. Borchelt, et al. (1996). "Endoproteolysis of presenilin 1 and accumulation of processed derivatives in vivo." Neuron **17**(1): 181-90.
- Tolia, A., L. Chavez-Gutierrez, et al. (2006). "Contribution of Presenilin Transmembrane Domains 6 and 7 to a Water-containing Cavity in the {gamma}-Secretase Complex." J Biol Chem **281**(37): 27633-42.

- Tu, H., T. Miyakawa, et al. (2002). "Functional characterization of the type 1 inositol 1,4,5-trisphosphate receptor coupling domain SII(+/-) splice variants and the *opisthokont* mutant form." Biophys J **82**: 1995-2004.
- Tu, H., O. Nelson, et al. (2006). "Presenilins form ER calcium leak channels, a function disrupted by mutations linked to familial Alzheimer's disease." Cell **126**: 981-993.
- Urban S., S. D., and M. Freeman. (2002). "Conservation of intramembrane proteolytic activity and substrate specificity in prokaryotic and eukaryotic Rhomboids." Curr Biol **12**: 1507-1512.
- Ute Dreses-Werringloer, J.-C. L., 2 Vale' rie Vingtdeux, 1 Haitian Zhao, 1 Horia Vais, 3 Adam Siebert, 3, J. K. Ankit Jain, 1 Anne Rovelet-Lecrux, 4 Didier Hannequin, 4 Florence Pasquier, 5 Daniela Galimberti, 6, et al. (2008). "Polymorphism in CALHM1 Influences Ca²⁺ Homeostasis, A β Levels, and Alzheimer's Disease Risk." Cell **133**: 1149-1161.
- Wolfe, M. S., W. Xia, et al. (1999). "Two transmembrane aspartates in presenilin-1 required for presenilin endoproteolysis and gamma-secretase activity." Nature **398**(6727): 513-7.
- Yagi, T., C. Giallourakis, et al. (2008). "Defective signal transduction in B lymphocytes lacking presenilin proteins." Proc Natl Acad Sci U S A **105**(3): 979-84.
- Yoo, A. S., I. Cheng, et al. (2000). "Presenilin-mediated modulation of capacitative calcium entry." Neuron **27**(3): 561-72.
- Young, L. T., S. J. Kish, et al. (1988). "Decreased brain [3H]inositol 1,4,5-trisphosphate binding in Alzheimer's disease." Neurosci Lett **94**(1-2): 198-202.
- Yu, G., F. Chen, et al. (1998). "The presenilin 1 protein is a component of a high molecular weight intracellular complex that contains beta-catenin." J Biol Chem **273**(26): 16470-5.
- Yu, H., C. A. Saura, et al. (2001). "APP processing and synaptic plasticity in presenilin-1 conditional knockout mice." Neuron **31**(5): 713-26.
- Zatti, G., Burgo, A., Giacomello, M., Barbiero, L., Ghidoni, R., Sinigaglia G., Florean, C., Bagnoli, S., Binetti, G., Sorbi, S., Pizzo, P., Fasolato, C. (2006). "Presenilin mutations linked to familial Alzheimer's disease reduce endoplasmic reticulum and Golgi apparatus calcium levels." Cell Calcium **39**: 539-550.
- Zekanowski, C., M. P. Golan, et al. (2006). "Two novel presenilin 1 gene mutations connected with frontotemporal dementia-like clinical phenotype: genetic and bioinformatic assessment." Exp Neurol **200**(1): 82-8.